Mathematical and numerical modelling of dispersion-managed solitons, autosolitons and self-similar optical pulses

Sonia Annarita Boscolo

Doctor of Philosophy

Aston University

May 2002

Aston University

Mathematical and numerical modelling of dispersion-managed solitons, autosolitons and self-similar optical pulses

Sonia Annarita Boscolo
Doctor of Philosophy

2002

Summary

This thesis presents theoretical investigation of three topics concerned with nonlinear optical pulse propagation in optical fibres. The techniques used are mathematical analysis and numerical modelling.

Firstly, dispersion-managed (DM) solitons in fibre lines employing a weak dispersion map are analysed by means of a perturbation approach. In the case of small dispersion map strengths, the average pulse dynamics is described by a perturbed nonlinear Schrödinger (NLS) equation. Applying a perturbation theory, based on the Inverse Scattering Transform method, an analytic expression for the envelope of the DM soliton is derived. This expression correctly predicts the power enhancement arising from the dispersion management.

Secondly, autosoliton transmission in DM fibre systems with periodical in-line deployment of nonlinear optical loop mirrors (NOLMs) is investigated. The use of in-line NOLMs is addressed as a general technique for all-optical passive 2R regeneration of return-to-zero data in high-speed transmission systems with strong dispersion management. By system optimisation, the feasibility of ultra-long single-channel and wavelength-division multiplexed data transmission at bit-rates $\geq 40\,\mathrm{Gbit\,s^{-1}}$ in standard fibre -based systems is demonstrated. The tolerance limits of the results are defined.

Thirdly, solutions of the NLS equation with gain and normal dispersion, that describes optical pulse propagation in an amplifying medium, are examined. A self-similar parabolic solution in the energy-containing core of the pulse is matched through Painlevé functions to the linear low-amplitude tails. The analysis provides a full description of the features of high-power pulses generated in an amplifying medium.

Key words: Nonlinear optics, Perturbation theory for optical solitons, Optical fibre communication systems, All-optical passive regeneration, Self-similar phenomena in optics.

To my parents and my friends,
close and far away.

"The world is not beautiful or ugly
but it is how you "see" it."

Acknowledgements

I have carried out the present research during my tenure of doctoral study with the Photonics Research Group, at the School of Engineering and Applied Science, Aston University, under the guidance of Dr. Sergei K. Turitsyn.

I would like to express my deep sense of appreciation to Dr. Sergei K. Turitsyn for his guidance, continuous support, creative ideas, and stimulating discussions for this research. I would also like to express my sincere appreciation to Prof. Keith J. Blow for his advice, valuable discussions, and useful suggestions. I am also much indebited to Dr. Jeroen H.B. Nijhof, who was with the Photonics Research Group, for his advice and kind assistance in solving several numerical problems.

I acknowledge Dr. Sergei K. Turitsyn, Prof. Keith J. Blow, Dr. Jeoren H.B. Nijhof, and Prof. Victor Yu. Novokshenov as coauthors of my papers.

I shall be grateful to all the past and present collegues in the Photonics Research Group for their discussions and continuing our friendships.

I feel thankful to my parents and all of my friends for their deep understanding about my research and giving me a great help and encouragement for accomplishing this research.

Contents

List of Figures

Abbreviations

GVD	group-velocity dispersion
SPM	self-phase modulation
XPM	cross-phase modulation
FWM	four-wave mixing
WDM	wavelength-division multiplexed
SMF	single-mode fibre
DSF	dispersion-shifted fibre
DCF	dispersion compensating fibre
EDFA	erbium-doped fibre amplifier
ASE	amplified spontaneous emission
SNR	signal-to-noise ratio
RZ	return-to-zero
NRZ	non-return-to-zero
NLS	nonlinear Schrödinger
IST	inverse scatttering transform
DM	dispersion-managed
FWHM	full-width at half-maximum
RMS	root-mean-square
NOLM	nonlinear optical loop mirror
GT	Gabitov-Turitsyn
2R	re-amplification, re-shaping
BER	bit error rate
PRBS	pseudo-random binary sequence
EE-PDF	effective core area enlarged positive dispersion fibre
NDF	negative dispersion fibre

Chapter 1

Introduction

1.1 Historical perspective and motivations

Propagation of optical pulses in nonlinear optical fibres is a classic fundamental problem of nonlinear optics with important practical applications in the development of communication systems. Soliton-based high bit-rate optical data transmission [1] is a nice example how the results of basic research can trigger the development of a novel approach to a very important practical problem. Other kinds of self-similar optical pulses are less known than solitons, but not of minor practical interest. An example is the generation and self-similar propagation of high-power, ultra-short pulses with parabolic intensity profiles in optical fibres with normal dispersion [2]. This section presents an historical perspective on the development of fibre-optic communication systems and optical solitons and solitary waves.

In generating and transmitting different types of optical pulses, it is important to understand the physical properties of optical fibres in order to take full advantage of their potential. Physical properties of optical fibres have been studied since the 1960s, such as their waveguide characteristics, chromatic dispersion, loss, and nonlinearity [3, 4]. Optical fibre cables guide waves by total internal reflection at the interface between the core layer having higher refractive index and the cladding layer having lower index. Boundary condition at the core-cladding interface permits a finite number of guided modes supported by fibres. When more than two guided modes propagate simultaneously in fibres, signals get distorted at the receiver because each mode propagates with different speed, which is the phenomenon known as multimode dispersion. In addition, chromatic dispersion of optical fibres brings about the dependence of group velocity on frequency. In the presence of dispersion, different spectral components of an optical pulse propagate at different group velocities, which leads to pulse broadening. This phenomenon is referred to as group-velocity dispersion (GVD), or simply fibre dispersion. GVD has two contributions: material dispersion and waveguide dispersion. Material dispersion originates from a physical property of the silica, i.e. a retarded response of bound electrons in silica for lightwave electric field, which gives frequency dependence of the refractive index. Waveguide dispersion arises from the geometry of the guided structure such as a core radius. Fibre loss, another limiting factor of transmission distance, originates from material absorption in the far-infrared region and Rayleigh scattering arising from random density fluctuation that takes place during fibre fabrication. Pure silica absorbs light at the wavelength $\sim 2\,\mu$m, while Rayleigh scattering loss is dominant at short wavelengths since it increases as λ^{-4}. Hence the fibre exhibits a minimum

loss at the wavelength in the vicinity of 1.55 μm. Nonlinear effects in optical fibres [5]-[7] have two major contributions: nonlinear refractive index arising from nonlinear electric polarization of bound electrons in the silica, and stimulated inelastic scattering arising from the excitation of vibrational mode of the silica. Stimulated scattering (Raman and Brillouin) phenomena result in intensity dependent loss or gain in signal power and become severe above certain power thresholds. However, the main problem of nonlinearity in optical fibre transmission systems comes from the nonlinear electric polarization. Since silica fibres do not exhibit second-order nonlinear effects due to the inversion symmetry of the medium, third-order nonlinear electric polarization (Kerr nonlinearity) contributes to the lowest order nonlinear effect in fibres. Since the Kerr effect induces intensity dependence of the refractive index of silica, it brings about intensity dependent phase shift. The nonlinear phase shift introduced by the optical field itself is called self-phase modulation (SPM), whereas the cross-phase modulation (XPM) is a phase shift which is induced by the other light copropagating with different frequencies or polarization components. These nonlinear phase shifts result in spectral broadening during propagation and, by the interplay with GVD, may produce considerable waveform distortion. In addition to phase modulations, once the phase matching conditions are satisfied, third-order nonlinearity induces a parametric process called four-wave mixing (FWM), where three copropagating optical fields generate the fourth electric field with a different frequency. This leads to inter-channel crosstalk in wavelength-division multiplexed (WDM) systems. Although silica fibres do not intrinsically exhibit high nonlinearity (the Kerr coefficient of the silica is of the order of $10^{-20}\,\mathrm{m^2\,W^{-1}}$), nonlinear effects accumulate over a long distance of propagation and may have a considerable impact because of their rather high efficiency due to the low loss and high density of lightwave over a small cross section in waveguide geometry.

To overcome the limitations imposed by the physical properties of optical fibres, there have been made a number of technical advances. The multimode dispersion can be avoided by the use of standard single-mode fibres (SMFs), that are designed to support only the fundamental mode of fibre so that all higher-order modes are cut off at the operating wavelength. Since SMF exhibits zero dispersion at the wavelength of 1.3 μm, lightwave systems at the early age were operated at this wavelength. Such primary systems, however, were limited mostly by fibre loss. Advances in fabrication technology of fibres had made it possible to achieve the minimum loss of $0.2\,\mathrm{dB\,km^{-1}}$ at the wavelength of 1.55 μm [8]. On the other hand, at this wavelength, GVD exceeds $15\,\mathrm{ps\,(nm\,km)^{-1}}$ for SMF and brings about significant pulse broadening during propagation. This difficulty was overcome by the use of dispersion-shifted fibres (DSFs) having minimum dispersion at 1.55 μm by a careful design of the index profile such that the zero dispersion wavelength is shifted from 1.3 μm to the vicinity of 1.55 μm. Now that we have almost precise control over the arbitrary choice of the GVD value, it is possible to fabricate fibres even with negative GVD that compensates for the high value of GVD in installed SMF. These fibres are referred to as dispersion compensating fibres (DCFs). In the early stage, electronic regeneration was employed periodically to compensate for the loss of fibres in transmission systems. It consists of detecting, amplifying, and re-emitting signals electrically. The electronic regenerators, however, include complicated signal processing, and they are not only low cost-effective but also impose a limit on transmission speed. A remarkable progress in optical fibre communication occurred in the early 1990s when erbium-doped fibre amplifiers (EDFAs), invented in 1987, became available

[9, 10]. These amplifiers were the first to achieve close to perfect linear amplifier performance. Light could continue propagating within a fibre for hundreds of kilometers using periodic optical amplification (every 40 to 80 km) to compensate for the fibre loss. Due to a large bandwidth of amplification by EDFAs, WDM signals can be simultaneously amplified without demultiplexing to each wavelength. Advances in optical amplifier technology dictated the usable wavelength window, which continues to grow rapidly.

As a result of the advent and deployment of optical amplifiers, fibre loss is not a major limitation in optical fibre transmission and the performance of optical amplifier systems is then limited by noise, chromatic dispersion, and nonlinearity. Indeed, EDFAs restated the significance of nonlinear effects, as lightwave systems making use of EDFAs operate at relatively high power in order to maintain the average power without being buried by noise. In addition to the nonlinear effects, amplified spontaneous emission (ASE) noise accumulates over multiple amplification stages, which was absent in conventional systems employing the electronic repeaters. There have been two principal approaches to cope with the effects of fibre nonlinearity and dispersion. In the first approach, that can be called "linear", both the chromatic dispersion and nonlinearity are considered to be detrimental factors, while in the second the nonlinear and dispersive effects are counterbalanced; such systems can be called "nonlinear" or more specifically, "soliton systems".

In the linear systems the signal power is kept as low as possible to minimize nonlinear pulse distortion. However, the power cannot be very small because of the noise and requirements on the signal-to-noise ratio (SNR). Since nonlinear effects cannot be compensated by passive methods, the only way to cope with them is to reduce the fibre nonlinearity itself by the use of fibres with large core area or by keeping the local GVD relatively large on purpose to suppress nonlinear effects while minimizing the average GVD by compensating for the cumulative GVD. The latter technique, referred to as dispersion management, reduces nonlinear effects by the help of GVD. Indeed, dispersion management, that consists of using multiple sections of constant dispersion fibre whose lengths and GVDs are elaborately chosen, can lower the average GVD of the entire link while keeping the GVD of each section large enough to reduce the impact of nonlinearity on signal transmission. The dispersion compensation technique, proposed in 1980 [11], has been used successfully both in long-haul communication systems and in the existing terrestrial links, most of which are based on SMF. The basic optical pulse equalizing system consists of a transmission fibre (SMF in the installed links or DSF in the long-haul systems) and an equalizer fibre with the opposite sign dispersion (DCF to compensate SMF or, for instance, SMF to compensate DSF with normal dispersion).

Considerable efforts have been made in linear transmission systems to cope with nonlinear effects. In addition to dispersion management or the use of new fibres with reduced nonlinearity, optical modulation in the return-to-zero (RZ) format helps reducing nonlinear effects rather than in the conventional non-return-to-zero (NRZ) format. NRZ has been used at first since it requires less bandwidth associated with the bit streams. NRZ has also been considered to suppress nonlinear effects by transmitting continuous waves over the total time slot of successive bits of ones and thus reducing the peak power. Nonlinearity, however, plays a crucial role even in the NRZ format as the bit-rate increases and the peak power is enhanced to keep the average power within one bit slot. For this reason, the RZ format, more tolerant to nonlinearity, has recently been employed. The pulse modulated in the RZ format propagating in a dispersion-

managed line is sometimes called the chirped RZ pulse or the nonlinear supported RZ pulse.

The nonlinear approach, by contrast, embraces the nonlinearity and attempts to extract the maximum possible benefits from it. In 1973 Hasegawa and Tappert [12] proposed to use fibre nonlinearity for compensation of chromatic spreading. The competition between spreading and nonlinear focusing in a conservative fibre leads to the formation of stationary pulses – optical solitons – which preserve their shape during propagation, where the nonlinear chirp arising from Kerr effect counteracts with the dispersion-induced chirp. Solitons thus do not suffer from either the pulse broadening due to chromatic dispersion or the spectral broadening due to SPM. This indicates their potential application to high-speed optical transmission as units of information. It is important to stress that the concept of optical soliton was elaborated initially for media with constant anomalous dispersion ($\partial^2 k/\partial\omega^2 < 0$). In fibres with constant normal dispersion ($\partial^2 k/\partial\omega^2 > 0$), focusing nonlinearity enhances the dispersion spreading, and usual "bright" solitons do not exist. We do not discuss here "dark" solitons, propagating on the background of a monochromatic wave of finite amplitude in defocusing media. In 1980 optical solitons were demonstrated experimentally in SMF by Mollenauer et al. [13].

The theory of optical solitons and their interactions was developed by Zakharov and Shabat in 1971 [14]. It was demonstrated that the nonlinear Schrödinger (NLS) equation, which describes plane self-focusing and one-dimensional self-modulation, is integrable by means of the Inverse Scattering Transform (IST) method (see also [15, 16]). An extensive family of exact solutions is represented by solitons, i.e. solitary wave packets that preserve their amplitude and velocity in an interaction, whereas their phase undergoes a discontinuity. The important thing is that the integrability of the NLS equation guarantees the stability of soliton propagation and, at the same time, indicates that any pulse of arbitrary shape launched with a proper amount of power evolves itself to a soliton (or solitons) during propagation whenever the nonlinearity is maintained large enough. The flexibility of solitons is an important property not only from a mathematical but also from a technical point of view.

An ideal optical soliton can propagate without distortion over long distances. Real optical lines, however, are not conservative and fibre loss eventually destroys the soliton. To retain the superbly consistent nature of the soliton, therefore, it is important to compensate for the loss. Progress on EDFAs and a new soliton transmission scheme which assumes the utilization of lumped amplifiers periodically installed in-line has enabled the development of a simple and promising soliton transmission system [17]-[19]. Indeed, Hasegawa and Kodama [17] showed that such "conventional" soliton lines inherit the basic features of conservative lines. Let us recall the main features of conventional soliton fibre communication systems without (or with a weak) dispersion management. The important feature of such systems is that the amplifier spacing is considerably shorter than the characteristic dispersion and nonlinear lengths, and therefore, both the dispersion and the nonlinearity can be treated as perturbations on the scale of one amplification period. To leading order, only the fibre loss and the periodic amplification are significant factors affecting the pulse evolution between two consecutive amplifiers. These factors cause the power oscillations, while the form of the pulse remains approximately unchanged. On larger scales nonlinearity and dispersion come into play and the pulse propagation in such systems is described by the path-averaged (guiding-center) soliton theory [17] (see also [18]). The average dynamics of the optical signal in this case is given to leading order by the integrable

[14] NLS equation. This makes it possible to use well-developed perturbation techniques (see e.g. [20]-[27]) to describe effects of numerous practical perturbations on the soliton propagation. Here we generally refer to the soliton solution of the NLS equation as the "conventional" soliton, wheter it is the solution of the unperturbed equation or the averaged equation.

However, conventional soliton-based communications face some technical difficulties unique to solitons. One of the most serious issues is the Gordon-Haus effect [28], i.e. a timing jitter which originates from random fluctuation of the carrier frequency of solitons caused by the nonlinear interaction with the ASE noise. The Gordon-Haus effect crucially limits the available capacity and transmission distance in soliton-based systems. Nonlinear interaction between two neighboring solitons in a single channel also degrades the performance since two solitons, when they are in-phase, attract with each other during propagation, resulting in their complete overlap at some distance [29]. To avoid the attraction, the interval between solitons should be set at least five times as large as the pulse width of the soliton. Moreover, in WDM transmissions, solitons in different channels could induce their timing jitter. As a consequence of the integrability of the NLS equation, solitons interact elastically and their amplitudes and velocities remain the same as those prior to the collision. A collision, however, can introduce nonlinear interactions between the wavelength channels through XPM and FWM. These effects affect soliton transmission in a manner slightly different from the case of the linear systems [30, 31]. XPM and FWM bring about central frequency shift [30] and the side band generation [31] respectively, during the collision process. The dispersion in conventional WDM soliton systems should not be too small so that different wavelengths travel at different speed and walk through other channels each other quickly, reducing the effects of XPM and FWM.

To overcome the limitations of the conventional soliton transmission, much effort has been placed on the development of "soliton control" techniques. Optical solitons, in fact, can be effectively stabilized by means of a periodical deployment of control elements, and this principle clearly divides the soliton dynamics from the other transmission formats [32]. Indeed, the combination of dissipative elements with nonlinear propagation leads to the presence of stable attractors that may enable for error-free long-haul connections. The stabilization of superposed perturbations to the soliton streams is usually explained as an all-optical regeneration of signals; from a practical viewpoint solitons that undergo pulse-to-pulse interactions and collisions may be reshaped and resynchronized, thus preserving the binary encoded information. Mathematically, the effect of control elements can be considered as a formation of autosolitons, i.e. solitary waves with parameters determined by the system parameters.

The simplest control method is to combine a bandpass filter with an amplifier [33]. Filters with narrow bandwidth inserted periodically are able to stabilize the amplitude and frequency of a soliton. This takes advantage of a unique property of solitons that their amplitude is always proportional to the inverse of their pulse width. Excessive amplification, for instance, leads to the narrowing of the width according to this property, thus the spectrum broadens. This broadened spectrum then goes through the bandpass filter where the spectral components outside the bandwidth are eliminated. The excess amplitude therefore can be diminished. In this principle, guiding filters give feedback against the variation of soliton amplitude and frequency. Linear waves such as ASE noise, on the other hand, are diffused in time domain by the filters, making it possible for only solitons to be selectively controlled in principle. The guiding filter, however,

requires excess gain in EDFA, which is necessary to compensate for the loss of soliton energy by the filtering action. The excess gain in turn amplifies linear waves within the filter bandwidth every time the pulse goes through a filter. This leads to significant growth of the noise and may even destroy the soliton [34]. To avoid the instability, several methods have been studied, such as sliding frequency filters [35] and synchronous amplitude and phase modulation [36, 37], which attempt to separate noise from solitons. In the sliding filtering approach, the center of the filter passband is successively displaced along the fibre, thereby giving more effective separation between the signal and noise than fixed filtering. The synchronous modulation method places phase and/or ampiltude modulators within the transmission path, driven synchronously with the bit-rate. These schemes have demonstrated successful soliton transmission over long distances, far beyond the limitation imposed by the instability. However, the sliding frequency filters, which require precise control of the central frequency at every stage, are troublesome in a practical application. The synchronous modulation is not compatible with WDM transmission, since the pulses in different channels propagating with different speeds have to be retimed separately, which requires demultiplexing and multiplexing of all the channels every time they go through modulators. Amplifiers having a nonlinear gain, or gain and saturable absorption in combination have also been suggested to reduce the problem of dispersive wave introduced by the use of filters [38, 34]. The key property of the nonlinearity in gain is to give an effective gain to the soliton and a suppression (or relatively small gain) to the noise.

Through a number of attempts to overcome the limitations of soliton-based systems, a significant breakthrough has finally come about: the discovery of dispersion-managed (DM) solitons. Though dispersion management was applied originally in the linear transmission systems, it has been discovered recently that this technique is also a very promising way to increase the transmission capacity of soliton-based communication lines. In [39] it has been numerically showed that solitons can propagate with reasonable power in SMF with large GVD by periodic dispersion compensation with DCFs at every amplifier and reducing the average dispersion. This was the first formulation in the literature of the idea of DM soliton transmission, even though a clear theoretical and practical description of this regime was not presented until fews years later. In [40]-[42] the DM pulse has been identified as a new information carrier – a stable periodic breather with features very different from those of the conventional soliton. Large variations of the dispersion (strong dispersion management) modify the soliton propagation fundamentally, inducing breathing-like oscillations of the pulse width during the amplification period and creating a nontrivial distribution of the phase in time (pulse chirp). This dynamics differs substantially from the guiding-center soliton propagation and that of the fundamental soliton of the NLS equation. Nevertheless, numerical simulations and experiments have demonstrated that it is possible to observe extremely stable propagation of a breathing soliton in fibre links with strong dispersion management. A classical means of categorising DM soliton propagation in a DM system is the map strength parameter S, defined as [40, 43]

$$S = \sum_i \frac{|\beta_2^{(i)} - \langle\beta_2\rangle| L_i}{\tau_{\mathrm{FWHM}}^2}, \tag{1.1}$$

where the sum extends to the fibre segments building up the dispersion map, $\beta_2^{(i)}$ and L_i are the GVD coefficients and lengths of the fibre sections, $\langle\beta_2\rangle$ is the average dispersion, and τ_{FWHM} is the minimum full-width at half-maximum (FWHM) pulse width. The values $S > 4$ and $S \ll 1$

refer to the strong and weak dispersion management, respectively. It has been observed [44] that stable pulses exist for $0 < S < 10$. There are two characteristic scales in the dynamics of a DM pulse: the fast dynamics corresponds to rapid oscillations of the pulse width, phase, and power due to periodic variations of the dispersion and periodic amplification; and the slow evolution is determined by the combined effects of nonlinearity and residual dispersion. The slow dynamics of the DM soliton then can be described by the propagation equation averaged over the fast oscillations [42]. The derivation of the path-averaged equation is outlined in Chapter 2. The use of a stable steady-state solution of the path-averaged equation as an information carrier provides stable data transmission along the fibre line.

An important feature of the DM soliton is that its energy is enhanced [40, 45, 46] in comparison with the soliton of the NLS equation of the same width and corresponding to the same path-averaged dispersion. The mechanism behind the increased energy requirement to form a stable pulse can be understood from the pulse evolution over one compensation period. Owing to the cycle of dispersive broadening and compression, the peak power of the pulse is generally lower than the initial launch power. Therefore the rate of SPM is reduced compared to the equivalent uniform fibre, and so higher launch power (and hence higher pulse energy) is needed for the nonlinearity to balance the path-averaged dispersion. The energy enhancement leads to an increase of the SNR [40] with a substantial improvement of system's performance. The chirp is a new and extremely interesting feature of the DM soliton – recall that the conventional soliton is unchirped. The soliton chirp leads to rapid rotation of the relative phase shift between neighboring solitons resulting into the suppression of interaction. An important consequence of the chirp of the DM soliton is that an input signal launched into the transmission line should be either chirped [47] or launched at some specific points of the dispersion map (for the case of a transform-limited input pulse) [43, 48]. Another surprising feature of the DM soliton is that it can propagate stably along a transmission line with zero or even normal average dispersion [49], in contrast to the fundamental soliton that propagates stably only in the anomalous dispersion region. Indeed, it has been found in [49] that DM solitons in zero or normal average dispersion exist for S larger than a critical value of 3.9. The possibility to transmit DM solitons at very low average dispersion allows a reduction of the Gordon-Haus timing jitter [50, 51]. Recall that the energy of the fundamental soliton is proportional to the fibre dispersion. Therefore, to keep the SNR large enough one must not operate too close to the zero-dispersion point. On the other hand, the timing jitter deriving from the Gordon-Haus effect is proportional to the fibre dispersion and it is preferable to transmit the soliton at wavelengths close to the zero-dispersion point. Thus it would be desirable to produce a finite-energy soliton pulse in the region of low fibre dispersion. Dispersion management allows for a low path-averaged dispersion, but a high local dispersion, thereby suppressing the Gordon-Haus jitter and the FWM effect [52] simultaneously. This technique is also found to be effective for reducing the intra-channel interactions between neighboring pulses [53] and the collision-induced timing jitter in a WDM system [54, 55]. The main features of the DM soliton which have been revealed by numerical simulations and experiments can be summarized as follows.

– The pulse width and chirp experience large oscillations during the compensation period leading to "breathing-like" soliton dynamics.

– The shape of the forming asymptotic pulse is not always hyperbolic secant as for the soliton

of the NLS equation, but varies with the increase of the strength of the map from a sech shape to a Gaussian shape and to a flatter waveform. The pulse shape varies along the compensation section from the monotonically decaying profile to a distribution with oscillatory tails.
– The time-bandwidth product varies with increase of the map strength from 0.32 corresponding to the sech-shaped soliton of the NLS equation to 0.44 corresponding to the Gaussian pulse and increases further with increase of the map strength.
– The energy of the stable breathing pulse is well above that of the soliton of the NLS equation with the same pulse width and of the corresponding average dispersion.
– The DM soliton can propagate stably at the zero path-averaged dispersion and even in the normal dispersion region.
– The central part of DM pulse is self-similar, but the far-field oscillating (and exponentially decaying) tails are not. There are some dips in the tails of the DM soliton at some specific points in the plane (z, t).

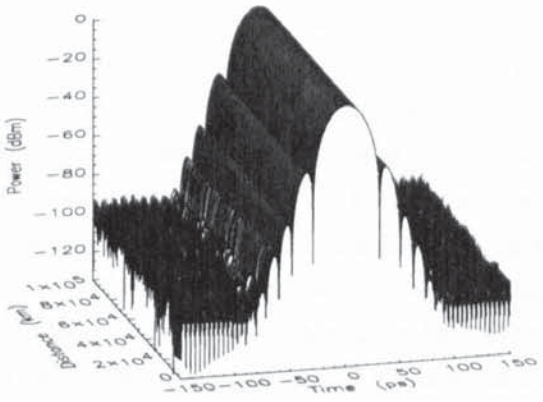

Figure 1.1: Stroboscopic evolution of DM soliton.

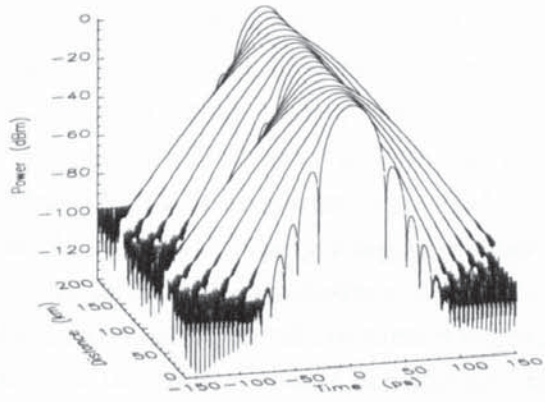

Figure 1.2: Evolution of DM soliton over one period of dispersion compensation cycle.

A typical example of DM soliton is shown in Fig. 1.1. Here we used a lossless two-step dispersion map, that comprises alternating 100 km fibre sections of $\beta_2^{(1)} = -5.1\,\mathrm{ps}^2\,\mathrm{km}^{-1}$ and $\beta_2^{(2)} = 4.9\,\mathrm{ps}^2\,\mathrm{km}^{-1}$. The map strength was $S \simeq 2.3$. The pulse is shown at the mid point of the anomalous section (on a logarithmic scale). Figure 1.2 shows the evolution during one period of the map. At the mid point of each section, the pulse has a curved (Gaussian) centre and linear (exponential) wings with dips. At these points, the pulse is totally unchirped and the pulse width is at its minimum. The dips are zeros, roughly periodic in t^2. At the boundary between sections, where the pulse is widest, it becomes more sech-like (exponential) and is strongly chirped. These observations are typical for strong and moderate dispersion maps.

Different theoretical approaches have been developed in the last fews years to describe the properties of the DM soliton, which include interesting numerical methods [40, 49, 53, 56], a variational approach [42], [57]-[62], a root-mean-square (RMS) momentum method [62, 63], multiscale analysis [64, 65], different averaging methods [46, 66], including averaging in the spectral domain [42, 57], Hamiltonian averaging [67], and an expansion of the DM soliton on the basis of the chirped Gauss-Hermite functions [66, 68]. In view of the important practical applications it is of interest to develop different alternative theoretical methods. Obviously, a

better understanding of the fundamental features of the information carriers in DM lines will lead to further progress in the improvement of the system's performance. An analytical description of path-averaged DM solitons in the regime of weak management is presented in Chapter 2.

Dispersion management is now regarded as a simple but powerful scheme to deal with nonlinear effects in both linear and nonlinear transmission systems. We emphasize again that linear systems take advantage of GVD to suppress nonlinear perturbations, whereas solitons positively exploit the SPM to cope with GVD. One of the advantages of DM solitons is that, in contrast to those linear systems employing post- or pre- transmission compensation of GVD, they are intrinsically a periodic system, giving more flexibility in constructing practical systems.

DM solitons share the fundamental and distinguishing property of the soliton format families of being capable to be effectively stabilized with properly designed elements of all-optical regeneration. The use of soliton control together with dispersion management can lead to significant improvement in the performance of soliton transmission systems. From the one hand, the DM soliton modulation format entails both a remarkable robustness to noise and dispersive perturbations and reduced transmission penalties in comparison with a purely linear RZ modulation format [69]. On the other hand, the periodic amplification, reshaping and retiming of the solitons may lead, in principle, to the asymptotic stabilization to a fixed value for the figure of merit of the transmission quality (e.g. the Q-factor) rather than a monotonic decay of the quality with distance as it occurs whenever regeneration is absent. Indeed, the action of control elements, such as for example guiding filters [70, 71] and synchronous modulators [72, 73], permits to counteract the timing jitter that is induced on the propagating pulse by pulse-to-pulse interactions and adjacent channel collisions in WDM transmissions. Additionally, a stabilization of soliton amplitude fluctuations is also achievable by the above control elements. It is important to point out the main difference between the control of DM solitons and that of NLS solitons. In conventional soliton systems, filters likely stabilize the pulse energy while modulators likely destabilize the pulse energy regardless of the location of filters or modulators. In DM systems, the periodic pulse dynamics with each dispersion map implies that the exact location of the above control elements in the map plays a key role. Lumped filters can cause instability of the pulse energy while modulators can stabilize the pulse energy regarding the insertion location [75, 72]. Therefore it is important to consider the proper insertion location of filters and modulators in the dispersion map in order to stabilize the pulse energy [74].

If modulators and filters are rather well-established devices in transmission systems using both conventional and DM solitons, other more efficient schemes require a methodological approach still under development. This is the case of optical regeneration based on SPM and filtering [76], where the efficiency of filtering is increased including a nonlinear spectral broadening of pulses, or optical control performed by nonlinear optical loop mirrors (NOLMs). Chapter 3 is devoted to the study of autosoliton transmission in DM systems with periodical in-line deployment of NOLMs as all-optical regenerators of signals. NOLMs are all-optical devices that exploit the Kerr effect to switch the parameters of optical pulses [77, 78]. Their basic principles and properties are described somewhere in Chapter 3. Here it is worth to point out that, thanks to their high nonlinear properties, in-line NOLMs can be employed as effective saturable absorbers [79]. Indeed, low-power background waves are discriminated against, while higher power pulses switch the NOLM into transmittance. Moreover, owing to its switching characteristic,

the NOLM can provide for stabilization of the pulse amplitude. Previous studies [79]-[82] have addressed the use of NOLMs to reshape and stabilize pulses in conventional soliton transmission systems. The use of dispersion management in conjunction with in-line NOLMs can be a powerful technique to achieve stable soliton propagation at high bit-rates and to enhance quality of the transmission, as it exploits a combination of the effects of dispersion management and the loop mirror intensity filtering action that allows for partial regeneration of pulse amplitude and shape, through suppression of noise accumulation and distortion. However, as NOLMs are insensitive to clock synchronism, they cannot ensure pulse retiming, thus the ensured optical regeneration may result in a less efficiency with respect to clock-sensitive elements such as modulators. Nevertheless, timing problems can be partially solved in many practical situations, because the saturable absorption action of NOLMs allows narrow bandwidth filters to be used without encountering pulse instability [83], which helps to suppress the timing jitter and reduces the effect of pulse-to-pulse interactions.

The deployment of in-line NOLMs in high-speed, strongly DM systems, such those that are used to upgrade the existing terrestrial links based on SMF, can be regarded as a different way of making positive use of the fibre nonlinearity. Indeed, the high values of local dispersion of SMF, together with the short pulse widths required to operate at high bit-rates, make the dispersion length in the fibre much shorter than the nonlinear length, implying a quasi-linear mode of propagation. In such a regime the intensity pattern changes rapidly along the fibre, and the effect of fibre nonlinearity tends to be averaged out. This scheme is, in some sense, opposite to soliton or DM soliton transmission, where pulses are characterised by a balance between nonlinearity and dispersion. As a consequence, pulses propagating in the quasi-linear regime are not stable in a mathematical sense; even though they can still be used in practical systems. When periodical in-line control by NOLMs is used, the effect of fibre nonlinearity is exploited in the regenerators rather than during propagation. It will be shown in Chapter 3 that, as a result, the quasi-linear propagation regime is changed into a stable, autosoliton propagation regime, which is strictly nonlinear.

Besides the well-known optical solitons, another example of nonlinear, self-similar pulse propagation in optical fibres is the propagation of high-intensity pulses with a parabolic intensity profile in fibres with normal dispersion [2]. It is worth to recall here that the establishment of self-similarity is a key element in the understanding of many widely differing nonlinear phenomena [84]. In particular, the presence of self-similarity can be exploited to obtain asymptotic solutions to partial differential equations describing a physical system by using the mathematical technique of symmetry reduction to reduce the number of degrees of freedom (see e.g. [85]). Although the powerful mathematical techniques associated with the analysis of self-similar phenomena have been extensively applied in certain areas of physics such as hydrodynamics, their application in optics has not been widespread. However, some important results have been obtained, with theoretical studies considering asymptotic self-similar behaviour in radial pattern formation [86], stimulated Raman scattering [87], the evolution of self-written waveguides in photosensitive materials [88], and the formation of Cantor set fractals in soliton systems [89]. In addition, self-similarity techniques have recently been applied to study ultrashort pulse propagation in high-gain optical fibre amplifiers with normal dispersion [90]. It has been shown that linearly chirped pulses having a parabolic intensity profile are approximate solutions of the NLS equation

with gain in the high-intensity limit. These results have been confirmed experimentally [91] and have extended previous theoretical and numerical studies of parabolic pulse propagation in optical fibres [2, 92]. A detailed analysis of the solutions of the NLS equation with gain and normal dispersion is the subject of Chapter 4. We note here that the self-similar parabolic solutions found in [90] should be contrasted with the well-known positive dispersion amplifier solitons whose amplitude and width are stabilized by the loss introduced from gain dispersion [93]. The self-similar parabolic pulses considered here are observed only when gain dispersion is negligible, and this is the case for many experimental situations in which high-gain broadband rare-earth fibre amplifiers are used [91, 94]. On the other hand, larger values of gain or narrower amplifier bandwidths require the analysis of the Ginzburg-Landau equation for examining the intermediate region between self-similar propagation and amplifier soliton formation [95]. We note also that the NLS equation with gain and anomalous dispersion has been analysed in [96]. It has been shown from numerical results and an equation-of-motion analysis that for such an equation solitons are the stable solutions. The physical mechanism behind the transition in the evolution from an initial binding of further solitons containing a large fraction of the total energy to propagation with a few stable solitons can be explained as follows [96]. Initially, if the gain length is sufficiently short compared with the soliton period, the pulse is amplified and this amplification leads to the binding of extra solitons. With the increased amplitude the nonlinear dynamical length scale is shorter than the gain length. The pulse can now compress sufficiently quickly to accomodate the gain, thus maintaining the new number of solitons.

The generation of high-power self-similar parabolic pulses from fibre amplifiers, aside from its being a further example of self-similar phenomenon in optics, is of fundamental practical interest. In particular, the linear chirp of pulses leads to highly efficient pulse compression to the sub-100 fs domain [94]. In addition, the initial pulse shape determines only the map towards the parabolic pulse that forms in the amplifier after some initial transient stage, while the asymptotic pulse characteristics are determined only by the initial pulse energy and the amplifier parameters. Moreover, all the incident pulse energy contributes to the output pulse. This is in contrast to the better known soliton solutions of the NLS equation in the absence of gain, which require accurate control of the input pulse energy and where a given input pulse develops into a soliton of fixed amplitude shedding the remaining energy into a continuum. "Parabolic fibre amplifiers" therefore have potential wide-ranging applications in many areas of current optical technology, allowing the generation of well-defined linearly chirped output pulses from an optical amplifier, even in the presence of input pulse distortions. We point out here that high-power parabolic pulses can be easily generated and measured experimentally thanks to the current availability of high-gain optical fibre amplifiers and to recent developments in methods of ultrashort pulse characterization [97]. Moreover, as predicted in [2] and experimentally demonstrated in [91], an attractive feature of high-power parabolic pulses is that they propagate self-similarly in normally dispersive fibre, allowing for highly nonlinear propagation over substantial fibre lengths without optical wave-breaking. Parabolic amplifiers thus allow access to a convenient fibre-based method of generating and transmitting high-power optical pulses, rivaling soliton propagation, stretched-pulse Gaussian pulse propagation [98], as well as existing chirped pulse amplification systems.

In view of their self-similar propagation and the ease with which they can be compressed, we expect that parabolic pulses will find wide application. Indeed, we anticipate that parabolic

pulse propagation in optical fibres may well become as important and as widely studied as the propagation of optical solitons.

The discussions in this section so far have focused on how nonlinear effects in optical fibres affect and why they play an important role in the generation and propagation of different kinds of stable (or quasi-stable) pulses that can be used in optical communication systems. The thesis will present theoretical studies on some of the issues addressed in this section. Theoretical models can provide guidance to and substantially accelerate experimental developments.

1.2 Overview

In Chapter 2, a perturbation theory of DM solitons for small dispersion map strengths is presented. In the case of a weak dispersion map, the path-average DM pulse dynamics can be described by a perturbed form of the NLS equation where the perturbation represents the small effects of the dispersion management. Using a perturbation theory scheme based upon the IST method, an analytical description of the evolution of the path-averaged soliton in the presence of such a perturbation is given. The derived analytic expression for the envelope of the DM soliton is shown to correctly predict the energy enhancement arising from the dispersion management. The theoretical results are verified by direct numerical simulations.

Chapter 3 is devoted to the study of autosoliton transmission in DM fibre systems with periodical in-line deployment of NOLMs as all-optical regenerators of signals. First, the compatibility of NOLMs with dispersion management for achievement of pulse stabilization and long-distance pulse transmission is demonstrated. Then, the use of in-line NOLMs is addressed as a general technique for all-optical passive 2R regeneration (i.e. without clock recovery) of RZ data in high bit-rate transmission systems with strong dispersion management. In particular, a feasibility of $40\,\mathrm{Gbit\,s^{-1}}$ single-channel stable soliton transmission over unlimited distances in standard fibre is numerically demonstrated. The tolerance of this result is investigated and the proposed method is extended to $80\,\mathrm{Gbit\,s^{-1}}$ data transmission. It is also demonstrated that the application of the proposed technique to systems where both amplitude noise and timing jitter are important limiting factors can dramatically improve the system's performance, allowing for transoceanic transmission distances. Finally, the application of $40\,\mathrm{Gbit\,s^{-1}}$ DM transmission guided by NOLMs to a WDM scheme is investigated. The use of specially designed WDM guiding filters coupled with NOLMs is proposed as a regeneration technique to enhance the transmission performance of WDM ($40\,\mathrm{Gbit\,s^{-1}} \times$ N channel) systems. By optimisation of the system, the feasibility of 150 GHz-spaced$\times$16 channel transmission over 25000 km of SMF is demonstrated.

In Chapter 4, a detailed mathematical analysis of the solutions of the NLS equation with gain and normal dispersion, that describes optical pulse propagation in an amplifying medium, is presented. A quasi-classical self-similar solution with parabolic temporal variation, that corresponds to the energy-containing core of the asymptotically propagating pulse in the amplifying medium, is constructed. The self-similar core is matched through Painlevé functions to the solution of the linearized equation, that corresponds to the low-amplitude tails of the pulse. The analytical solution proves to reproduce accurately the numerically calculated solution of the NLS equation.

Chapter 5 draws the conclusions of the thesis by summarizing the overall results and envisaging possible future developments.

Chapter 2

A perturbative analyisis of dispersion-managed solitons

2.1 Introduction

An essential step in the development of a theory of the DM solitons was done by Gabitov and Turitsyn in 1996 [42]. In the assumption of smallness of the local nonlinearity with respect to the local (not average) dispersion, they derived an equation describing the average dynamics of the optical pulse envelopes in fibre links with periodical pulse amplification and dispersion compensation. Although it is an Hamiltonian system, the Gabitov-Turitsyn (GT) equation is not integrable in a general case. Recently Zakharov discussed the limit of strong dispersion management and demonstrated that the system is integrable in this limit [99] (see also [100]). In the opposite limiting case of weak dispersion management the system is close to the NLS equation, which is known to be integrable by the IST method [14]-[16].

In this chapter we study the weak dispersion management case. The regime of weak management may be considered to not be of much interest because it loses the well-known advantages offered by strong dispersion management. Indeed, it is characterised by negligible pulse breathing, small pulse chirp, and low power enhancement. However, the weak regime still covers many practical situations. Moreover, analytical methods developed for weak management are formally valid for map strengths $S \ll 1$, and therefore their predictions may become less accurate for stronger dispersion maps (such as when the average dispersion becomes very small or even zero). Nevertheless, these predictions often can work well even when the strength of the map is of the order of one; this includes the practically important case when the variations of the local dispersion are much larger than the average (residual) dispersion. The analytical method presented here proves to be valid for map strengths up to 0.7[101].

DM solitons in systems with weak dispersion maps have been considered already in [46, 64]. In [46] a Lie transform technique has been used to describe the features of the carrier pulse ("dressed" soliton). In the limit where the amplifier spacing (or the periodic distance) is shorter than the path-averaged dispersion and nonlinear lengths, pulse propagation in a fibre with periodic variation of dispersion and nonlinearity can be theoretically analysed using the guiding-center theory [17]. The basic idea is to transform the perturbed system into an averaged equation by using the Lie transformation. The averaged equation to leading order is a NLS equation with

renormalization coefficient before the nonlinear term, whose soliton solutions are the so-called guiding-center solitons. The real waveform is obtained by inverting the Lie transformation of the guiding-center soliton solution [46]. This inversion adds dressing to the guiding-center soliton; thus such a pulse is called (a guiding-center) dressed soliton. In [64] a multiple-scale averaging technique has been employed to analyse the dynamics of DM solitons. Considering the asymptotic limit where the dispersion map period is shorter than the scales corresponding to the path-averaged dispersion and nonlinearity, second-order averaging and a near-identity transformation have been used to derive an evolution equation valid for general dispersion maps and applicable to both RZ and NRZ pulses. Applying the equation to the case of solitons, an analytic expression for the power enhancement arising from the dispersion management [40] has been obtained. Because of the practical importance of the problem, it is of evident interest to develop different analytical methods to describe the properties of the DM solitons. A variety of complementary mathematical methods can be advantageously used to find an optimal and economical description of any specific practical application.

In this chapter we present a perturbation theory of DM solitons for small dispersion map strengths [101]. In the case of a weak dispersion map, the average DM pulse dynamics can be described by a perturbed form of the NLS equation where the perturbation represents the small effects of the dispersion management. Using a perturbation theory scheme based upon the IST method [25], we give an analytical description of the evolution of the path-averaged soliton in the presence of such a perturbation. Numerical [40] and analytical [102] works have previously shown that the shape of the DM soliton is mainly determined by the strength of the dispersion map (cf. Eq. (1.1)): the DM soliton shape is close to hyperbolic secant for weak dispersion maps and it changes to a Gaussian shape and to even flatter waveform as the map strength is increased. Then, in the case of the weak map strengths, the stable asymptotic pulse can be presented as the sech-shaped soliton of uniform fibres with small deviations that account for the dispersion management effects. The perturbation method presented here allows us to calculate such deviations from the sech-shaped soliton. The derived analytic expression for the envelope of the DM soliton is shown to correctly predict the power enhancement arising from the dispersion management [40]. The theoretical results are verified by direct numerical simulations.

The chapter is organized as follows. In Section 2.2, we introduce the basic model governing optical pulse propagation in a cascaded transmission system with varying dispersion and we outline the derivation of the GT equation. We also present the result in [99] for the integrability of the averaged model in a strong dispersion management limit. Section 2.3 is devoted to the development of the perturbation theory in the case of a weak dispersion management. As result of this approach, analytic expressions for the DM soliton envelope and the power enhancement are derived. In Section 2.4 we compare the theoretical predictions with the results of numerical simulations. A summary of the results is presented in the concluding section.

2.2 Basic equations

The evolution of optical pulses in a fibre link with periodical pulse amplification and dispersion compensation is described by the modified NLS equation (see e.g. [102])

$$iA_z + d(z)A_{tt} + c(z)|A|^2A = 0. \tag{2.1}$$

Here z is the propagation distance, normalized to the dispersion compensation length L (in [km]); t is the retarded time, measured in units of the parameter t_0 (in [ps]); $A(z,t)$ is an envelope of electric field, normalized to the parameter $\sqrt{P_0}$ (in [$W^{1/2}$]). Periodic functions $d(z) = -\beta_2(z)L/(2t_0^2)$ and $c(z) = c_0(z)\exp[2\int_0^z dz'\, G(z')]$, $c_0(z) = \sigma(z)P_0L$, $G(z) = L(-\gamma(z) + \sum_{k=1}^{N} r_k\delta(z-z_k))$, describe, respectively, the varying dispersion and the signal power oscillations due to loss and amplification. Parameter β_2 is the first order group-velocity dispersion measured in [ps^2km^{-1}]. It is customary to express β_2 in terms of the associated dispersion coefficient D by $\beta_2 = -\lambda_0^2 D/(2\pi c_l)$, where λ_0 is the carrier wavelength, c_l is the speed of light, and D is measured in [ps (nm km)$^{-1}$]. The nonlinear coefficient is given by $\sigma = 2\pi n_2/(\lambda_0 A_{\text{eff}})$, where n_2 is the nonlinear refractive index, and A_{eff} is the effective fibre area. The loss coefficient $\gamma = 0.05\ln(10)\alpha$ ([km^{-1}]) accounts for the fibre attenuation along an amplifier span, where α is given in [dB km^{-1}]. We write β_2, σ, and γ as functions of z to account for the change of these parameters from fibre to fibre. We assume periodic amplification with the period Z_a; $z_k = kZ_a/L$ ($k = 1,\ldots,N$) are the amplifier locations; and r_k is the amplification coefficient that compensates the fibre losses over the distance Z_a. We assume that the dispersion is compensated periodically with a period L, though possibly with some uncompensated average dispersion $\langle\beta_2\rangle$. Thus, the normalized chromatic dispersion presents a sum of a rapidly (over one compensating period) varying local dispersion and a constant residual dispersion, $d(z) = \tilde{d}(z) + \langle d\rangle$, where $\langle\tilde{d}\rangle = 0$. Here and throughout this work, $\langle\cdot\rangle$ represents the path-average over the period L.

We study here the propagation regime where the compensation length L and the local dispersion length $Z_{\text{dis}} \sim t_0^2/|\beta_2|$ are much smaller than the nonlinear length $Z_{\text{NL}} = 1/(\sigma P_0)$ and the scale corresponding to the residual (path-averaged) dispersion $Z_{\text{RD}} \sim t_0^2/|\langle\beta_2\rangle|$. Such a condition is usually satisfied in real transmission lines. In this limit the main factors that affect the pulse evolution during one compensation period are local dispersion, loss, and amplification, and one may treat the nonlinearity and the residual dispersion as perturbations. The DM pulse dynamics then can be considered on fast and slow scales. The fast dynamics corresponds to the oscillations of the pulse phase, width, and peak power over one period due to the dispersion compensation and periodic amplification, while the slow evolution corresponds to an accumulation of small deviations from the periodic oscillations over many periods due to nonlinear effects and residual dispersion. The slow dynamics of the DM soliton then can be described by the propagation equation (2.1) averaged over the fast oscillations.

The path-averaged equation in the spectral domain has been derived in [42, 57]. The basic idea of this approach is rather simple. In the linear propagation regime a pulse bandwidth (spectral width) is constant and does not vary with propagation. In the spectral domain only the pulse phase experiences fast oscillations during a compensation period due to rapidly varying local dispersion. Therefore, to leading order, effects of nonlinearity and the small residual dispersion can be accounted for as a slow evolution of the envelope of the quasi-linear solution. This decomposition of DM pulse dynamics in rapid oscillations of the phase and slow evolution

of the amplitude can be effectively realized in the spectral domain by applying the following Fourier-like transform [42, 57]

$$A(z,t) = \int_{-\infty}^{+\infty} \mathrm{d}\omega\, \hat{u}(z,\omega) \exp\left[-i\omega t - i\omega^2 R_0(z)\right]. \tag{2.2}$$

Here $\mathrm{d}R_0(z)/\mathrm{d}z = \tilde{d}(z)$, $\langle R_0 \rangle = 0$; and $\hat{u}(z,\omega)$ is assumed to be a slowly varying function of z.

The resulting equation with $\hat{u}$ can now be averaged directly. Since $\hat{u}$ varies slowly, in the first approximation it can be taken outside of the averaging integral. The result is an integro-differential equation in the spectral domain describing the slow evolution of $\hat{u}(z,\omega)$

$$\begin{aligned} & i\frac{\partial \hat{u}(z,\omega)}{\partial z} - \omega^2 \langle d \rangle \hat{u}(z,\omega) \\ & + \int_{-\infty}^{+\infty} \mathrm{d}\omega_1 \mathrm{d}\omega_2 \mathrm{d}\omega_3\, \delta(\omega_1 + \omega_2 - \omega_3 - \omega) \langle K(\omega_1^2 + \omega_2^2 - \omega_3^2 - \omega^2) \rangle \hat{u}_{\omega_1} \hat{u}_{\omega_2} \hat{u}^*_{\omega_3} = 0, \end{aligned} \tag{2.3}$$

where

$$\langle K(\Delta\Omega) \rangle = \langle c(z) \exp[-i\Delta\Omega R_0(z)] \rangle. \tag{2.4}$$

This is the GT equation [42] (see also [57, 65]).

Without loss of generality, throughout the chapter we focus on a lossless model, $c(z) = c_0 = const$. When the compensation period is much larger than the amplification distance, $L \gg Z_a$, the inclusion of periodic amplification and dispersion compensation can be handled, in fact, as separate problems [43]. We consider in this model a two-step dispersion map, whose $\tilde{d}(z)$ is given by

$$\tilde{d}(z) = \begin{cases} \tilde{d}_1, & \text{for } 0 < z < l_1 \\ \tilde{d}_2, & \text{for } l_1 < z < 1 \end{cases} \tag{2.5}$$

where $l_1 + l_2 = 1$ and $\tilde{d}_1 l_1 + \tilde{d}_2 l_2 = 0$. In such a case the kernel $\langle K \rangle$ can be written as

$$\langle K(\Delta\Omega) \rangle = c_0 \frac{\sin(\mu\Delta\Omega/2)}{\mu\Delta\Omega/2}, \quad \text{with } \mu = \tilde{d}_1 l_1, \tag{2.6}$$

where parameter μ is a characteristic of the strength of the map.

2.2.1 Strong dispersion management limit

Here we briefly summarize the result of Zakharov in [99]. The key idea of taking a strong management limit is to find an approximate function for the kernel $\langle K \rangle$. First we note for large μ

$$\begin{aligned} \delta(\Delta\Omega) &= \frac{1}{2\pi} \lim_{\mu\to\infty} \int_{-\mu/2}^{\mu/2} \mathrm{d}x\, e^{i\Delta\Omega x} = \frac{1}{\pi} \lim_{\mu\to\infty} \left(\frac{\mu}{2} \frac{\sin(\mu\Delta\Omega/2)}{\mu\Delta\Omega/2} \right) \\ &\simeq \frac{\mu}{2\pi c_0} \langle K(\Delta\Omega) \rangle, \end{aligned} \tag{2.7}$$

from which we have

$$\langle K(\Delta\Omega) \rangle \simeq \frac{2\pi c_0}{\mu} \delta(\Delta\Omega) = \pi c_0 \delta(\mu\Delta\Omega/2). \tag{2.8}$$

Notice that the kernel becomes so small for strong management, implying that the equation becomes almost linear. Then Eq. (2.3) may be written in the form

$$i\frac{\partial\hat{u}(z,\omega)}{\partial z} - \omega^2\langle d\rangle\hat{u}(z,\omega) + \frac{\pi c_0}{\mu}\hat{u}(z,\omega)\int_{-\infty}^{+\infty} d\omega_1 \frac{|\hat{u}_{\omega_1}|^2}{|\omega-\omega_1|} = 0. \tag{2.9}$$

Here the integral may be taken as a principal sense, in other words, this equation is valid up to logarithmic accuracy. One of the main features of this equation is that the amplitudes of the Fourier harmonics are constants of motion (which implies that the spectral power $|\hat{u}(z,\omega)|^2$ is preserved during propagation). In this sense, the GT equation is integrable in the strong limit.

2.3 Perturbation theory for weak dispersion management

In the limit $\mu = 0$, $\langle K(\Delta\Omega)\rangle = c_0$ and Eq. (2.3) reduces to the Fourier transform of the NLS equation, with dispersion $\langle d\rangle$ and nonlinear coefficient c_0. Here we study the case $\mu \ll 1$ [101]. In this limit we can add to the NLS equation a perturbation term represented in the spectral domain by an integral with a kernel of $c_0 - \langle K(\Delta\Omega)\rangle$. The perturbed NLS equation in the spectral domain may then be written in the form

$$\begin{aligned} &i\frac{\partial\hat{q}(z',\omega)}{\partial z'} - \frac{1}{2}\omega^2\hat{q}(z',\omega) + \int_{-\infty}^{+\infty} d\omega_1 d\omega_2\, \hat{q}_{\omega_1}\hat{q}_{\omega_2}\hat{q}^*_{\omega_1+\omega_2-\omega} \\ &= \int_{-\infty}^{+\infty} d\omega_1 d\omega_2 \left\{1 - \frac{\sin[\mu(\omega-\omega_1)(\omega-\omega_2)]}{\mu(\omega-\omega_1)(\omega-\omega_2)}\right\}\hat{q}_{\omega_1}\hat{q}_{\omega_2}\hat{q}^*_{\omega_1+\omega_2-\omega} \equiv i\hat{F}(z',\omega). \end{aligned} \tag{2.10}$$

Here we have normalized the space coordinate and the field amplitude by: $z' = 2|\langle d\rangle|z$, $\hat{q} = [c_0/(2|\langle d\rangle|)]^{1/2}\hat{u}$. Finally, an inverse Fourier transform leads to

$$i\frac{\partial q}{\partial z'} + \frac{1}{2}\frac{\partial^2 q}{\partial t^2} + |q|^2 q = iF. \tag{2.11}$$

The Fourier operator $\mathcal{F}$ and its inverse are defined here by $\hat{f} \equiv \mathcal{F}(f) = (1/2\pi)\int_{-\infty}^{+\infty} dt\, f(t)\exp(i\omega t)$, $f \equiv \mathcal{F}^{-1}(\hat{f}) = \int_{-\infty}^{+\infty} d\omega\, \hat{f}(\omega)\exp(-i\omega t)$, for any function f. Note that here we restrict ourselves to the case of anomalous average dispersion ($\langle d\rangle > 0$) and "bright" solitons. Eq. (2.11) describes the propagation of optical pulses in a nonideal dispersive single-mode optical fibre, with perturbing influences represented by the complex term iF.

A perturbation theory formulated within the "natural" framework of inverse scattering theory has been developed in [25] to investigate the effects of various perturbations on soliton propagation down an optical fibre. First, we briefly recall the main results of this theory and then we apply these results to the particular form for F considered here.

With F set to zero, Eq. (2.11) is integrable using the IST method [14]-[16]. In particular, it has the exact single-soliton solution

$$q(z',t) \equiv q_s = 2\eta_1 e^{-2i\xi_1 t + 2i(\eta_1^2-\xi_1^2)z'}\,\mathrm{sech}[2\eta_1(t+2\xi_1 z')]. \tag{2.12}$$

The parameters η_1 and ξ_1 characterize the soliton; $2\eta_1$ is its height and inverse width, $2\xi_1$ is its velocity. The action of the perturbation iF on the soliton q_s modifies this in two distinct ways. The soliton parameters, which were constant of the motion in the unperturbed case, now vary with distance down the fibre; if the perturbation is small, this change is adiabatic [20].

The perturbation is also responsible for the generation of a background radiation field $\delta q(z',t)$, which is superimposed on the soliton pulse so that, at any location z',

$$q(z',t) = q_s + \delta q(z',t). \tag{2.13}$$

We will be interested here in the case when $F \neq 0$, but still a small perturbing influence on the propagating soliton. In this limit, we will derive an analytic expression for the perturbing field. A knowledge of the basic techniques of IST theory is assumed, and is summarized in Appendix A. Full details can be found in [14]-[16], and [20]-[27].

Two main results were achieved in [25], which find useful application in our study on Eq. (2.11). The first result is exact and is true for any form of the perturbation F, which need not be small. It states that, under the action of the perturbation iF, the infinity of conserved quantities C_n, $n = 0, 1, 2, \ldots$, associated with the unperturbed equation [16], evolve according to

$$\frac{\mathrm{d}C_n}{\mathrm{d}z'} = \int_{-\infty}^{+\infty} \mathrm{d}t\, [F^*, F](2i\mathcal{L})^n \begin{bmatrix} q \\ q^* \end{bmatrix}. \tag{2.14}$$

$\mathcal{L}$ is the integro-differential operator associated with the squared eigenfunctions obtained from the linear eigenvalue problem connected with the unperturbed form of Eq. (2.11) [14]-[16], and is defined in Eq. (A.8). For the derivation of Eq. (2.14) the reader is referred to Appendix A.

The second result describes the generation of the radiation field. In the IST theory, scattering data are summarized by the coefficients a and b [15, 16] (see Appendix A). A generalized form for the evolution equation for the spectral parameter b has been derived in [23]; this reads

$$\frac{\partial b}{\partial z'} = 2i\zeta^2 b + \int_{-\infty}^{+\infty} \mathrm{d}t\, [F^*, F]\check{\Phi}. \tag{2.15}$$

The first term follows using standard manipulations for the unperturbed system; the bilinear spinor $\check{\Phi} = [\phi_1\bar{\psi}_1, \phi_2\bar{\psi}_2]^T$ arises in the squared eigenfunction problem associated with Eq. (2.11); $\phi = [\phi_1, \phi_2]^T$, $\bar{\phi}$, ψ, and $\bar{\psi}$ are two-component spinor Jost function solutions of the linear eigenvalue problem, and $\zeta = \xi + i\eta$ is a complex eigenvalue [14]-[16]. All the mentioned quantities are briefly discussed in Appendix A. The spectral parameter $b(\xi, z')$ is a measure of the radiation field present in the pulse. For a single soliton in an unperturbed fibre, b is zero and remains zero as the soliton propagates; the presence of the perturbation changes b in accordance with Eq. (2.15), so that b is first order in the perturbing term. The last term in Eq. (2.15) is the source which generates the radiation field. We will be interested in the case when $\zeta = \xi$ is real and where $\check{\Phi}$ is approximated by its solitonic expression. Then, the integral in Eq. (2.15) is the projection of the perturbation F onto a set of "dressed" continuum modes (the Jost functions), labeled by the parameter ξ, in much the same way that a spectral component of a source F is found by projecting onto a continuum mode $\exp(i\omega t)$ in simple Fourier analysis. Indeed, in the absence of the soliton, $\check{\Phi} = [\exp(-2i\xi t), 0]^T$, and the source term is simply the conjugate of the Fourier component of F, with 2ξ the transform variable. We will make then the identification $\omega \equiv 2\xi$. Following [25], rather than work with the spectral parameter $b(\omega, z')$, let us introduce an associated field $f(z',t)$, such that its transform $\hat{f}(\omega, z') \equiv \mathcal{F}(f(z',t))$ is related to $b(\omega, z')$ by

$$\hat{f}(\omega, z') = \frac{b^*(\omega, z')}{\omega^2 + 4\eta_1^2}, \tag{2.16}$$

where η_1 is the soliton parameter. Simple manipulation of Eq. (2.15) then leads to the evolution equation for $\hat{f}$,

$$i\frac{\partial \hat{f}}{\partial z'} = \frac{\omega^2}{2}\hat{f} + \frac{i}{\omega^2 + 4\eta_1^2}\int_{-\infty}^{+\infty} \mathrm{d}t\, \left([F^*, F]\check{\Phi}\right)^*. \tag{2.17}$$

Finally, an inverse Fourier transform produces the evolution equation for the associated field f [25],

$$i\frac{\partial f}{\partial z'} = -\frac{1}{2}\frac{\partial^2 f}{\partial t^2} + i\int_{-\infty}^{+\infty} \mathrm{d}t\mathrm{d}\omega\, \frac{e^{-i\omega t}}{\omega^2 + 4\eta_1^2}\left([F^*, F]\check{\Phi}\right)^*. \tag{2.18}$$

Equation (2.18) generalizes a similar version given in [26]. Having found the evolution equation for f, the next step is to link this to the perturbing field δq. It can be shown that [25, 26]

$$2\pi\delta q(z', t) = -\frac{\partial^2 f}{\partial t^2} + 2\gamma\frac{\partial f}{\partial t} - \gamma^2 f + q_s^2 f^*, \tag{2.19}$$

where $\gamma = -q_s^{-1}\partial q_s/\partial t$. Hence, the algorithm for finding δq is first to solve Eq. (2.18) for the associate field $f(z', t)$, then to find $\delta q(z', t)$ from this, using Eq. (2.19).

Equation (2.18) appears very difficult to solve, since analytic forms are not generally known for ϕ_i, etc. Hovewer, in the perturbative limit considered here, these Jost function components can be approximated by their appropriate expressions for the single-soliton state, and the integrals can then be easily evaluated. We will require in particular the solitonic expressions for ϕ_1 and ϕ_2, together with that one for the spectral parameter a; these are

$$\begin{aligned} a(\xi) &= \frac{\xi - i\eta_1}{\xi + i\eta_1}, \\ \phi_1 &= \frac{e^{-i\xi t}}{\xi + i\eta_1}(\xi - i\eta_1 \tanh 2\eta_1 t), \\ \phi_2 &= -\frac{i\eta_1}{\xi + i\eta_1} e^{-i\xi t - 2i\eta_1^2 z'} \operatorname{sech} 2\eta_1 t. \end{aligned} \tag{2.20}$$

To simplify the algebra, and with no loss of generality, we have set the (constant) soliton parameter $\xi_1 = 0$ –a Galilean transformation effects this change. Finally, we remind that Eq. (2.11) implies the following symmetry relationships [16]

$$\begin{aligned} &[\bar{\phi}_1, \bar{\phi}_2] = [\phi_2^*, -\phi_1^*] \\ &\bar{a}(\xi) = a^*(\xi), \quad \xi \text{ real}, \\ &\bar{b}(\xi) = b^*(\xi), \quad \xi \text{ real}. \end{aligned} \tag{2.21}$$

We apply now the illustrated analysis to the case when the perturbation F has the form [cf. Eq. (2.10)]

$$F = -i\int_{-\infty}^{+\infty} \mathrm{d}\omega_1 \mathrm{d}\omega_2 \mathrm{d}\omega\, e^{-i\omega t}\left\{1 - \frac{\sin[\mu(\omega - \omega_1)(\omega - \omega_2)]}{\mu(\omega - \omega_1)(\omega - \omega_2)}\right\} \hat{q}_{\omega_1}\hat{q}_{\omega_2}\hat{q}^*_{\omega_1 + \omega_2 - \omega}, \tag{2.22}$$

with parameter $\mu \ll 1$. In order to simplify the above equation, we use the approximation $1 - \sin[\mu(\omega - \omega_1)(\omega - \omega_2)]/\mu(\omega - \omega_1)(\omega - \omega_2) \approx 1/6[\mu(\omega - \omega_1)(\omega - \omega_2)]^2$ valid for small μ. By setting also $\omega_3 = \omega_1 + \omega_2 - \omega$, we can write

$$F = -i\frac{\mu^2}{6}\int_{-\infty}^{+\infty} \mathrm{d}\omega_3\, e^{i\omega_3 t}\hat{q}^*_{\omega_3}\left[\int_{-\infty}^{+\infty} \mathrm{d}\omega_j\, e^{-i\omega_j t}(\omega_j - \omega_3)^2\hat{q}_{\omega_j}\right]^2, \quad j = 1 \text{ or } 2, \tag{2.23}$$

from which, by using well-known properties of the Fourier transform, we get

$$F(q,q^*) = -i\frac{\mu^2}{6}\left[q^*\left(\frac{\partial^2 q}{\partial t^2}\right)^2 + 4\frac{\partial q}{\partial t}\frac{\partial q^*}{\partial t}\frac{\partial^2 q}{\partial t^2} + 2q\frac{\partial^2 q}{\partial t^2}\frac{\partial^2 q^*}{\partial t^2} + 4\left(\frac{\partial q}{\partial t}\right)^2\frac{\partial^2 q^*}{\partial t^2} + 4q\frac{\partial q}{\partial t}\frac{\partial^3 q^*}{\partial t^3} + q^2\frac{\partial^4 q^*}{\partial t^4}\right]. \tag{2.24}$$

Since the perturbation is assumed to be small, which amounts to assuming an adiabatic deformation of the soliton, we can replace q in the above equation by the single-soliton form q_s [cf. Eq. (2.12)]; then, carrying out the required derivatives leads to

$$F(q_s,q_s^*) = -\frac{256}{3}i\mu^2\eta_1^7 e^{2i\eta_1^2 z'}\operatorname{sech}^3 2\eta_1 t\left(19\operatorname{sech}^4 2\eta_1 t - 21\operatorname{sech}^2 2\eta_1 t + 4\right). \tag{2.25}$$

Consider first an investigation of the effects of the perturbation F on the soliton parameters ξ_1 and η_1, after which an analytic expression for the generated field δq will be derived.

The trace formulae [16], which give the conserved functionals C_n for the unperturbed form of Eq. (2.11) in terms of the spectral data, are stated in Eq. (A.15). From these, since $N = 1$ (by assumption, that is a single soliton), we can deduce the evolution equations for ξ_1 and η_1; these are

$$\frac{\mathrm{d}\eta_1}{\mathrm{d}z'} = \frac{1}{4}\frac{\mathrm{d}C_0}{\mathrm{d}z'}, \quad \frac{\mathrm{d}\xi_1}{\mathrm{d}z'} = -\frac{i}{8\eta_1}\frac{\mathrm{d}C_1}{\mathrm{d}z'} - \frac{\xi_1}{4\eta_1}\frac{\mathrm{d}C_0}{\mathrm{d}z'}, \tag{2.26}$$

where the evolution of C_0 and C_1 is given by Eq. (2.14) for $n = 0$ and 1,

$$\frac{\mathrm{d}C_0}{\mathrm{d}z'} = \int_{-\infty}^{+\infty}\mathrm{d}t\,(F^*q + Fq^*), \quad \frac{\mathrm{d}C_1}{\mathrm{d}z'} = \int_{-\infty}^{+\infty}\mathrm{d}t\left(-F^*\frac{\partial q}{\partial t} + F\frac{\partial q^*}{\partial t}\right). \tag{2.27}$$

In the adiabatic limit considered here, we can evaluate the integrals in the above equations for $q = q_s$; it is easy then to verify that these integrals are zero, so that C_0 and C_1 are conserved quantities (i.e., independent of z'). It follows that the change in the soliton parameters ξ_1 and η_1 is $O(\mu^4)$.

Consider next the perturbing field. To $O(\mu^2)$, the soliton parameters remain constant. Then ξ_1 can self-consistently be set to zero. The soliton forms for ϕ_1 and ϕ_2 are given in Eqs. (2.20). Similar expressions for $\bar{\psi}_1$ and $\bar{\psi}_2$ are readily deduced using Eqs. (A.4), with (2.21). However, since b is required to $O(\mu^2)$, we may replace $\bar{\psi}$ with $\bar{a}\phi$, where $\bar{a}(\xi) = a^*(\xi)$ is given by the first of Eqs. (2.20).

To get the evolution equation for b, or equivalently for f, it remains to evaluate the integral [cf. Eq. (2.18)]

$$I = \int_{-\infty}^{+\infty}\mathrm{d}t\,[F^*(q_s,q_s^*), F(q_s,q_s^*)]\begin{bmatrix}\phi_1\bar{\psi}_1\\ \phi_2\bar{\psi}_2\end{bmatrix}. \tag{2.28}$$

Using the analytic forms for ϕ_i, etc. noted above (with $\omega = 2\xi$), together with Eq. (2.25), it is easy to show that

$$\begin{aligned} F^*\phi_1\bar{\psi}_1 + F\phi_2\bar{\psi}_2 = &\frac{256}{3}i\mu^2\eta_1^7 e^{-2i\eta_1^2 z'}\frac{e^{-i\omega t}}{\omega^2 + 4\eta_1^2}\left[152\eta_1^2\operatorname{sech}^9 2\eta_1 t + (19\omega^2 - 244\eta_1^2)\right. \\ &\times \operatorname{sech}^7 2\eta_1 t - (21\omega^2 - 116\eta_1^2)\operatorname{sech}^5 2\eta_1 t + 4(\omega^2 - 4\eta_1^2)\operatorname{sech}^3 2\eta_1 t \\ &\left. -4i\eta_1\omega(19\operatorname{sech}^7 2\eta_1 t - 21\operatorname{sech}^5 2\eta_1 t + 4\operatorname{sech}^3 2\eta_1 t)\tanh 2\eta_1 t\right]. \end{aligned} \tag{2.29}$$

By substituting Eq. (2.29) into Eq. (2.28) and using standard integrals involving hyperbolic functions, we get, after simple manipulations,

$$I = \frac{32}{3}\pi i\mu^2\eta_1^4 e^{-2i\eta_1^2 z'}\,\mathrm{sech}\left(\frac{\pi\omega}{4\eta_1}\right)\left[\frac{19}{20160}\frac{(\omega^2+4\eta_1^2)^3}{16\eta_1^4} + \frac{1}{5040}(95\omega^2 - 188\eta_1^2)\frac{(\omega^2+4\eta_1^2)^2}{16\eta_1^4}\right.$$
$$\left. + \frac{1}{2520}(197\omega^2 + 1268\eta_1^2)\frac{(\omega^2+4\eta_1^2)}{4\eta_1^2} + \frac{3}{35}(\omega^2+4\eta_1^2)\right]. \tag{2.30}$$

Now, the easiest way to find the associated field $f(z',t)$ is to solve first for its Fourier transform $\hat{f}(\omega,z')$, and then to transform back to f. The evolution equation for $\hat{f}$ reads [cf. Eq. (2.17)]

$$\frac{\partial\hat{f}}{\partial z'} + i\frac{\omega^2}{2}\hat{f} = Ce^{2i\eta_1^2 z'}. \tag{2.31}$$

Here, $C = \exp(-2i\eta_1^2 z')I^*/(\omega^2+4\eta_1^2)$ is a coefficient that does not depend on z'. The general integral of the above equation reads

$$\hat{f}(\omega,z') = Ae^{-i\frac{\omega^2}{2}z'} - \frac{2iCe^{2i\eta_1^2 z'}}{\omega^2+4\eta_1^2}, \tag{2.32}$$

where A is an arbitrary constant. Since we look for a stationary solution in z', i.e. $q(z',t) = R(t)\exp(ikz')$ where R and k are real, we must set $A = 0$. Then, substituting Eq. (2.30) into Eq. (2.32) gives the explicit form for $\hat{f}$

$$\hat{f}(\omega,z') = -\frac{8}{21}\pi\mu^2\eta_1^4 e^{2i\eta_1^2 z'}\,\mathrm{sech}\left(\frac{\pi\omega}{4\eta_1}\right)\left(\frac{133}{1920\eta_1^4}\omega^2 + \frac{197}{180\eta_1^2}\frac{\omega^2}{\omega^2+4\eta_1^2}\right.$$
$$\left. + \frac{533}{45}\frac{1}{\omega^2+4\eta_1^2} - \frac{169}{1440\eta_1^2}\right). \tag{2.33}$$

Finally, taking the inverse Fourier transform of the above equation, by means of standard integration techniques, produces the required form for f

$$f(z',t) = -\frac{2}{315}\pi\mu^2\eta_1^3 e^{2i\eta_1^2 z'}\left\{168\,\mathrm{sech}\,2\eta_1 t + 133\,\mathrm{sech}^3 2\eta_1 t\right.$$
$$\left. + 448\left[-2\eta_1 t\sinh 2\eta_1 t + \cosh 2\eta_1 t\ln(2\cosh 2\eta_1 t)\right]\right\}. \tag{2.34}$$

Having found f, the perturbing field δq is obtained directly from Eq. (2.19); this reads

$$\delta q(z',t) = \frac{16}{45}\mu^2\eta_1^5 e^{2i\eta_1^2 z'}\left(8\,\mathrm{sech}\,2\eta_1 t + 40\,\mathrm{sech}^3 2\eta_1 t - 95\,\mathrm{sech}^5 2\eta_1 t\right.$$
$$\left. + 64\eta_1 t\,\mathrm{sech}\,2\eta_1 t\tanh 2\eta_1 t\right). \tag{2.35}$$

2.3.1 Prediction of the soliton power enhancement

The perturbative solution of Eq. (2.1) reads

$$A(z,t) = \left(\frac{2\langle d\rangle}{\sigma P_0 L}\right)^{1/2}\int_{-\infty}^{+\infty} d\omega\,\hat{q}(z',\omega)\exp\left[-i\omega t - i\omega^2 R_0(z')\right], \quad z' = 2\langle d\rangle z. \tag{2.36}$$

Here, $R_0(z')$ is the accumulated dispersion function for the map, as defined in Eq. (2.2), and $\hat{q}(z',\omega)$ is the Fourier transform of the solution of Eq. (2.11), $q(z',t) = q_s + \delta q(z',t)$, with q_s

and δq given by Eqs. (2.12) and (2.35), respectively. Equation (2.36) allows the description of some features of the path-averaged DM soliton, in the perturbative limit of small dispersion map strengths. In particular we derive here an expression for the soliton power enhancement –compared with the constant dispersion case–, first observed in [40].

If we consider the pulse at the mid point of one of the fibre segments making up the dispersion map, then $R_0 = 0$ and (2.36) reduces to

$$A(z,t) = \left(\frac{2\langle d\rangle}{\sigma P_0 L}\right)^{1/2} q(z',t). \tag{2.37}$$

Hence, the pulse features are simply described by the function $q(z',t)$. This function contains a free parameter η_1 which determines the amplitude and the width of the pulse (cf. Eqs. (2.12) and (2.35)). We denote here the scaled pulse power $|q_s + \delta q|^2$ by $G(t;\eta_1)$, to stress its dependence on η_1, for a given value of the perturbation parameter μ. The peak power (at $t = 0$) is given by

$$G(0;\eta_1) = \left(2\eta_1 - \frac{752}{45}\mu^2\eta_1^5\right)^2, \tag{2.38}$$

and is plotted in Fig. 2.1 in a suitable range of η_1, for different values of μ. The relation

$$G(t_{\mathrm{FWHM}};\eta_1) = \frac{1}{2}G(0;\eta_1) \tag{2.39}$$

defines the FWHM t_{FWHM} of the pulse as an implicit function of η_1. This solution is shown in Fig. 2.2, for the same range of values of η_1. Finally, Fig. 2.3 shows the peak power against the pulse width. Equations (2.38) and (2.39) allow one to calculate the peak power $2\langle d\rangle G(0)/(\sigma P_0 L)$ of the DM soliton corresponding to a fixed t_{FWHM}. This is then compared with the peak power of a soliton of equal FWHM t_{FWHM} in a uniform fibre with the same path-averaged dispersion $\langle d\rangle$, $2\langle d\rangle G_{sol}(0)/(\sigma P_0 L)$, where

$$G_{sol}(0) = \frac{(1.76)^2}{t_{\mathrm{FWHM}}^2}. \tag{2.40}$$

This comparison results in the following expression for the peak power enhancement in terms of parameter μ

$$\frac{G(0)}{G_{sol}(0)} = 1 + \alpha\mu^2 + O(\mu^4), \tag{2.41}$$

where the interpolation parameter α is found to have a value of approximately 2.9.

The next step is to link the perturbation parameter μ to the dispersion map strength. For a dispersion map as defined in this section, the strength of one element can be characterized by [40, 43] (cf. Eq. (1.1))

$$S = \left|\frac{\tilde{\beta}_2^{(1)}L_1 - \tilde{\beta}_2^{(2)}L_2}{2t_0^2}\right|, \tag{2.42}$$

where $\beta_2^{(1,2)} = \tilde{\beta}_2^{(1,2)} + \langle\beta_2\rangle$ and L_1, $L_2 = L - L_1$ are the GVD coefficients and lengths of the two fibre segments, in physical units. Here, we choose the time parameter t_0 to be $t_0 = \tau_{\mathrm{FWHM}}/\sqrt{2}$, where τ_{FWHM} is the minimum FWHM pulse width. The perturbation parameter μ can be expressed as

$$\mu = \frac{S}{2}, \tag{2.43}$$

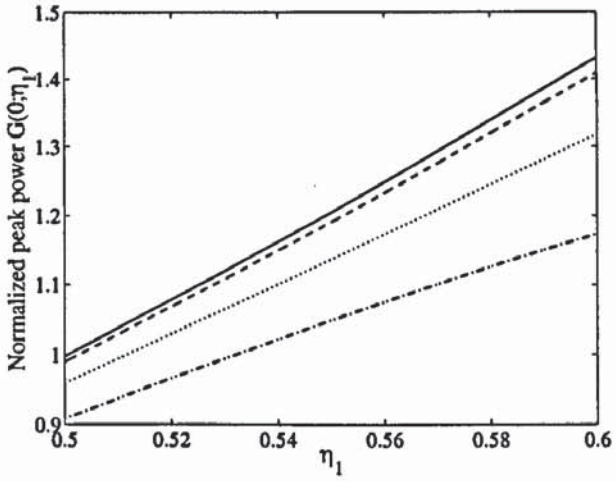

Figure 2.1: Peak power against soliton parameter η_1. Solid curve, $\mu = 0.05$; dashed curve, $\mu = 0.1$; dotted curve, $\mu = 0.2$; dash-dot curve, $\mu = 0.3$.

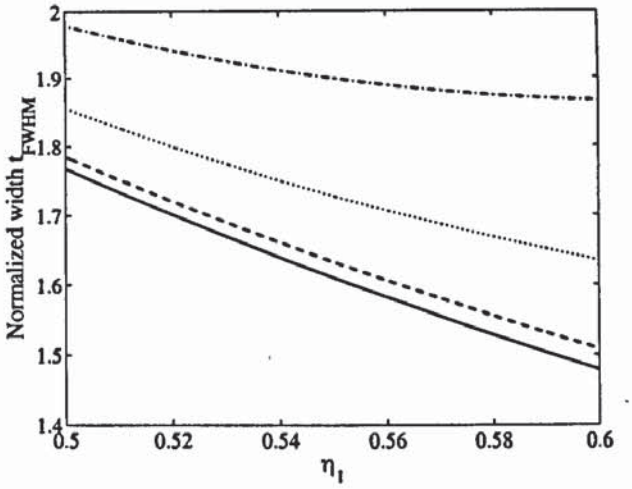

Figure 2.2: Full-width at half-maximum against soliton parameter η_1. Legend as in Fig. 2.1.

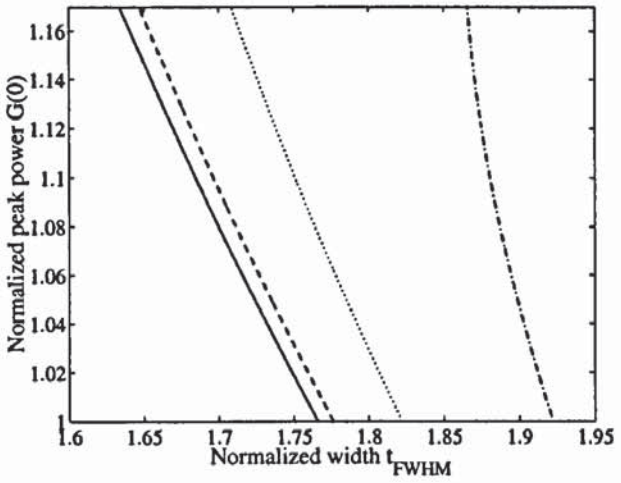

Figure 2.3: Peak power against full-width at half-maximum. Legend as in Fig. 2.1.

and then Eq. (2.41) becomes

$$\frac{G(0)}{G_{sol}(0)} = 1 + \beta S^2 + O(S^4), \tag{2.44}$$

where $\beta = \alpha/4 \approx 0.72$. This result, obtained in the limiting case of small S, is in agreement with the empirical formula discovered through numerical simulations [40], where a value of $\beta \approx 0.7$ was found.

2.4 Numerical simulations and comparison with the theory

In this section a comparison between the predictions of the perturbation analysis developed in the previous section and the results of full-numerical simulations is presented, in order to investigate the validity of the perturbation theory.

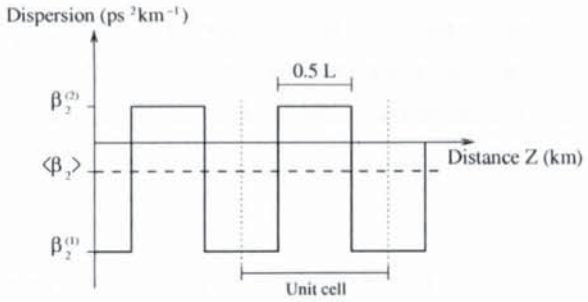

Figure 2.4: The dispersion compensation map used in calculations.

Our simulations are based on numerical integration of the NLS equation

$$i\frac{\partial E}{\partial Z} - \frac{1}{2}\beta_2(Z)\frac{\partial^2 E}{\partial T^2} + \sigma|E|^2 E = 0 \tag{2.45}$$

using the dispersion map shown in Fig. 2.4. This comprises equal lengths $L_1 = L_2 = L/2$ of alternating anomalous and normal fibres, with dispersions $\beta_2^{(1)} = \tilde{\beta}_2 + \langle\beta_2\rangle$ and $\beta_2^{(2)} = -\tilde{\beta}_2 + \langle\beta_2\rangle$ respectively. The unit cell is defined to start and end at the mid point of one of the fibres [103]. In all the examples presented we have chosen $L_1 = L_2 = 100\,\text{km}$, and $\langle\beta_2\rangle = -0.01\,\text{ps}^2\text{km}^{-1}$. The nonlinear coefficient is taken to be $\sigma \simeq 2.57\,(\text{W km})^{-1}$ in both fibres; fibre attenuation is neglected, which is consistent with the case discussed in Section 2.2.

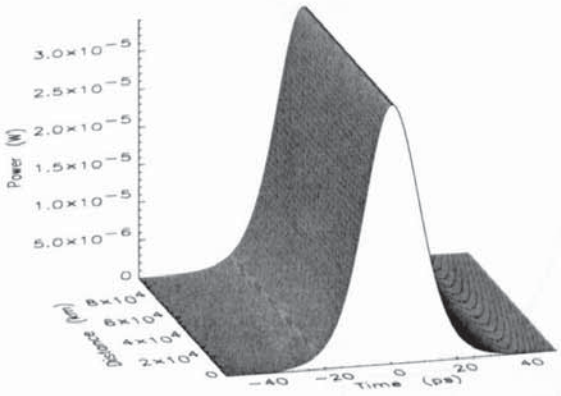

Figure 2.5: Asymptotic pulse profile at the beginning of each unit cell. Here $\tilde{\beta}_2 = -0.8\,\text{ps}^2\text{km}^{-1}$.

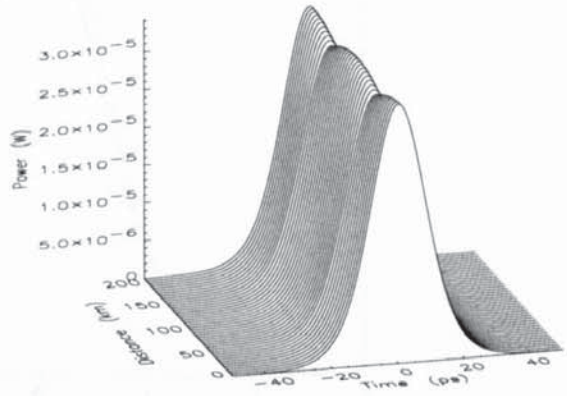

Figure 2.6: Evolution of the pulse shown in Fig. 2.5 over one period of dispersion compensation cycle.

We have launched Gaussian pulses into a transmission line with the dispersion maps defined above, with a FWHM pulse width of 20 ps, and the proper energy. Using the averaging technique presented in [104], we have obtained long distance stable soliton-like pulses that return to their original shapes after each map period. Figure 2.5 shows the intensity profile of such a stable asymptotic pulse at the start of each unit cell, for a map with $\tilde{\beta}_2 = -0.8\,\text{ps}^2\text{km}^{-1}$. The evolution of the same pulse within one unit cell is shown in Fig. 2.6. It can be seen that for the weak dispersion maps considered here, the shape of the stable soliton is not significantly different to the hyperbolic secant shape of uniform fibres, though the soliton exibits an enhanced power.

The analytical solution which has been compared with the stable solution of numerical simulations is given in Eq. (2.36). The power and time have been scaled here using the peak power P and the width τ_{FWHM} of the numerical solution at the mid point of each section, i.e. $P_0 = P$, and $t_0 = \tau_{\mathrm{FWHM}}/\sqrt{2}$. In physical units the perturbation parameter μ then reads

$$\mu = -\frac{\tilde{\beta}_2 L}{2\tau_{\mathrm{FWHM}}^2}. \tag{2.46}$$

Since the perturbation theory is expected to work for small μ, we have considered here dispersion maps with values of μ between 0.05 and 0.3.

For a given numerical solution, the determination of the free parameter η_1, which arises in the analytical solution (cf. Eqs. (2.12) and (2.35)), is somewhat arbitrary. We have chosen to set η_1 at the value for which the peak powers of the analytical and numerical solutions are matched. This gives a simple relationship between η_1 and μ

$$\eta_1 - \frac{376}{45}\eta_1^5\mu^2 = \frac{1}{2}\left(\frac{\sigma P_0 L}{2\langle d\rangle}\right)^{1/2}, \tag{2.47}$$

if the analytical solution amplitude is evaluated at the mid point of a section (where $R_0 = 0$). Equation (2.47) can then be solved for η_1 in terms of μ.

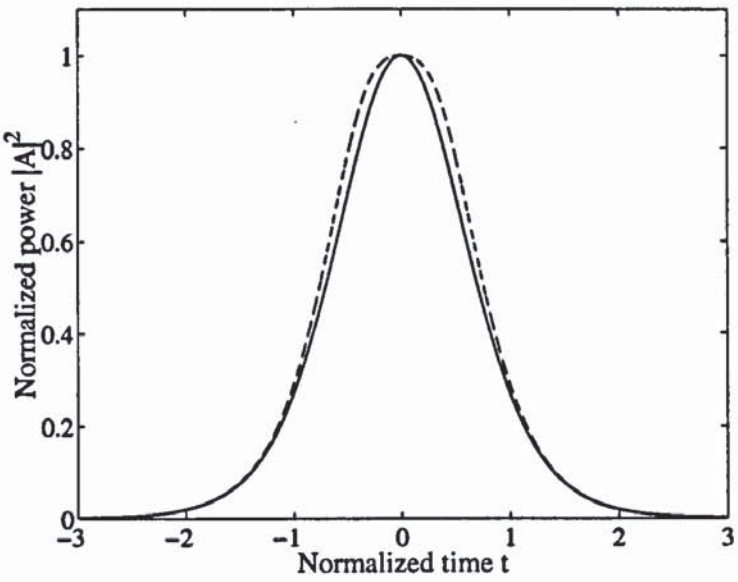

Figure 2.7: Pulse shapes obtained with the numerical (solid curve) and the analytical (dashed curve) NLS equation solutions, shown at the beginning of the periodic cell, for $\mu = 0.2$ ($\tilde{\beta}_2 = -0.8\,\mathrm{ps^2km^{-1}}$).

Figure 2.7 compares the normalized pulse powers obtained from the numerical and the analytical solutions, at the beginning of each unit cell, for a map with $\tilde{\beta}_2 = -0.8\,\mathrm{ps^2km^{-1}}$, i.e. for $\mu = 0.2$. It can be seen that the agreement is very good, as one would expect for weak perturbations. To establish better the degree of accuracy of the theoretical results, we have also compared the difference in power – at the same point of the map – of both the analytical and the numerical solution with the exact soliton solution of the NLS equation with constant dispersion, $A_s = (2\langle d\rangle/(\sigma P_0 L))^{1/2} 2\eta_1 \operatorname{sech} 2\eta_1 t$. Figure 2.8 shows the results of this comparison for two different values of μ, $\mu = 0.1$ (corresponding to $\tilde{\beta}_2 = -0.4\,\mathrm{ps^2km^{-1}}$) and $\mu = 0.2$. It

can be seen that the scaling factor between the two pairs of curves is of the order of μ^2. This is consistent with our expectations, since the correction δq to q_s is $O(\mu^2)$ (cf. Eq. (2.35)). On the other hand, the difference between the analytical and the numerical curves corresponding to the same μ is not exactly of order μ^4, as one would expect from the perturbation theory, because the path-averaged dispersion is not vanishingly small compared to the local dispersion. The path-averaged dispersion in the numerical simulations has been chosen as a realistic value. Reduction of $\langle\beta_2\rangle/\tilde{\beta}_2$ would make the difference between the two curves closer to order μ^4.

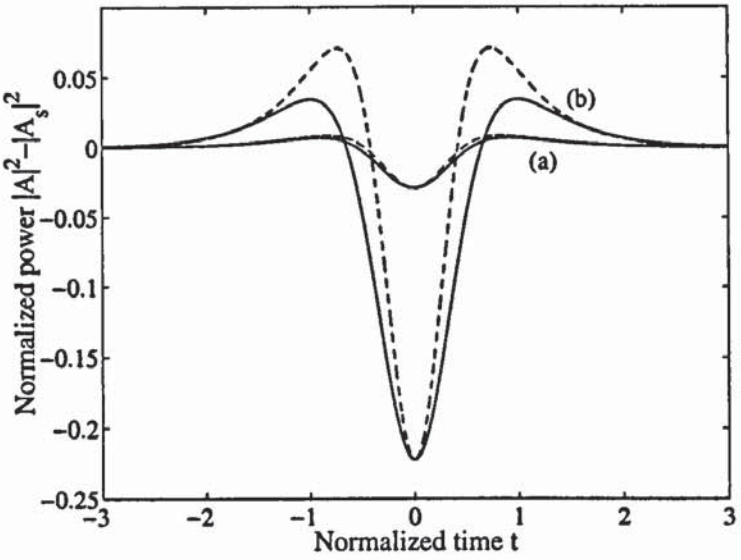

Figure 2.8: Difference in power with the sech soliton, $|A(t)|^2 - |A_s(t)|^2$, for the numerical (solid curve) and analytical (dashed curve) solutions, for (a) $\mu = 0.1$ ($\tilde{\beta}_2 = -0.4\,\mathrm{ps^2km^{-1}}$), and (b) $\mu = 0.2$ ($\tilde{\beta}_2 = -0.8\,\mathrm{ps^2km^{-1}}$).

In conclusion, we can affirm that Eqs. (2.12) and (2.35) predict the pulse shape very well. For values of μ above ~ 0.35, however, the analytical solution becomes double peaked and is no longer a good pointwise approximation to the solution. We can then set the limit of validity of our perturbation analysis at the value $\mu = 0.35$ (i.e. $S = 0.7$), which is in good agreement with the results achieved in [64].

2.5 Conclusion

In this chapter we have developed a perturbation theory to describe path-averaged DM solitons in transmission lines with a weak dispersion map. The analytic expression for the soliton envelope obtained by this approach predicts a pulse shape and a power enhancement which are in good agreement with the results of direct numerical simulations. Thus we are confident that the results presented in this chapter can be useful in applications to practical systems with weak dispersion management. Analytical results can be especially important in the optimisation problems when numerical simulations require a lot of computer time.

Chapter 3

Dispersion-managed autosoliton transmission and all-optical passive regeneration by the use of in-line nonlinear optical loop mirrors

3.1 Introduction

The central topic of this chapter is the study of autosoliton transmission in DM fibre systems with periodical in-line deployment of NOLMs as all-optical regenerators of signals.

DM solitons have been attracting considerable interest recently in RZ format optical communication systems because of their superb characteristics which are not observed in conventional solitons. In particular, as described in Chapter 1, dispersion management gives the benefits of high local and low average dispersion, while allowing pulses with higher energies to propagate [40, 45, 46]. Indeed, the energy enhancement, which increases with increasing map strength (cf. Eq. (1.1)), relaxes the linear relation between dispersion and energy, and thus makes it possible to reduce the Gordon-Haus timing jitter through the use of low average dispersion [50, 51], while maintaining a good SNR [40]. Moreover, the high local dispersion efficiently suppresses interchannel crosstalk in WDM systems [55]. By using these properties, it is possible to make a new transmission line with higher bit-rate and/or longer transmission distance compared to a conventional soliton transmission system. Another promising application of this technology is the upgrade of an already installed SMF base into a high-speed system operating at single-channel bit-rates of $40\,\mathrm{Gbit\,s^{-1}}$ and above.

However, the transmission performance of a DM soliton system with small average dispersion may be strongly degraded by linear waves. Indeed, the propagation of nonlinear stationary pulses in real fibre links is always accompanied by a radiative background (or linear mode). These dispersive waves originate from amplifier noise or from the mismatch between the input pulse and the truly stationary pulse. Small average dispersions prevent the separation of the linear wave from the signal, which delays the formation of a stationary pulse.

Moreover, when dispersion management is used for operation at $40\,\mathrm{Gbit\,s^{-1}}$ on standard fibre, the high values of local dispersion together with the short pulse widths required result in high map strengths beyond the range where stationary DM solitons exist [44]. In this regime of high map strengths, to which we refer as the quasi-linear regime, carrier pulses periodically

experience large temporal broadening, and the effect of fibre nonlinearity tends to be averaged out. As remarked in Chapter 1, this scheme is, in some sense, opposite to soliton or DM soliton transmission, where the nonlinearity plays an important role in preserving the pulse shapes. Even though pulses in the quasi-linear regime are not stable in a strict mathematical sense, they can still be successfully used in practical systems. However, the nonlinear impairements that are allowed to accumulate by the remaining order of the field can impose severe limits to transmission. Indeed, nonlinear intra-channel pulse-to-pulse interactions are considered to be one of the main limiting factors inhibiting channel bit-rates of $40\,\mathrm{Gbit\,s^{-1}}$ or beyond in RZ transmission in strongly DM fibres (see [105]-[109] and references therein). Such interactions are caused by strong temporal overlap between adjacent pulses which is due to large pulse breathing within one management period. They take two different forms [106, 107], which are usually referred to as intra-channel XPM and FWM. The intra-channel XPM shifts the frequencies of the interacting pulses, resulting in timing jitter, while the intra-channel FWM causes amplitude fluctuation of the main signals and generation of ghost pulses in the zero bit slots.

Transmission control methods both passive, which make use of guiding filters (with fixed or sliding frequency) [70, 71] and active, which make use of in-line synchronous modulation [72, 73] have been studied in order to stabilize DM RZ transmissions against the above-mentioned perturbations. Such control elements – discussed in Chapter 1 – are shown to reduce the timing jitter that is induced in the propagating pulse by interaction with amplifier noise, pulse-to-pulse interactions in both single-channel and WDM transmissions, and noise accumulation, and to achieve stabilization of pulse amplitude fluctuations. However, guiding filters require excess gain in order to compensate for the filter-induced loss, which in turn may enhance the accumulation of the linear mode. In addition, filtered DM pulses can suffer from additional instabilities, depending on the location of lumped filters [75], owing to the opposite direction of the filter action on stabilizing energy against spectrum fluctuation. Whereas the synchronous modulation may also not be effective as long as the linear wave is not shed away. Introduction of nonlinear gain, that is realized by use of polarization controllers [38] and fast saturable absorbers [110], has also been proposed to stabilize DM soliton transmissions by suppression of the growth of the linear mode [111]. Thanks to the DM soliton power enhancement, nonlinear gain may be more beneficial to DM solitons than to conventional solitons [110].

The use of in-line NOLMs as saturable absorbers (also termed intensity filters) [79] may be an alternative to the above schemes. It is useful to clarify here the application and motivation for wishing to place NOLMs into a transmission line. The NOLM (see its brief description in the following section) filters out low-intensity noise and dispersive waves from higher power signals through an effective saturable absorption (i.e. a decreasing attenuation with increasing optical power), and thus avoids pulse instabilities that are caused by interaction of such background radiation with the carrier pulse [80]. Fibre NOLMs have an ultrafast response (sub-picosecond) which most saturable absorbers do not. For instance, traditional semiconductor saturable absorbers have nanosecond response times. Moreover, NOLMs have a different switching characteristic owing to which they can provide negative feedback control of the amplitude of pulses, thus allowing for stabilization of the pulse amplitude against small changes in the input power. The dual function of intensity filtering and pulse amplitude control is probably the most attractive feature that distinguish NOLMs from other saturable absorbers. These characteristics

indicate that the use of in-line NOLMs can be a very effective technique for all-optical passive 2R regeneration (alternatively termed quasi-regeneration) of signals. Indeed, loop mirror intensity filtering allows for partial regeneration of pulse amplitude and shape, through suppression of noise accumulation and pulse distortion. On the other hand, as a NOLM introduces no temporal or spectral reference point into the system, it can not ensure pulse retiming, thus it does not directly improve the timing jitter in the system. Nevertheless, the noise suppression allows narrow bandwidth filters to be used without encountering pulse instability [83]. But solving timing problems is not the primary aim of including NOLMs into a transmission system.

After a brief review of the basic properties of the NOLM (Section 3.2), in Section 3.3 we present a numerical study of DM autosoliton transmission assisted by in-line NOLMs [112]. We demonstrate that stable pulse propagation over long distances is achievable in such a line, with a significant increase in the SNR. In the following sections we describe the use of in-line NOLMs as a general technique for all-optical passive 2R regeneration of RZ data in high-speed transmission systems with strong dispersion management. Specifically, in Section 3.4 we demonstrate that the application of the proposed technique to SMF-based systems mainly affected by amplitude noise may achieve stable single-channel data transmission over practically unlimited distances at bit-rates $\geq 40\,\mathrm{Gbit\,s^{-1}}$ [113, 114]. In Section 3.5 we describe the use of the technique in transoceanic $40\,\mathrm{Gbit\,s^{-1}}$ transmission systems where both intra-channel XPM and FWM are significant limiting factors [115]. Finally, in Section 3.6 we study the application of the $40\,\mathrm{Gbit\,s^{-1}}$ DM transmission guided by NOLMs to a WDM scheme [116, 117].

3.2 The nonlinear optical loop mirror

The NOLM was originally proposed by Doran and Wood [77] and experimentally demonstrated by Blow et al. [118] and Islam et al. [119]. We now briefly review its basic principles and properties. The device consists of a four-port directional coupler, the outputs of which are connected by a loop of fibre. Normal operation has the light being reflected back out of the input port. If a π phase shift occurs in the interferometer, then a "fringe shift" occurs which in this case corresponds to the light being transmitted through the output port. The phase shift comes from the fibre nonlinearity (SPM) which is different for the two counter-propagating pulses in the loop, because they have different intensities as a result of a breaking of the loop symmetry. Unbalancing of the NOLM can be achieved with an asymmetric coupler [77], or alternatively with a gain/loss element asymmetrically placed in the loop [78]. Other variations include using two fibres with different dispersive properties within the loop [120].

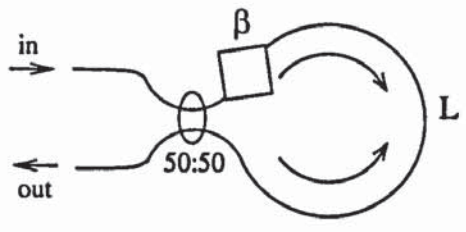

Figure 3.1: Schema of the NOLM.

In what follows, we will use a gain/loss-unbalanced NOLM (see Fig. 3.1). It incorporates a 50:50 coupler and an amplifier/attenuator with power gain/loss β. The continuous-wave (cw) input-output power mapping of the NOLM is given by [78]

$$P_{\text{out}} = \frac{\beta}{2g} P_{\text{in}} \left\{ 1 - \cos \left[\frac{\sigma(\beta - 1) L_{\text{eff}}}{2} P_{\text{in}} \right] \right\}. \tag{3.1}$$

Here, P_{out} and P_{in} are the output and input powers, respectively; σ is the nonlinear coefficient of the loop fibre; $g = \exp(2\gamma L)$, where L is the loop length, and γ is the loss coefficient [km^{-1}] of the loop fibre; and $L_{\text{eff}} = (1 - 1/g)/(2\gamma)$. Note that the configuration with an attenuator, $\beta = \Delta$, is similar to the configuration with an amplifier, $\beta = G$, provided that pre-amplification is included with gain G' such that $G'\Delta = G$. The first scheme avoids possible pulse instability due to in-loop amplification, at the expense of a reduced switching performance.

It can be shown [79] that operation of the NOLM in the region just after the first peak of the switching curve is stable against small fluctuations in the input power. Indeed, locally there is a saturable gain: if the pulse power increases, the NOLM's transmissivity decreases, and vice versa, returning the pulse toward its original state. The main advantage of using gain/loss-unbalanced NOLMs instead of coupler-unbalanced NOLMs as saturable absorbers is that the first provide higher discrimination against low-power radiation [121, 82], owing to their amplitude cubing effect at low energies (see Eq. (3.1)). On the other hand, because gain/loss-unbalanced NOLMs have sharper switching peaks, the portion of the switching curve on which operation is stable is smaller. However, this limitation can be easily overcome (see following sections) by placing the operation point only slightly past the switching peak.

We point out that the approximation of the NOLM's transmissivity by the cw transfer characteristic (3.1) is unsatisfactory in the case of intensity-modulated data streams, because significant pulse shaping takes place within the arms of the loop. Therefore, it is important to explicitely model pulse propagation within the loop mirror fibre by numerical integration of the NLS equation. However, the cw transfer function can still give a good estimate of the NOLM's characteristics needed to adapt the NOLM to a transmission line, as we will see in Section 3.4.

Previous studies [79]-[82] have addressed the use of NOLMs to reshape and stabilize pulses in transmission systems employing fibres with constant dispersion. In the following sections we study the application of NOLMs to DM transmission schemes.

3.3 Dispersion-managed autosoliton transmission guided by in-line nonlinear optical loop mirrors

In this section we examine the feasibility of optical pulse transmission in periodically amplified DM systems with in-line NOLMs [112]. The main goal is the demonstration of the compatibility of the NOLM with dispersion management for achievement of stable pulse transmission.

The basic section of the periodic system used as the model in our simulations is shown in Fig. 3.2. The normal- and the anomalous-dispersion fibre segments that build up the dispersion map are both 20 km long, and have dispersion of $\beta_2^{(1)} = 4.9\,\text{ps}^2\text{km}^{-1}$ and $\beta_2^{(2)} = -5.1\,\text{ps}^2\text{km}^{-1}$ respectively, which gives a path-averaged dispersion of $\langle \beta_2 \rangle = -0.1\,\text{ps}^2\text{km}^{-1}$. The effective area is taken to be $A_{\text{eff}}^{(1,2)} = 50\,\mu\text{m}^2$ in both fibres, and fibre attenuation is $\alpha^{(1,2)} = 0.2\,\text{dB km}^{-1}$.

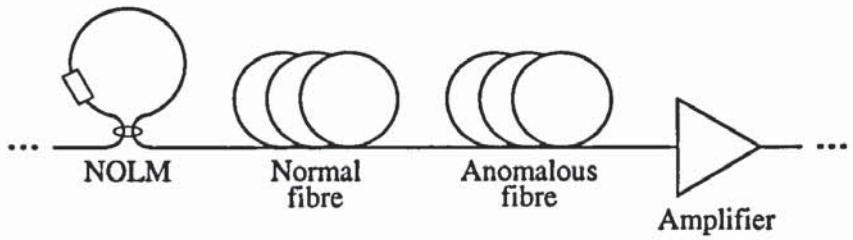

Figure 3.2: Schematic diagram of one element of the periodic transmission system.

The NOLM incorporates a coupler with a power-splitting ratio of 50:50, and a 6 km loop of DSF with zero dispersion and an attenuation of $\alpha = 0.6\,\mathrm{dB\,km^{-1}}$; the effective area of the loop fibre is assumed to be $A_{\mathrm{eff}} = 25\,\mu\mathrm{m}^2$, which makes the NOLM highly nonlinear. The symmetry between the two directions around the loop is broken by a loss element, inserted at one end of the loop, which subjects the pulses to a power attenuation of $\Delta = 6\,\mathrm{dB}$. An amplifier located at the end of the section compensates for fibre attenuation and loss from the NOLM. ASE noise is included in the calculations, but no filter is added at the amplifier.

A stable pulse (an ideal information carrier) that is propagating in the transmission system must be periodically reproduced at the output of each section. Considering the transformation of the pulse after propagation in one section as the Poincaré mapping of the input pulse into the output one, we find the stable solutions by determination of the fixed points of such a mapping in the space energy - pulse width - chirp. We call these stable pulses autosolitons, meaning that their characteristics are fixed by the system parameters. We use the following two-step procedure to rapidly find the converging pulse parameters. In a first run of simulations the pulse energy is fixed. Gaussian pulses are launched into the system, with a FWHM pulse width of 5.0 ps, and the pulse energy is restored at the end of each section, which means conceptually that we have variable amplifier gain. This restoration is done for a sufficient number of iterations for the pulse's width and chirp to reach a steady state; then, the amplifier gain also converges to some value. Then we perform a second run with a fixed amplifier gain, to check the stability of the pulse energy: Gaussian pulses with the stationary width and chirp are used as initial waveforms for the complete system with amplifiers, where the amplifier gain is set to the asymptotic value.

We find that stable propagation is possible over very long distances for pulse energies at the start of each cycle (NOLM input) between 2.2 and 2.4 pJ. The optimal pulses settle quickly to a steady state and their stable pulse shape for the system at the start of each cycle differs from the input Gaussian shape mostly in that the pulse develops low-power symmetric side-lobes. These background pedestals are removed by the NOLM through saturable absorption. The NOLM also subjects the pulses to a negative chirp (through SPM), while the pulse width is not significantly changed by the NOLM, because the loop fibre is dispersionless.

The cw input-output power mapping for the NOLM used in calculations is shown in Fig. 3.3. The peak power of the pulse before the NOLM is slightly beyond the first peak of the switching curve. Even in this region, however, the NOLM still loses a substantial fraction of the incident power. This loss could easily be reduced, because the attenuation in the loop fibre is set to a pessimistic value, and unbalancing of the NOLM is achieved with a loss element.

An example of a stable pulse with an energy of 2.25 pJ is shown in Fig. 3.4 as it settles to a steady state. Before the NOLM, the stable FWHM pulse width and the average chirp are 4.4 ps

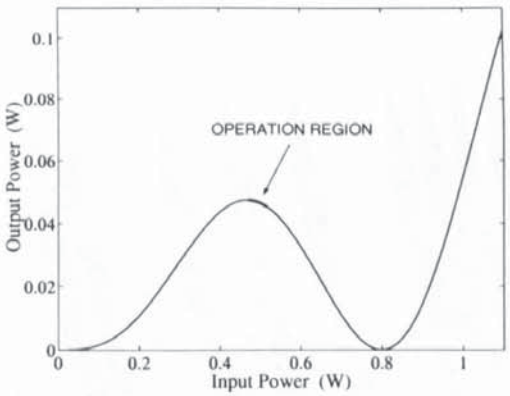

Figure 3.3: Cw switching curve of the NOLM.

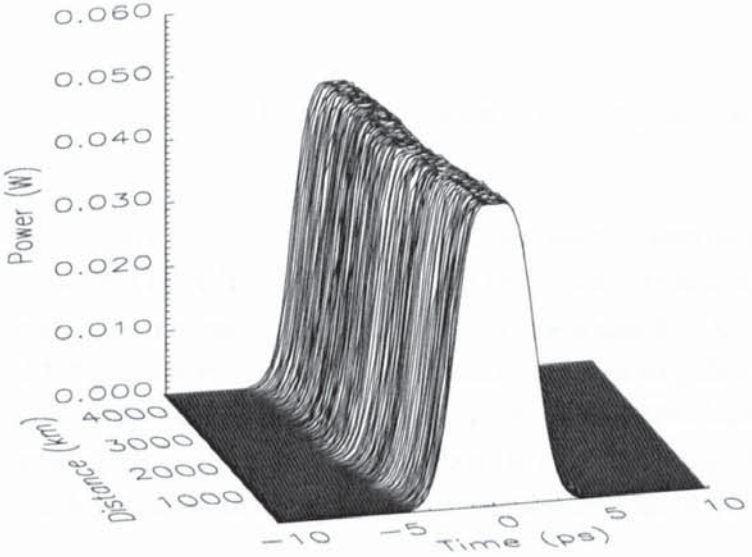

Figure 3.4: Stroboscopic evolution of a 2.25 pJ pulse as viewed at the NOLM output.

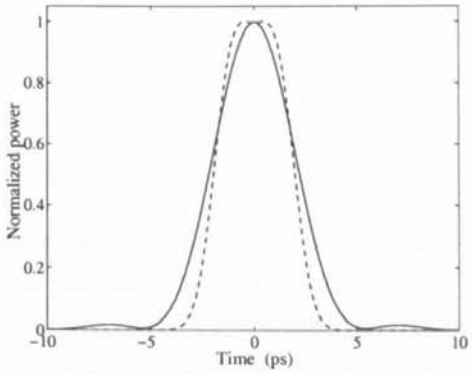

Figure 3.5: Stable pulse shapes. Solid curve, NOLM input; dashed curve, NOLM output.

and 0.13 THz^2, respectively. The pulse profile is taken at the NOLM output, where the pulse has an energy of 0.19 pJ, a FWHM of 4.0 ps, and an average chirp of $-0.16\,\mathrm{THz}^2$. The corresponding stable pulse shapes at the NOLM input and output are shown in Fig. 3.5. The waveform of the pulse after passing through the NOLM is clean, and the flat top is due to the maximum power that can be switched by the NOLM. The pulse undergoes a small position shift, 2 ps over 4000 km; this is basically the Gordon-Haus timing jitter, and introducing NOLMs as saturable absorbers does not improve system's performance in this respect. Timing jitter suppression could be achieved by the use of guiding filters [70, 71], or, for instance, by reduction of loss in the NOLM, since that reduces the amplifier gain required and hence the amount of noise. Another possibility would be to reduce further the average dispersion of the dispersion map [46]. We point out, however, that the main goal of the present work is not the optimisation of the system's characteristics, but the demonstration of stable DM pulse transmission through the action of in-line NOLMs. Optimisation of the system will lead to further improvement of its performance.

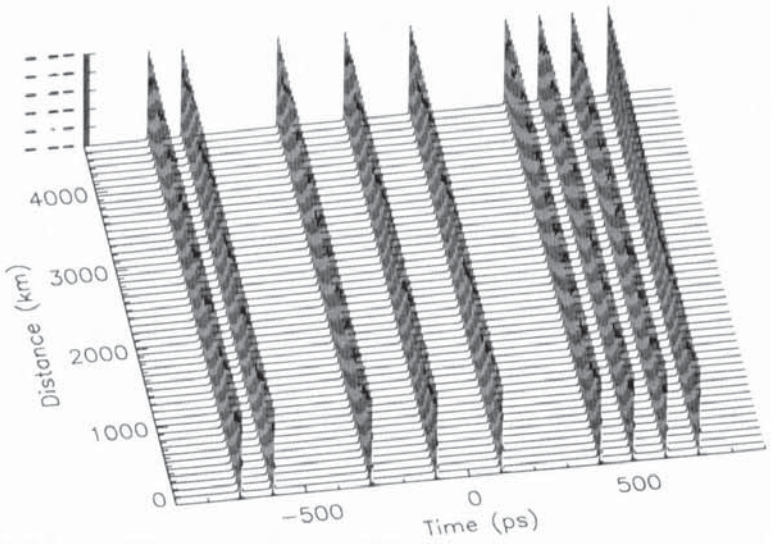

Figure 3.6: Example simulation of a 4.4 ps pulse train with data ⟨1100101010011110⟩.

Figure 3.6 shows a typical simulation result taken at each amplifier output for a 4.4 ps pulse train with data ⟨1100101010011110⟩ and a bit period of 100 ps (corresponding to the 10 Gbit s^{-1} data rate), propagating to 4000 km. In this simulation Gaussian filters with a FWHM bandwidth of 1.2 THz are included simply to limit the pulse-to-pulse interactions, and the filters do not have a significant effect on pulse propagation, as the filter bandwidth is approximately ten times the bandwidth of the pulses used. There is no discernible evidence of perturbations or distortions, which indicates that the data can be recovered for the full system length studied.

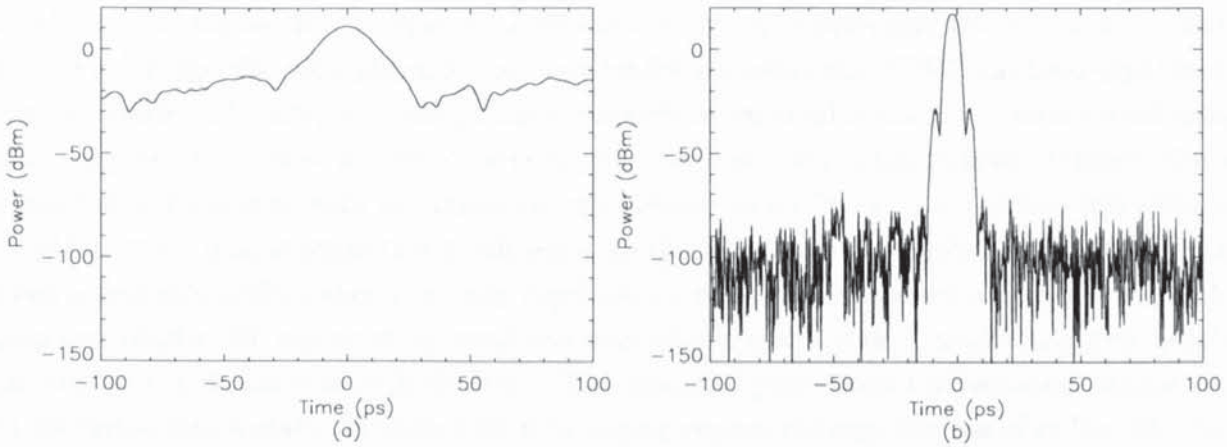

Figure 3.7: Pulse waveforms after 4000 km in DM systems with (a) guiding filters and (b) NOLMs.

To demonstrate the effectiveness of the NOLM in suppressing noise we compare pulse propagation in the transmission system with NOLMs with propagation in the same line without NOLMs. In the latter scheme Gaussian filters with a FWHM bandwidth of 0.24 THz are located after each amplifier to reduce the ASE noise effect. Gaussian pulses are launched into the system with the energy that they would have at the NOLM output and with the proper

width and chirp. Figure 3.7 shows a comparison between the waveforms of a 0.19 pJ pulse at a propagation distance of 4000 km for the systems without and with NOLMs. The waveforms are those at the starting point of the DM cycle. The substantial suppression of radiation by the introduction of NOLMs can clearly be seen; the SNR is ~ 60 dB higher in the system with NOLMs. It is also important to point out that, unlike in the system without NOLMs, the SNR stabilizes and does not degrade any furhter after a short distance.

In conclusion, we have demonstrated the feasibility of stable autosoliton propagation over long distances in periodically amplified DM transmission system with in-line NOLMs. NOLMs are very effective in suppressing the buildup of ASE noise and dispersive waves. The issues of determining the NOLM's optimal characteristics within the constraints of the DM scheme and of applying NOLMs to practical transmission systems will be addressed in the following sections.

3.4 All-optical passive 2R regeneration of dispersion-managed RZ data at 40 and 80 Gbit s^{-1} using in-line nonlinear optical loop mirrors

The problem of increasing the channel data rate to 40 Gbit s^{-1} and beyond and the error-free transmission distance in SMF is attracting much attention because of the immediate application to the upgrade of existing terrestrial links. A promising upgrading method is the use of a RZ modulation format together with dispersion management. However, as described in Section 3.1, the intra-channel nonlinear effects [105]-[109] can be significant for strongly DM systems operating in the quasi-linear regime, such as SMF-based systems with bit-rates ≥ 40 Gbit s^{-1}. These effects may lead to serious transmission penalties, specifically timing and amplitude jitter and the ghost pulse generation at the zero bits [106, 107].

In this and the following sections we study the use of in-line NOLMs as a general technique for all-optical passive 2R regeneration of RZ data in high-speed strongly DM systems. To date, 40 Gbit s^{-1} single-channel DM transmission over a few thousand km of SMF has been experimentally demonstrated [122]-[124]. Also, transoceanic distances at 40 Gbit s^{-1} can be achieved using in-line regeneration based on synchronous modulation [125, 126]. Though active regeneration is a possible method to provide for unlimited transmission at 40 Gbit s^{-1}, in practice this solution could be not optimal in terms of cost efficiency. In this section, we numerically demonstrate that when a system's performance is mainly degraded by pulse distortion and amplitude noise, the proposed passive 2R regeneration technique may enable stable data transmission over practically unlimited distances at high bit-rates. Therefore, the quasi-linear transmissison regime may be converted into a stable nonlinear bit-overlapping regime through the use of in-line NOLMs. Specifically, we show the feasibility of distance-unlimited transmission of a 40 Gbit s^{-1} single-channel RZ data stream over SMF [113]. We investigate the tolerance of this result [114] and we extend the proposed method to 80 Gbit s^{-1} data transmission.

3.4.1 System description

As a sample system for demonstration of the technique, we used a symmetric dispersion map similar to that in [127] (see Fig. 3.8). This DM scheme represents a practical upgrade of a link

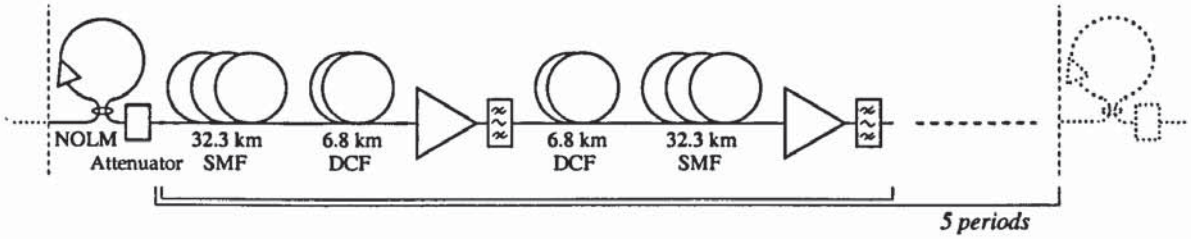

Figure 3.8: Schematic diagram of one element of the periodic transmission system.

with SMF by means of DCFs. The transmission line is composed of an equal number of 32.3 km SMF and 6.8 km DCF. The map consists of an alternation of two different fibre combinations: a SMF-DCF and a DCF-SMF block. A role of prechirping in such a map is minimized since the chirp-free points are located exactly at the beginning and the middle of the map [128]. The dispersion coefficients are $D^{(1)} = 15.0\,\mathrm{ps\,(nm\,km)^{-1}}$ for the SMF and $D^{(2)} = -71.2\,\mathrm{ps\,(nm\,km)^{-1}}$ for the DCF at 1550 nm, giving an average dispersion of $\langle D \rangle = 0.009\,\mathrm{ps\,(nm\,km)^{-1}}$ which is slightly anomalous. The effective area is $A_{\mathrm{eff}}^{(1)} = 70\,\mu\mathrm{m}^2$ for the SMF and $A_{\mathrm{eff}}^{(2)} = 30\,\mu\mathrm{m}^2$ for the DCF. The attenuation is $\alpha^{(1)} = 0.22\,\mathrm{dB\,km^{-1}}$ in the SMF and $\alpha^{(2)} = 0.65\,\mathrm{dB\,km^{-1}}$ in the DCF. A combination of an EDFA to compensate for the energy losses and a fixed Gaussian filter follows each of the two blocks. The amplifier has a typical noise figure of 4.5 dB and a power gain of 11.9 dB. The bandwidth of the filter B is taken to be approximately 1.5 times the bandwith of the pulses used and the product $B\tau_{\mathrm{FWHM}}$ is kept constant, τ_{FWHM} being the pulse width. Note that the use of such strong guiding filters is allowed by the saturable absorption action of the NOLMs [83]. Narrow bandwidth filters give in turn timing jitter reduction. The NOLM is placed into the transmission line every five periods of the dispersion map (as shown in Fig. 3.8). The NOLM incorporates a 50:50 coupler, and a loop of DSF with zero dispersion, an attenuation of $\alpha = 0.3\,\mathrm{dB\,km^{-1}}$, and an effective area of $A_{\mathrm{eff}} = 25\,\mu\mathrm{m}^2$. Unbalancing of the NOLM is achieved with an asymmetrically placed EDFA close to the loop coupler. The loop amplifier has the same noise figure as the in-line amplifiers.

Optimisation procedure

We use here a simple procedure to make the NOLM compatible with the DM line. This optimisation procedure is not exact, to the extent that it makes use of the cw assumption for the NOLM's transfer function; nevertheless it still gives a good estimate of the NOLM's characteristics imposed by the constraints of the DM scheme. We require two conditions to be satisfied. We make the NOLM operate in the stable region just after the first peak of the switching curve (cf. Eq. (3.1)),

$$\frac{\sigma(G-1)(1-1/g)}{4\gamma} P_{\mathrm{in}} = \pi(1+a), \quad 0 \le a < 1, \tag{3.2}$$

and we demand the pulse peak power at the starting point of the DM cycle to equal the peak power at the NOLM input. To fullfill these conditions, first we fix a suitable value for the loop length, $L = 3\,\mathrm{km}$ throughout this work. Then, from Eq. (3.2) we calculate the loop gain G for a given input power P_{in}, which is chosen as a reasonable peak power for the particular dispersion

map considered. Using this value of G in Eq. (3.1), we calculate

$$\frac{P_{\text{out}}}{P_{\text{in}}} = \frac{G}{2g}[1 + \cos(a\pi)] = \mu, \tag{3.3}$$

which is greater than 1 in the range of P_{in} used in our simulations, and we restore the peak power of pulses after the NOLM by the use of an attenuator with a power loss of $1/\mu$. The cw input-output power mapping of the NOLM is plotted in Fig. 3.9 for $P_{\text{in}} = 3.5\,\text{mW}$, which gives $G = 172.9$ (22.4 dB) and $1/\mu = 1/105.4$ (−20.2 dB). Here, $a = 1/3$.

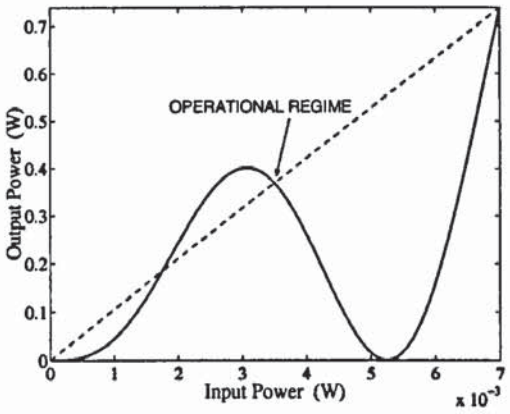

Figure 3.9: Cw switching curve of the NOLM.

We point out that we can equivalently use the loop length L as free parameter and fix $\mu = 1$ in Eq. (3.3), which releases the constraint of the power post-restoration. However, this results in very long loop lengths that are not practical. We also note that the value chosen for L is only an example, and changing the loop length is just a matter of rescaling G and μ.

3.4.2 Single pulse stabilization

We first demonstrate stabilization of single pulse propagation compared with the system without NOLMs. To simplify, no noise is added at the amplifiers in these simulations. Chirp-free Gaussian-shaped pulses are launched at the NOLM input (see Fig. 3.8), with different peak powers and pulse widths. An example of these pulses with a launch peak power of 3.5 mW and a FWHM of 5.0 ps is shown in Fig. 3.10 as it propagates over 7820 km. The pulse profile is taken at the NOLM input. Figure 3.10 also shows the same pulse at the starting point of the DM cycle as it propagates through the system without NOLMs. The effectiveness of the NOLM in stabilizing the pulses can be clearly seen. For the system without NOLMs, in fact, the pulse peak power decreases gradually with propagation distance, as the pulse width increases. This result was to be expected because the strength of the map used here, $S = 49$, is well outside the range where stable propagation of conventional DM solitons has been observed [44]. In other words, the considered propagation regime is quasi-linear. On the other hand, when NOLMs are incorporated into the system, the pulse settles to a steady state after a short initial transition distance. Figure 3.11 shows the pulse stabilization (at the NOLM input point) in the plane RMS pulse width - chirp (see their definition below). It can be seen that the asymptotic stable pulse corresponds to the fixed point (width = 2.4 ps, chirp = $-0.008\,\text{THz}^2$). The stationary

pulse peak power is 3.6 mW.

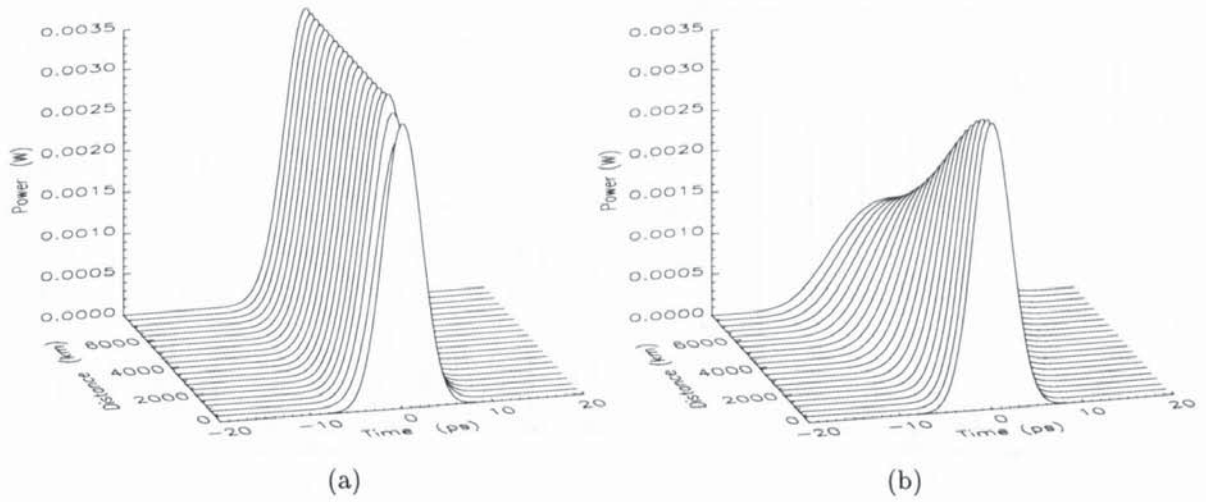

Figure 3.10: Propagation of a pulse with a launch peak power of 3.5 mW and a FWHM of 5.0 ps in the system (a) with NOLMs (plot taken at the NOLM input) and (b) without NOLMs.

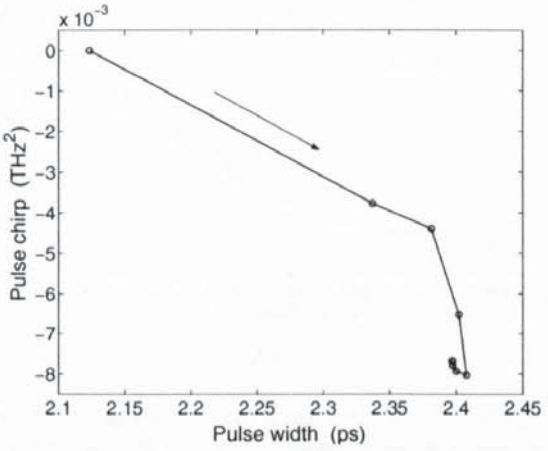

Figure 3.11: Acqusition of the steady state in the plane RMS pulse width - chirp.

The periodical deployment of NOLMs into the system changes the quasi-linear propagation regime into a stable autosoliton propagation regime, which is strictly nonlinear. This can be clearly seen from Fig. 3.12 that shows the evolution of the stationary RMS pulse width, chirp, and bandwidth over one period of the system (spacing between two consecutive NOLMs). The insets show the evolution of the same pulse characteristics over one period of the system without NOLMs (one dispersion map period). In both systems the pulse width breathes over a wide range, leading to a bit-overlapping regime in transmission of data at high bit-rates. From the bandwidth variation one may see that SPM does not significantly affect the pulse evolution in the system without NOLMs. Indeed, the net change in the bandwidth from the dispersion map is small (+0.05 %). On the other hand, in the system with NOLMs the pulse bandwidth exhibits a large net change within one NOLM span (−62 %), indicating that the pulse dynamics is nonlinear. Another interesting feature emerging from Fig. 3.12 is a gradual decrease in the amplitude of the chirp oscillations as the pulse covers the distance between two consecutive

NOLMs. This autosoliton dynamics is periodically reproduced at the output of each section.

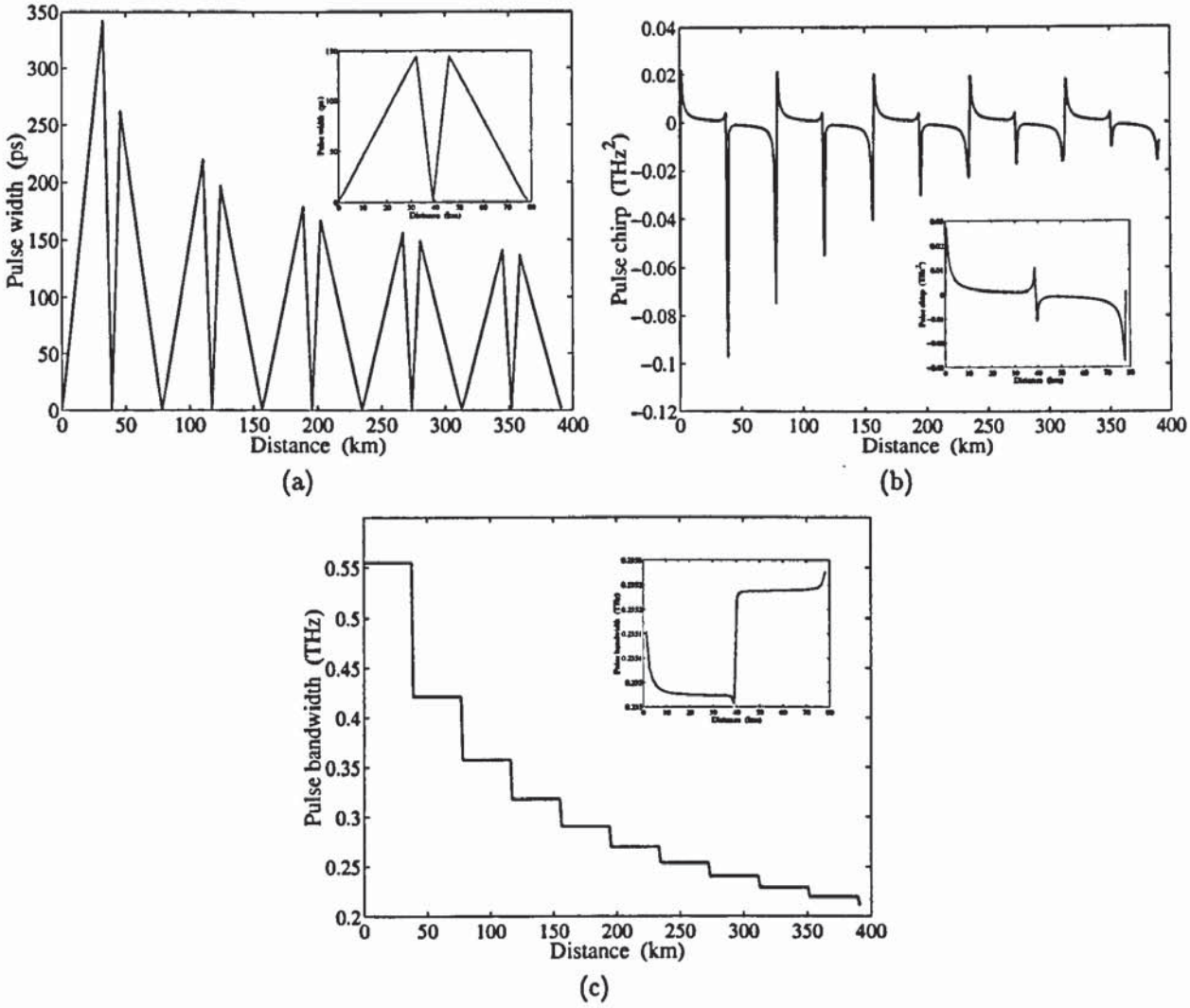

Figure 3.12: Evolution of the stationary RMS (a) pulse width, (b) chirp, and (c) bandwidth over one period of the system. Insets, evolution of the same quantities over one period of the system without NOLMs.

RMS quantities

The RMS pulse width τ, chirp C, and bandwidth Ω are defined as [63]

$$\tau = \left[\frac{\int \mathrm{d}t\, t^2|u|^2 - (\int \mathrm{d}t\, t|u|^2)^2}{\int \mathrm{d}t\, |u|^2}\right]^{1/2}, \quad C = \frac{\mathrm{Im}\int \mathrm{d}t\, u^2(u_t^*)^2}{\int \mathrm{d}t\, |u|^4},$$
$$\Omega = \left[\frac{\int \mathrm{d}\omega\, \omega^2|\hat{u}|^2 - (\int \mathrm{d}\omega\, \omega|\hat{u}|^2)^2}{\int \mathrm{d}\omega\, |\hat{u}|^2}\right]^{1/2}. \tag{3.4}$$

Here, u is the field amplitude and $\hat{u}$ its Fourier transform.

3.4.3 Transmission at 40 and 80 Gbit s^{-1}

Next we examine the system's performance at 40 and 80 Gbit s^{-1} data rate in terms of maximum propagation distance corresponding to a bit error rate (BER) of more than 10^{-9}. We estimate

here the BER by means of the standard Q-factor: $Q = (\mu_1 - \mu_0)/(\sigma_1 + \sigma_0)$, where $\mu_{1,0}$ are the mean levels of 1's and 0's and $\sigma_{1,0}$ are the standard deviations. If the levels of 1's and 0's are assumed to have a Gaussian distribution, $Q = 6$ is equivalent to a BER of 10^{-9}. The data stream is modelled by a pseudo-random binary sequence (PRBS) of length $2^6 - 1$ using Gaussian pulses with the stationary peak power, width, and chirp reached during single pulse propagation. The ASE noise is included in these simulations. The receiver is modelled by an optical filter with the same bandwidth as the in-line filters. The photodiode is modelled as a square law detector followed by a fourth-order Bessel-Thomson electrical filter with a cut-off frequency equal to the bit-rate. For each set of pulse parameters six simulations are performed for bit patterns with identical parameters and the instantaneous Q-factor is calculated as the mean value. The Q-factor is evaluated just before the NOLM location.

Study of the operating regime for passive regeneration and distance-unlimited transmission at 40 Gbit s^{-1}

An example of simulations at 40 Gbit s^{-1} is given in Fig. 3.13, which shows the evolution of the Q-factor over 40000 km transmission distance. Here, we used input pulses with a peak power of 3.5 mW and a FWHM of 5.0 ps, that give the best performance of the system without NOLMs. A maximum error-free transmission distance of approximately 3900 km is found without NOLMs. For the system with NOLMs the Q-factor stabilizes and does not degrade any furhter after a short distance. This result demonstrates that stable soliton transmission over practically unlimited distances at 40 Gbit s^{-1} is possible, where unlimited transmission means here that after some stage, the accumulation of noise and timing jitter through the transmission system is stabilized, yielding nondecaying Q-factor > 6.

Figure 3.14 shows the tolerance limits of this result to the parameters of the input pulses. It can be seen that 7.0 ps is the largest pulse width allowing for distance-unlimited transmission. For larger pulse widths, we observe long-distance transients in the evolution of Q, which are due to the growing effect of pulse-to-pulse interactions. For pulse widths less than 2.0 ps, the effect of timing jitter becomes more important. One may also see that a FWHM of 3.0 ps is the optimal initial pulse width for operation of the system investigated here, giving the widest range of allowed initial peak powers. We point out that for peak powers below the lower limit of the working region the Q-factor sharply drops below six after some distance, while for peak powers above the upper limit we observe a gradual decay in the evolution of Q. The mean value around which the stable Q-factor fluctuates against the input pulse peak power is plotted in Fig. 3.15 for the different input pulse widths considered here. It can be seen that for a given pulse width, increasing the allowed peak power produces an increase in the mean value of the stable Q. It is also clear from Fig. 3.15 that a 3.0 ps pulse width gives the best performance of the system in terms of the highest Q-value achievable.

An example of pattern dynamics and eye-diagrams of the 40 Gbit s^{-1} data signal is given in Figs. 3.16 and 3.17. This example corresponds to the set of initial pulse parameters of Fig. 3.13. Figure 3.16 shows the pattern propagation over 3900 km in the system without NOLMs, and over 40000 km in the system with NOLMs (plot taken at the NOLM input). For the system without NOLMs the eye-diagram is taken at the maximum transmission distance of 3900 km. One may see that the intra-channel FWM -induced amplitude noise dramatically affects the

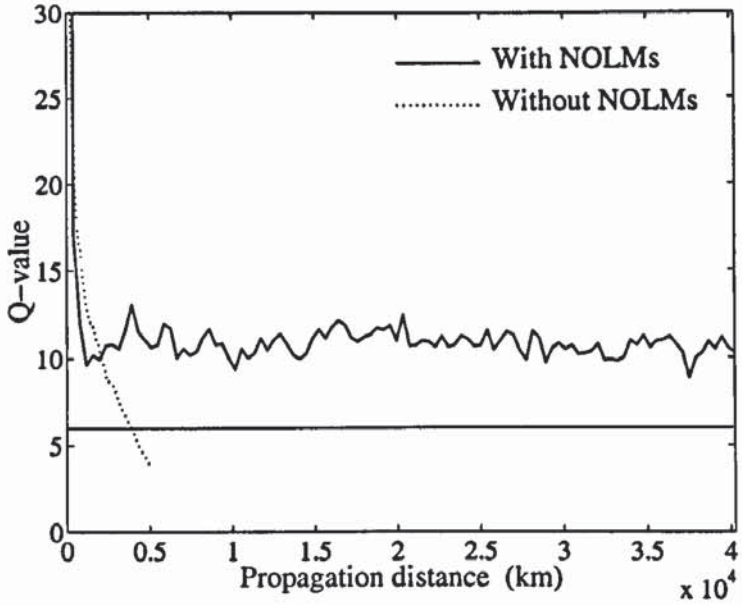

Figure 3.13: Q-values versus propagation distance for 40 Gbit s^{-1} transmission.

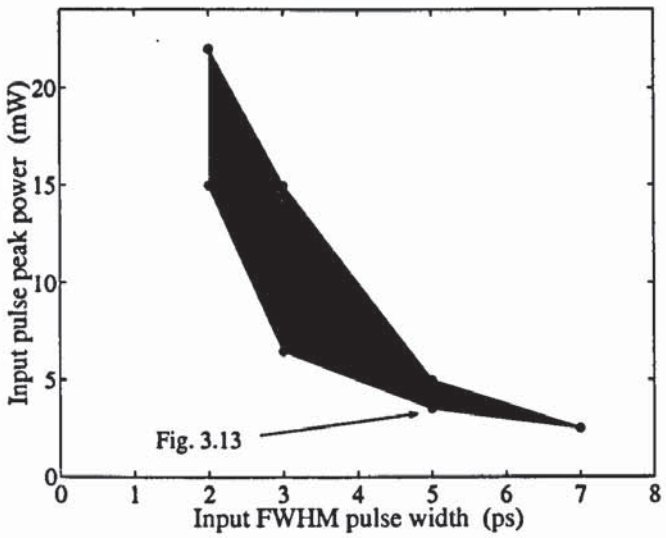

Figure 3.14: Limits of operation of the 40 Gbit s^{-1} system in the plane pulse width - peak power.

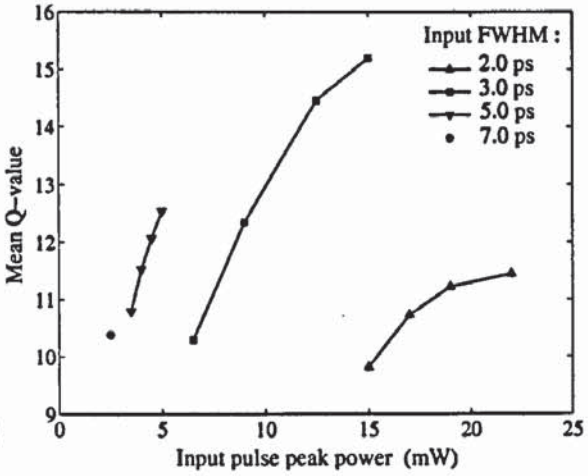

Figure 3.15: Mean value of the stable Q versus input pulse peak power.

quality of the transmission. For the system with NOLMs the eye-diagram is taken at the same distance and after 40000 km transmission. It is seen that the background is almost completely suppressed by the saturable absorption action of the NOLMs, and the amplitude jitter of ones is also slightly reduced, leading to an almost perfect restoration of the initial pattern at the end of transmission. The eye-diagram reveals that the system will eventually be dominated by timing jitter, but still at 40000 km the accumulation of timing jitter is not enough to produce degradation of the Q-factor.

As one may infer from the single pulse dynamics (cf. 3.4.2), the considered transmission regime is bit-overlapping. Indeed, for the initial pulse parameters of Fig. 3.13, the maximum FWHM pulse width, $\tau_{\mathrm{FWHM}}^{\mathrm{max}}$, ranges from 540 ps (first compensation period) to 310 ps (last compensation period) in one period of the system, and $\tau_{\mathrm{FWHM}}^{\mathrm{max}} \gg T = 25$ ps, where T is the bit

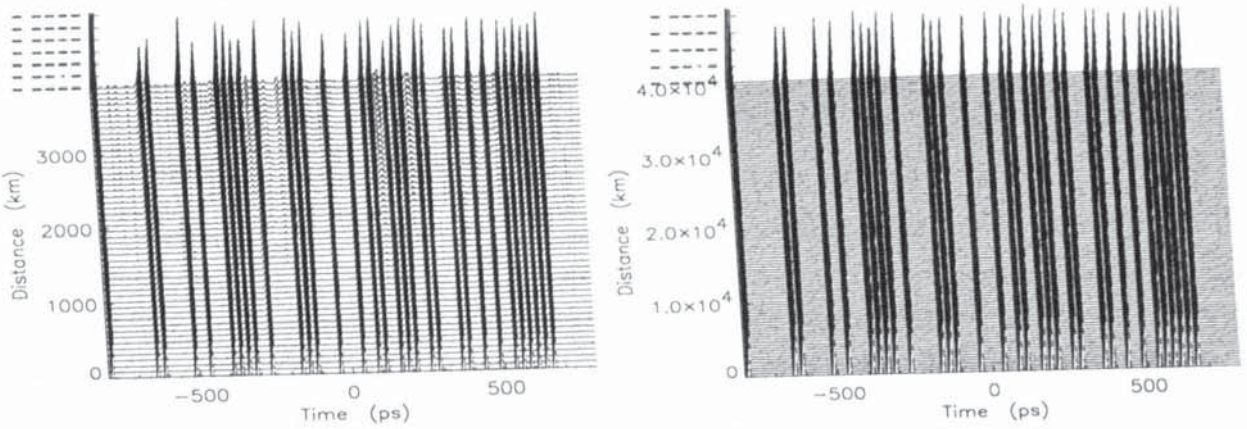

Figure 3.16: Propagation of a 40 Gbit s^{-1} $2^6 - 1$ PRBS (a) over 3900 km in system without NOLMs and (b) over 40000 km in system with NOLMs.

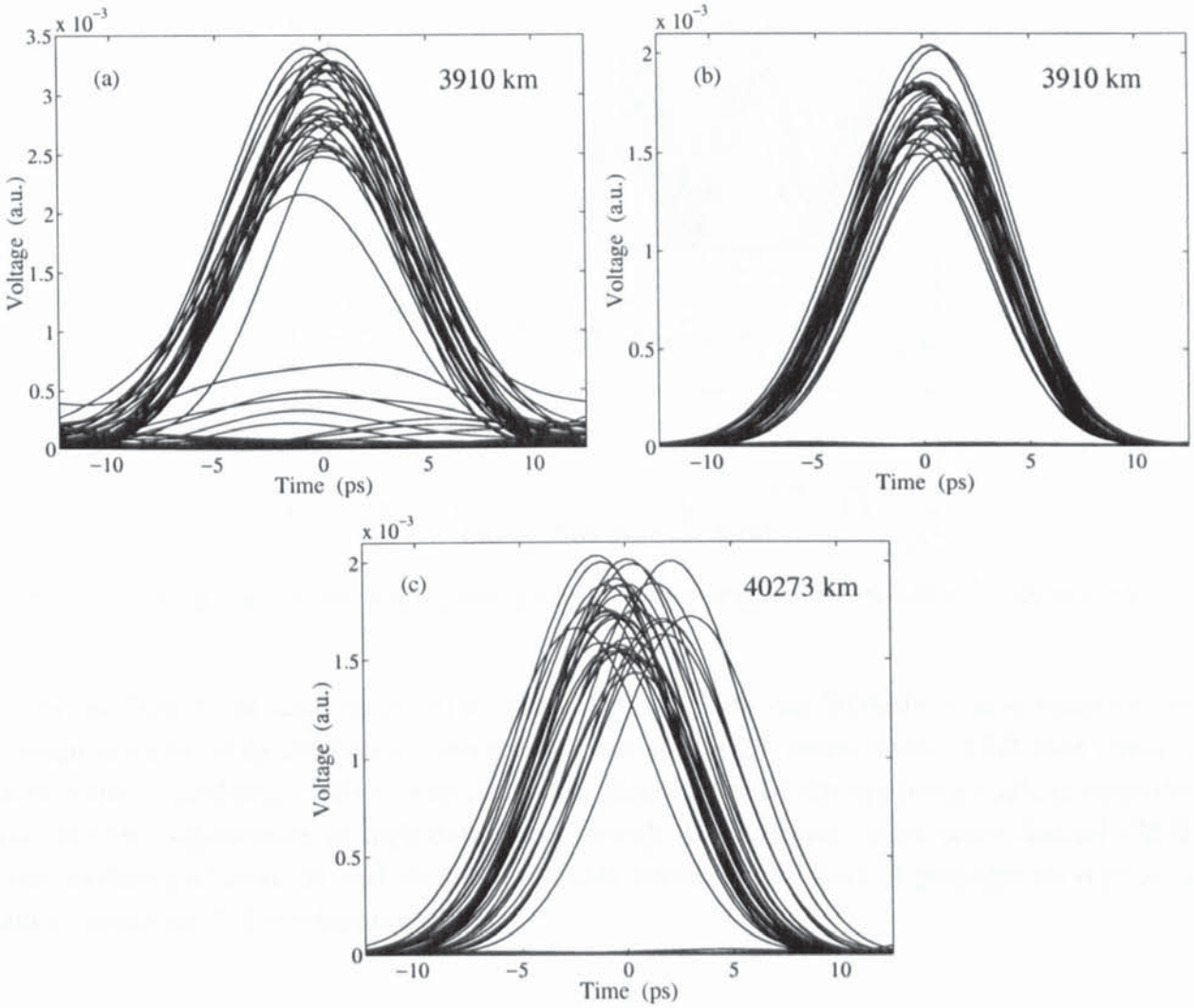

Figure 3.17: 40 Gbit s^{-1} data eye-diagrams in systems (a) without NOLMs and (b), (c) with NOLMs.

slot. The maximum number of overlapped pulses in one compensation period can be estimated as $N \simeq (2/5)f$ for a bit slot five times as large as the minimum FWHM, $f = \tau_{\mathrm{FWHM}}^{\mathrm{max}}/\tau_{\mathrm{FWHM}}^{\mathrm{min}}$ being

the expansion ratio. This gives N ranging from 43 to 25 in one period of the system. Therefore, we can say that the NOLMs stabilize the bit-overlapping transmission, through conversion of a quasi-linear mode of propagation into a nonlinear propagation regime.

Sample transmission at 80 Gbit s^{-1}

To demonstrate the potential of our technique, we also ran simulations at 80 Gbit s^{-1} data rate. An example is given in Fig. 3.18, which shows the evolution of the Q-factor with propagation distance and the eye-diagram after 40000 km transmission, for an input peak power of 6.5 mW and a pulse width of 3.0 ps. We point out that in this case the pulse parameters were not optimised. Even though passive regeneration of the data stream is still achievable after 40000 km. The long-distance transient in the evolution of Q is due to pulse-to-pulse interactions, that become more important at very high bit-rate, as the eye-diagram clearly shows.

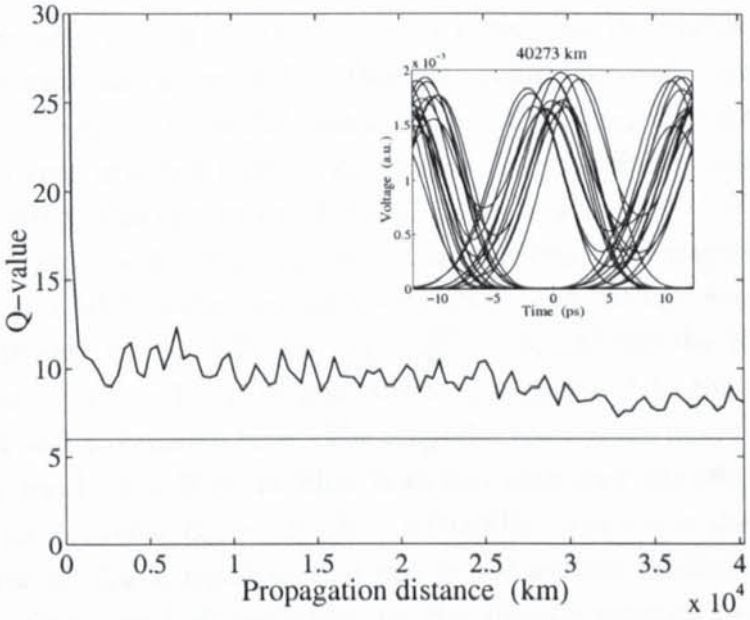

Figure 3.18: Q-value versus propagation distance and eye-diagram for 80 Gbit s^{-1} transmission.

In conclusion, we have demonstrated that the use of in-line NOLMs in DM transmission systems dominated by amplitude noise can achieve passive 2R regeneration of RZ data streams at bit-rates $\geq$ 40 Gbit s^{-1}. This is an indication that the use of this approach could obviate the need for full-regeneration in high data rate, strongly DM systems, when intra-channel FWM poses serious problems. In such systems, NOLMs impose a new kind of propagation regime: a stable, nonlinear, bit-overlapping regime.

3.5 Passive quasi-regeneration in transoceanic 40 Gbit s^{-1} RZ transmission systems with strong dispersion management

In this section we discuss the use of in-line NOLMs as a method of all-optical passive quasi-regeneration of bit streams in high-speed RZ transmission systems with strong dispersion man-

agement, when both intra-channel XPM and FWM are important limiting factors. We numerically demonstrate that the quasi-regeneration of signals performed by NOLMs dramatically improves the system's performance, allowing for 40 Gbit s^{-1} RZ transmission over transoceanic distances [115].

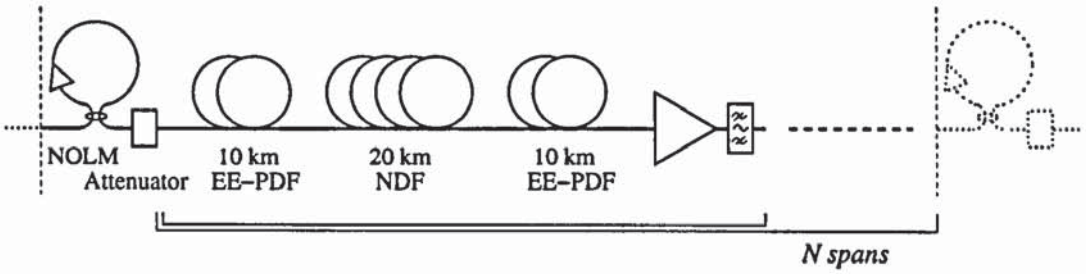

Figure 3.19: One period of the transmission system.

As a sample system for our study we used a symmetric dispersion map (see Fig. 3.19) similar to the experimental setup [129]. This dispersion flattened transmission scheme has been proved to be beneficial to WDM transmission. Each amplifier span consists of 20 km-long effective core area enlarged positive dispersion fibre (EE-PDF) and 20 km-long negative dispersion fibre (NDF). The dispersion $D^{(1)}$ and dispersion slope $S^{(1)} = \mathrm{d}D^{(1)}/\mathrm{d}\lambda$ of the EE-PDF are 20 ps (nm km)$^{-1}$ and 0.06 ps (nm^{2}km)$^{-1}$ respectively. The magnitude of dispersion and dispersion slope of the NDF is the same as the EE-PDF, and the sign is opposite. The effective area is $A_{\mathrm{eff}}^{(1)} = 110\,\mu\mathrm{m}^2$ for the EE-PDF and $A_{\mathrm{eff}}^{(2)} = 30\,\mu\mathrm{m}^2$ for the NDF. The attenuation is $\alpha^{(1)} = 0.2\,\mathrm{dB\,km}^{-1}$ in the EE-PDF and $\alpha^{(2)} = 0.24\,\mathrm{dB\,km}^{-1}$ in the NDF. Each span also includes an EDFA and a Gaussian filter. The amplifier has a noise figure of 4.5 dB and a power gain of 9 dB. The bandwidth B of the filter is chosen such that the effective system's FWHM bandwidth over one period is $B_{\mathrm{eff}} = B/\sqrt{n} = 0.093$ THz, where n is the number of filters per period. This value of B_{eff} is equal to that one of the system studied in Section 3.4 for the same pulse width. One period of the system, i.e. the distance between two consecutive NOLMs, amounts to N $(= n)$ amplifier spans. Characteristics and operation of the NOLM are the same as described in Section 3.4.

First single chirp-free Gaussian-shaped pulses are launched into the system, with a FWHM pulse width of 6.0 ps and different peak powers. We point out that the use of such a pulse width may ensure both a sufficient separation between carrier pulses for 40 Gbit s^{-1} transmission and a reasonably narrow spectral bandwidth, which is desirable for WDM applications. The NOLM allows for pulse stabilization (cf. 3.4.2). The stationary pulse peak power, width, and chirp reached during single pulse propagation are then used as input parameters for transmission of a $2^6 - 1$ PRBS data stream at 40 Gbit s^{-1}. The system's performance is examined in terms of maximum transmission distance corresponding to a Q-value of more than 6 (equivalent to a BER of 10^{-9}). The Q-factor is evaluated just before the NOLM location. An example of these simulations is given in Fig. 3.20. Here the spacing between NOLMs was 400 km ($N = 10$), and input pulses with a peak power of 1.5 mW were used. Figure 3.20 also shows the result achieved without NOLMs for the same input pulse parameters. It can be seen that the deployment of NOLMs extends the error-free transmission distance from 3000 km to 26400 km. Figure 3.21

shows the eye-diagrams of the 40 Gbit s^{-1} data signal for the systems without and with NOLMs. For the system without NOLMs the eye-diagram is taken at the maximum transmission distance of 3000 km. One may see that amplitude noise and timing jitter severely affect the quality of the transmission. For the system with NOLMs the eye-diagram is taken at the same distance and at the maximum transmission distance of 26400 km. It is seen that the background is almost completely suppressed by the action of the NOLMs, and the amplitude jitter of ones is also slightly reduced. One can also see that the eye is closed after 26400 transmission mainly due to a significant accumulation of timing jitter through the transmission system.

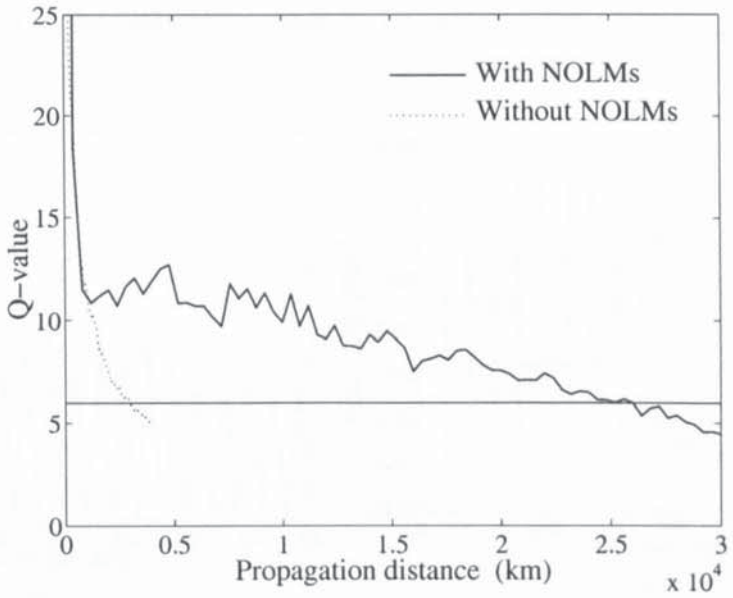

Figure 3.20: Q-values versus propagation distance.

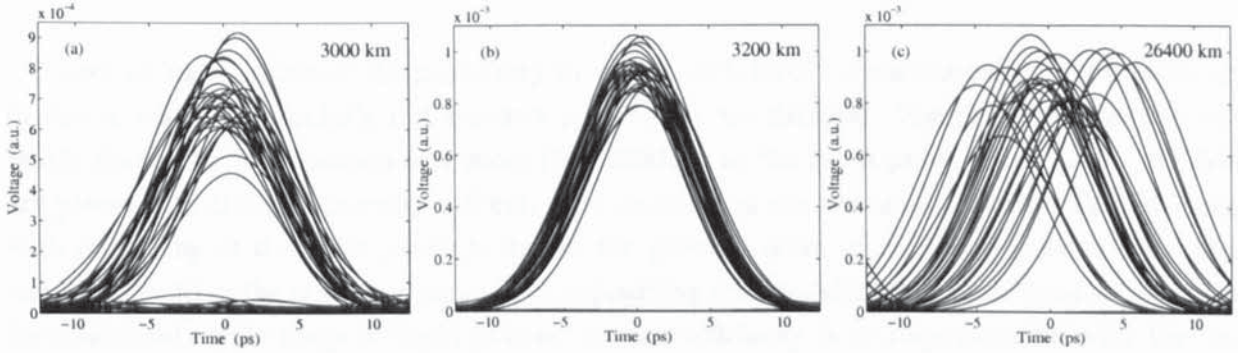

Figure 3.21: Eye-diagrams in systems (a) without NOLMs and (b), (c) with NOLMs.

We point out that under the same NOLM spacing of 400 km, with the same strength of filtering for the system, and for the same input pulse width, practically unlimited transmission was possible in the system studied in Section 3.4 (cf. Fig. 3.14), owing to a substantially lesser accumulation of timing jitter. As we have seen, in both systems strong dispersion management is used and the intra-channel FWM is a limiting factor in transmission performance. The saturable absorption action of in-line NOLMs efficiently suppresses this effect. Unlikely the

system reported in Section 3.4, the system studied here is also significantly affected by intra-channel XPM. A possible reason for such a behaviour may be inferred from the single pulse dynamics. Figure 3.22 shows the evolution of the stationary RMS pulse width, chirp, and bandwidth over one period of the system, for the same input pulse parameters of Fig. 3.12. From a comparison with Fig. 3.12, one may see that the pulse dynamics is qualitatively the same for the two configurations, but the pulse spreading is more than twice larger for the configuration in Section 3.4. This implies that adjacent pulses spend more time in a strong bit-overlapping regime. Following [107], the intra-channel XPM -induced frequency shift per unit distance is proportional to the time derivative of the interacting pulse's intensity. The derivative reduces with pulse broadening. Moreover, the sign of the derivative changes across the region of overlap so that the net effect of the interaction tends to be canceled out.

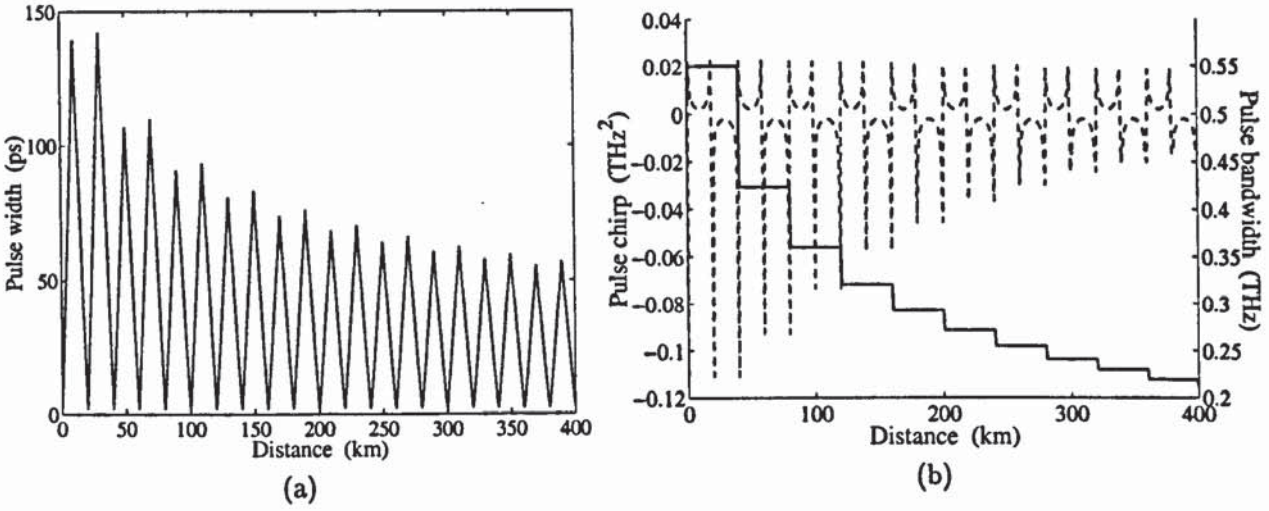

Figure 3.22: Evolution of the stationary RMS (a) pulse width, (b) chirp (dashed line), and bandwidth (solid line) over one period of the system.

Next we have examined the possibility to achieve 40 Gbit s^{-1} transmission over transoceanic distances when some pulse's and system's parameters are changed. Figure 3.23 shows the tolerable limits of a transmission over more than 9000 km to the input pulse power, when NOLMs are placed into the system every 400 km. The decrease in the maximum transmission distance with increasing of the pulse power is due to the growing effect of nonlinear interactions. The results show that the system is capable of supporting transmission over transoceanic distances for a relatively wide range of input powers. As cost efficiency is an important issue for the design of ultra-long transmission systems, it would be desirable to utilize the minimum number of NOLMs necessary to achieve a given transmission distance. Figure 3.24 shows the tolerance of a transoceanic transmission to the spacing between two consecutive NOLMs. We point out that in this case the pulse parameters were not optimised. The decrease in the transmission distance with increasing of the NOLM separation was to be expected, because the signal reshaping is less frequent during transmission. The relative flatness of the last part of the curve is of interest because it shows that a transmission distance of more than 9000 km is achievable with a NOLM separation of 600 - 700 km, which means by deploying only about fifteen NOLMs or even less in the system.

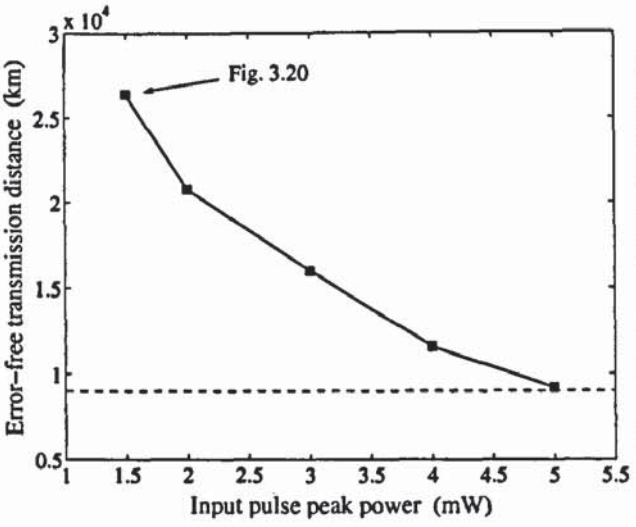

Figure 3.23: Maximum error-free transmission distance versus input pulse peak power.

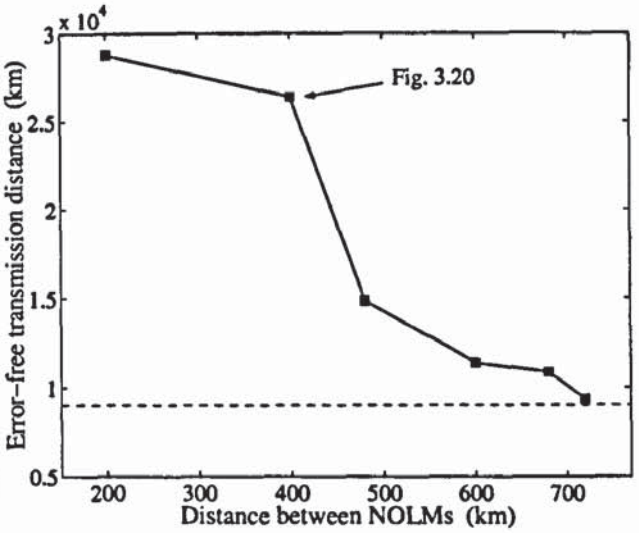

Figure 3.24: Maximum error-free transmission distance versus distance between NOLMs.

In conclusion, we have demonstrated that the all-optical quasi-regeneration method based on the use of in-line NOLMs may enable transoceanic transmission distances in 40 Gbit s^{-1} RZ strongly DM systems limited by both timing jitter and amplitude noise.

3.6 Passive regeneration scheme for 40 Gbit s^{-1}-based WDM dispersion-managed RZ transmission

Increasing the channel bit-rate of WDM systems to 40 Gbit s^{-1} and beyond offers a number of advantages, including an increased link capacity and a reduced number of channels required to achieve a given capacity. Such systems will be required to operate over the SMF most commonly installed in current networks. To date, 20 Gbit s^{-1}-based WDM experiments with a total capacity of 1 Tbit s^{-1} over a few thousand km have been reported using a combination of conventional SMF and dispersion slope compensating fiber [130, 131]. 40 Gbit s^{-1}×16 channel WDM transmission over 1000 km through a DM SMF-based line without active modulation has also been experimentally demonstrated [132]. Ultra-long, high capacity transmission over SMF is still a challenge to be resolved. It has been shown recently that appropriate filtering is a promising technique that enables substantial advance in improving the performance of 40 Gbit s^{-1} WDM systems [133]. In this section we propose a technique of all-optical passive 2R regeneration for 40 Gbit s^{-1} WDM RZ transmission based on specially designed WDM guiding filters and in-line NOLMs [116, 117]. In Section 3.4 we have demonstrated the feasibility of distance-unlimited transmission of a 40 Gbit s^{-1} single-channel data signal over SMF without active control. The key to success was the loop mirror intensity filtering action, that allowed for regeneration of pulse amplitude and shape. Here we describe the application of 40 Gbit s^{-1} DM transmission guided by NOLMs to a WDM scheme. A study of two channel transmission is presented in 3.6.2 [116]. The potential of the proposed technique is revealed by examples of ultra-long transmission with a channel spacing of 300 and 150 GHz. The tolerance of the system's performance to the input pulse parameters is also investigated. In 3.6.3 we apply

numerical modelling to system optimisation and we investigate the flexibility of the technique by extending its application to N channel transmission [117]. As an outcome, the feasibility of 150 GHz-spaced×16 channel transmission over 25000 km of SMF is demonstrated.

3.6.1 Modelled system

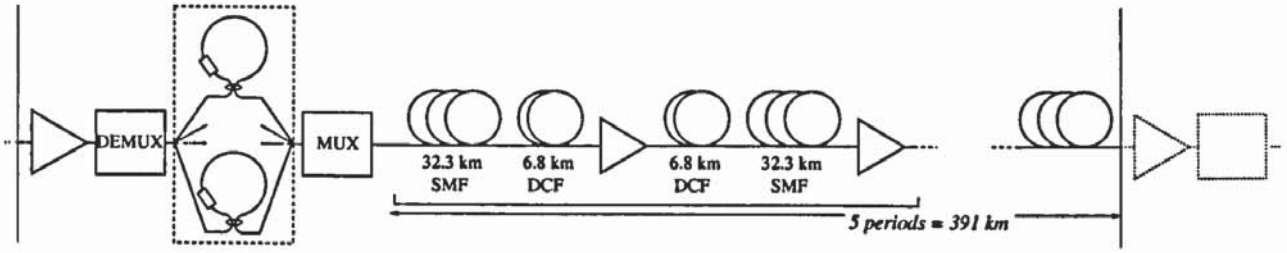

Figure 3.25: One element of the periodic WDM transmission system.

The WDM transmission scheme used for demonstration of the technique is depicted in Fig. 3.25. This configuration is similar to the single-channel transmission scheme reported in Section 3.4, except that we use here one NOLM for each channel. This avoids XPM-induced wave distortion inside the loop mirror. The dispersion map is fully described in Section 3.4. The EDFA has a noise figure of 4.5 dB and a power gain of 11.6 dB. An identical NOLM for each channel is placed into the transmission line every five periods of the dispersion map. The loop fibre has the same characteristics as described in Section 3.4. Unbalancing of the NOLM is achieved here with an asymmetrically placed attenuator close to the loop coupler. We require that the NOLM operates in the region just after the first peak of the switching curve and we demand the output power to equal the input one. These two conditions are satisfied by choosing the power loss Δ of the loop attenuator and adding an extra-gain G' to the amplifier immediately preceding the NOLM. Note that this NOLM's configuration is equivalent to the amplifier-unbalanced configuration of Section 3.4 (cf. Section 3.2). Moreover, we remove here the power post-restoration by properly adjusting the pre-amplification.

The demultiplexer and multiplexer placed before and after the NOLM respectively are modelled by optical filters. For a 300 GHz channel spacing, we use super-Gaussian filters with an amplitude transfer function $f(\nu) = \exp[-((\nu-\nu_k)/\Delta\nu)^6]$, where k is the channel number. When narrowing the channel spacing to 150 GHz it is preferable to employ filters with very sharp edges, to enable a clean separation between the channels. To keep at the same time a filter guiding action, we use in this case specially designed filters with an amplitude transfer function

$$f(\nu) = \exp\left[-\left(\frac{\nu-\nu_k}{\Delta\nu'}\right)^{14} - \left(\frac{\nu-\nu_k}{\Delta\nu''}\right)^{2}\right]. \tag{3.5}$$

Such a design, in fact, enables filters to perform simultaneously two functions: WDM channel separation and channel guiding. Indeed, the super-Gaussian part of the transfer function provides for sharp edges, while the Gaussian part allows for a guiding top (see Fig. 3.26). The value of 14 for the parameter controlling the degree of edge sharpness in (3.5) is chosen after performing a number of simulations.

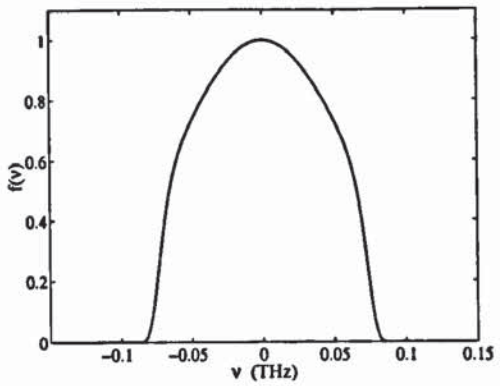

Figure 3.26: WDM filtering for 150 GHz channel spacing.

3.6.2 Two channel transmission

First we describe the application of the proposed technique to two channel transmission without performing any system optimisation. An in-line optical filter following each amplifier is used in these simulations just to limit the bandwidth of the noise. It is Gaussian-shaped and has a FWHM bandwidth of $B = 1.06\,\mathrm{THz}$. The bandwidths of the WDM filters are $\Delta\nu = 0.14\,\mathrm{THz}$ ($B = 0.235\,\mathrm{THz}$) for 300 GHz channel spacing, and $\Delta\nu' = 0.075\,\mathrm{THz}$ ($B = 0.139\,\mathrm{THz}$) and $\Delta\nu'' = 0.09\,\mathrm{THz}$ ($B = 0.106\,\mathrm{THz}$) for 150 GHz channel spacing.

An example of single pulse propagation in the 150 GHz-spaced channels WDM system is shown in Fig. 3.27. On the top, the pulse stabilization at the NOLM input point is shown. Here, the pulse is centered on $t = 0$ and the centre frequency of the in-line filters is correspondingly shifted. On the bottom, the evolution of the stationary pulse characteristics over one period of the system is illustrated. It is interesting to note that the WDM filtering significantly modifies the pulse dynamics, if compared to the dynamics in the single-channel transmission system that is shown in Fig. 3.12.

Each of the two channels carries a $40\,\mathrm{Gbit\,s^{-1}}$ 2^6-1 PRBS data stream using Gaussian pulses with the stationary peak power, width, and chirp reached during single pulse propagation. The launch point is the input of the amplifier preceding the NOLM. The cut-off frequency of the electrical filter at the receiver is 40 GHz as for single-channel transmission. The Q-factor for each channel is evaluated just before the NOLM location. An example of the system's performance for 300 GHz-spaced two channel transmission is given in Fig. 3.28, which shows the evolution of the Q-factor for both channels over 40000 km transmission distance. Here the pulse's parameters at the launch point were 0.33 mW peak power (corresponding to 3.9 mW at the starting point of the DM cycle), 4.2 ps FWHM pulse width, and $-0.003\,\mathrm{THz}^2$ chirp, the power loss of the loop attenuator was $\Delta = -18.7\,\mathrm{dB}$, and the extra-gain of the amplifier preceding the NOLM was $G' = 21.8\,\mathrm{dB}$. Figure 3.28 demonstrates that passive regeneration of both channels is still achievable after 40000 km transmission.

Figure 3.29 shows an example of the transmission performance with 150 GHz-spaced two channels. In this example input pulses with a peak power of 0.13 mW (corresponding to 1.8 mW at the starting point of the DM cycle), a FWHM of 9.1 ps, and a chirp of $-0.004\,\mathrm{THz}^2$ were used, and the in-loop attenuation and the pre-amplification were $\Delta = -21.7\,\mathrm{dB}$ and $G' = 26.2\,\mathrm{dB}$ respectively. It can be seen that an error-free transmission distance of 25000 km is possible for both channels. To see if the WDM performance is limited by single-channel performance,

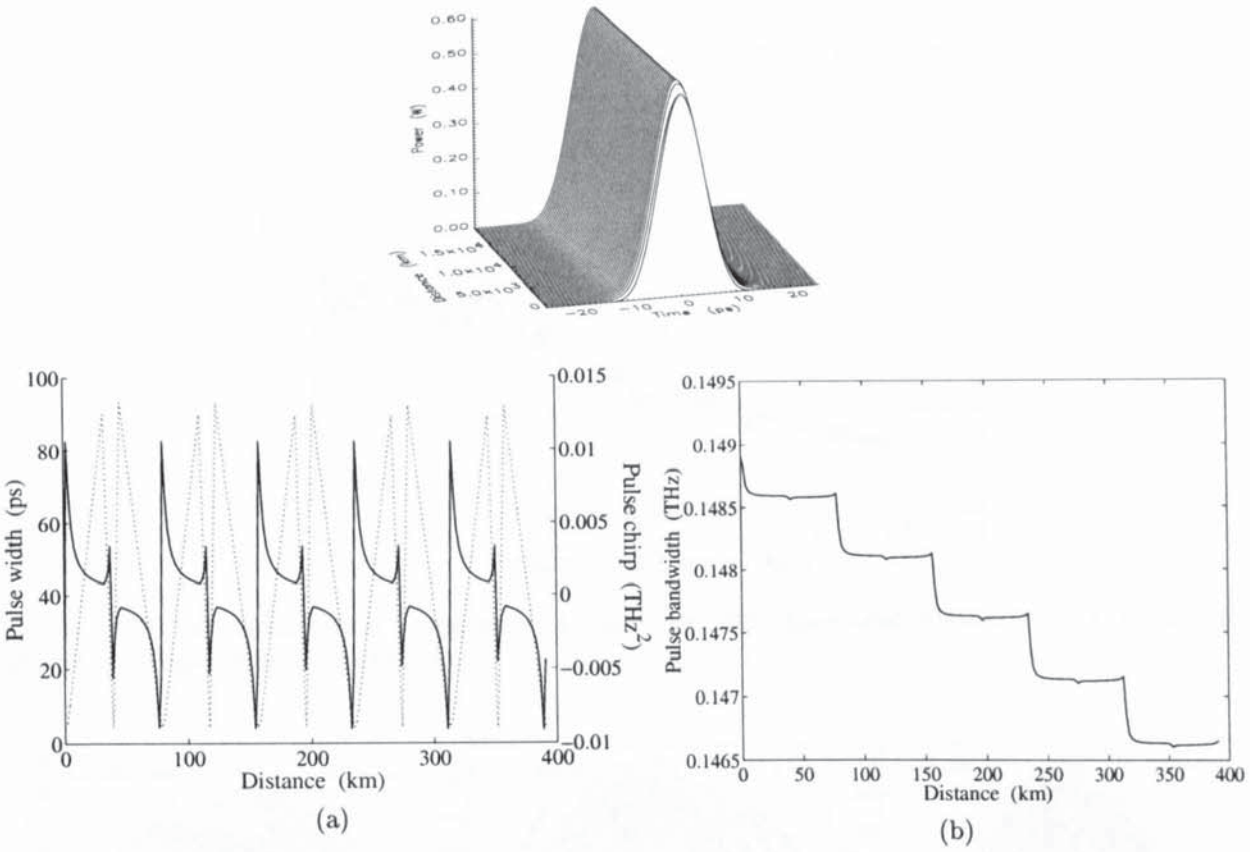

Figure 3.27: Single pulse propagation in the 150 GHz-spaced channels WDM system. Top, pulse stabilization at the NOLM input point. Bottom, evolution of the stationary RMS (a) pulse width (dotted line) and chirp (solid line), and (b) bandwidth over one period of the system.

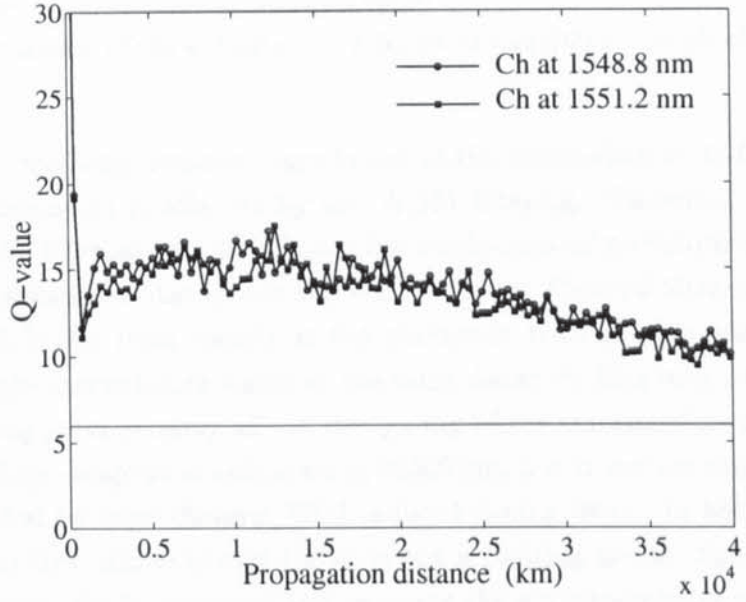

Figure 3.28: Q-values versus propagation distance for 300 GHz-spaced-40 Gbit s^{-1}×2 WDM transmssion.

we switched off one of the two channels and transmitted the other one through the WDM system. In this case an error-free transmission over 38700 km was possible (see Fig. 3.29). This result demonstrates that the WDM transmission performance is mainly limited by inter-channel

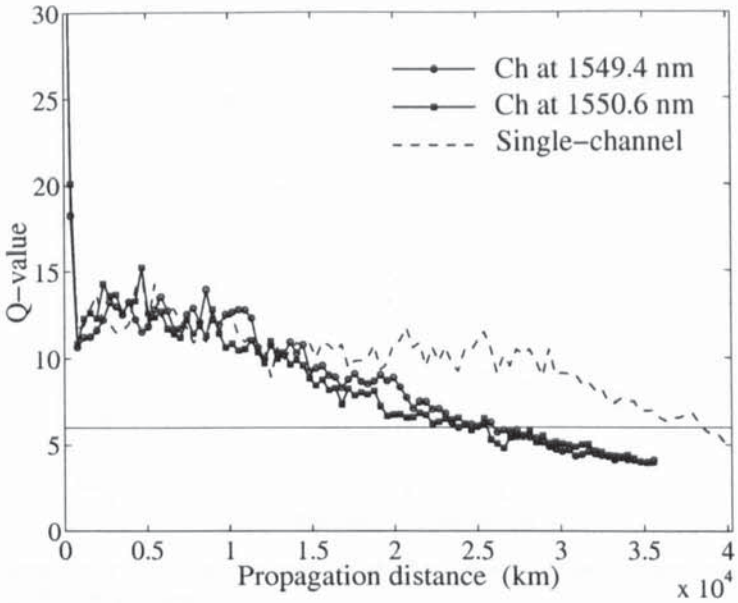

Figure 3.29: Q-values versus propagation distance for 150 GHz-spaced-40 Gbit s^{-1} × 2 WDM and 40 Gbit s^{-1} single-channel transmission.

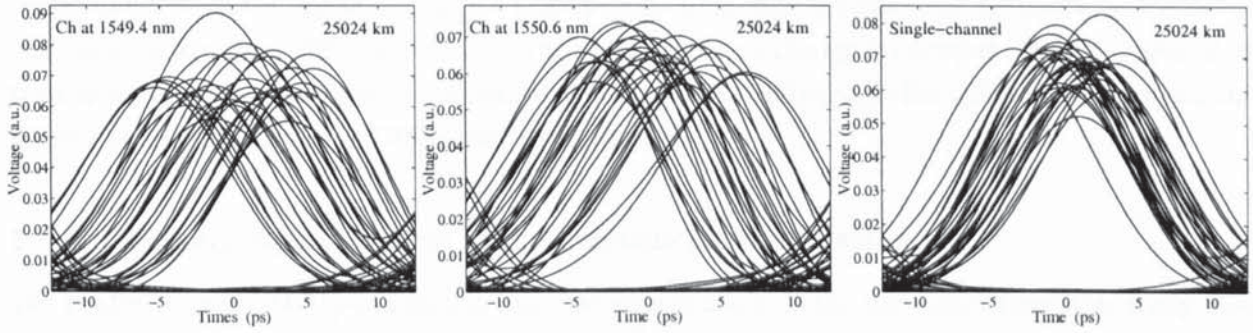

Figure 3.30: Eye-diagrams of the 40 Gbit s^{-1} × 2 WDM and 40 Gbit s^{-1} single-channel data signals.

crosstalk. However, the long-distance degradation of the single-channel Q-factor indicates that single-channel transmission is affected by the WDM filtering. Therefore, we expect that by optimising the WDM filtering we can enhance the single-channel performance and consequently also increase the transmission distance in the WDM system. Figure 3.30 shows the eye-diagrams of the two channel WDM data signals at the maximum transmission distance, and the eye-diagram of the single-channel data signal at the same distance. One may see that inter-channel XPM-induced timing jitter severely affects the quality of the transmission in the WDM system. The single-channel eye-diagram is still open at 25000 km, but it reveals that the system will be eventually dominated by intra-channel XPM-induced timing jitter. In both WDM and single-channel systems, in fact, intra-channel FWM is not a limiting factor, due to the action of the NOLMs in suppressing the background and reducing the amplitude jitter of ones.

Next we examine the tolerance of the performance of the 150 GHz-spaced channels system to the parameters of the input pulses. We remark that the stationary pulse width for the system is strictly fixed by the system's filtering. Indeed, we find that for a given input power, the FWHM pulse width at the launch point stabilizes on 9.1 ps during single pulse propagation, for any initial width. This allows, in principle, for a wide range of launch pulse widths to be used

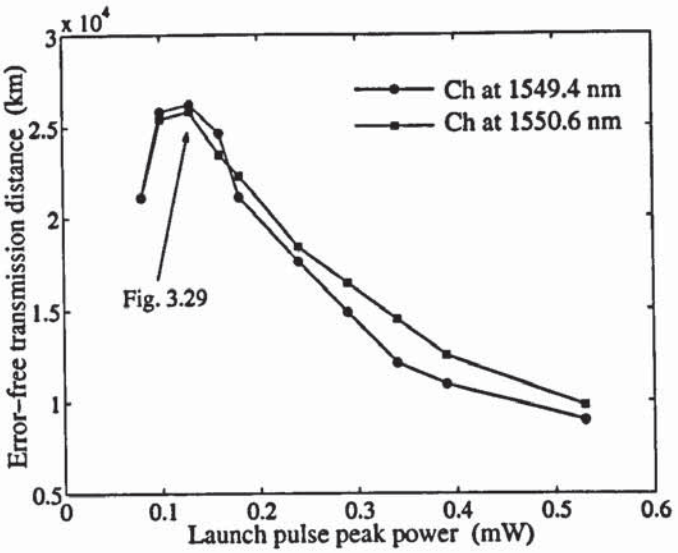

Figure 3.31: Maximum error-free transmission distance versus launch pulse peak power for 150 GHz-spaced-40 Gbit s^{-1} × 2 WDM system.

in WDM transmission. Figure 3.31 shows the maximum error-free transmission distance for both channels versus the launch pulse peak power. One may see that the system's performance degrades by less than 20% for ±40% power deviation from the optimal value. It is also seen that transmission over a transoceanic distance of 9000 km is still possible for both channels when the launch power deviates of +310% from its optimum.

3.6.3 System optimisation and N channel transmission

We analyse here 150 GHz-spaced× N channel transmission. One may infer from the study presented in the previous paragraph that a good system's performance depends sensibly on the proper balance between the edge-cutting and the guiding effects of the WDM filtering. Therefore, we perform here an optimisation of the ratio $\Delta\nu'/\Delta\nu''$ for the filter transfer function (3.5). Moreover, in the present study we remove the in-line filters to avoid channel asymmetry effects when increasing the number of channels. In addition, the bandwidth of the electrical filter at the receiver is set to 25 GHz which is chosen after performing a range of simulations.

Figure 3.32 shows the maximum error-free transmission distance for each channel as a function of the ratio $\Delta\nu'/\Delta\nu''$ for four channel WDM transmission. Here $\Delta\nu'$ was set to 0.075 THz, corresponding to a FWHM bandwidth of $B = 0.139$ THz which is slightly less than the channel spacing, and $\Delta\nu''$ was allowed to vary. It can be seen that a transmission distance of more than 30000 km is possible for all channels when $\Delta\nu'/\Delta\nu''$ is equal to 0.9375.

Figure 3.33 shows the Q-value evolution for four channel WDM and single-channel transmission, using the optimal WDM filtering. In this example input pulses with a peak power of 0.14 mW (corresponding to 1.7 mW at the starting point of the DM cycle), a FWHM of 9.4 ps, and a chirp of -0.005 THz^2 were used. One may see that single-channel transmission over practically unlimited distances is possible in the optimised WDM system. This result corresponds to the result reported in Section 3.4 using a single-channel transmission scheme, and indicates that the WDM performance is only affected by inter-channel effects. Figure 3.33 also shows the eye-diagram of one of the four channels at the maximum transmission distance and the single-channel

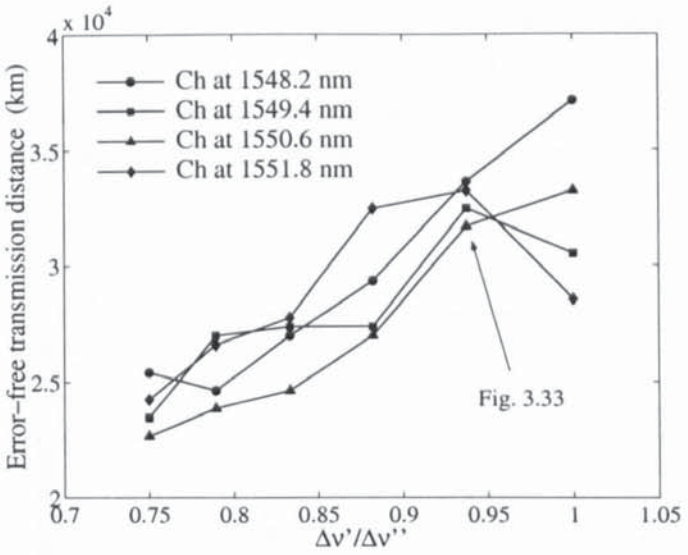

Figure 3.32: Maximum error-free transmission distance versus $\Delta\nu'/\Delta\nu''$ for 150 GHz-spaced-40 Gbit s^{-1} × 4 WDM system.

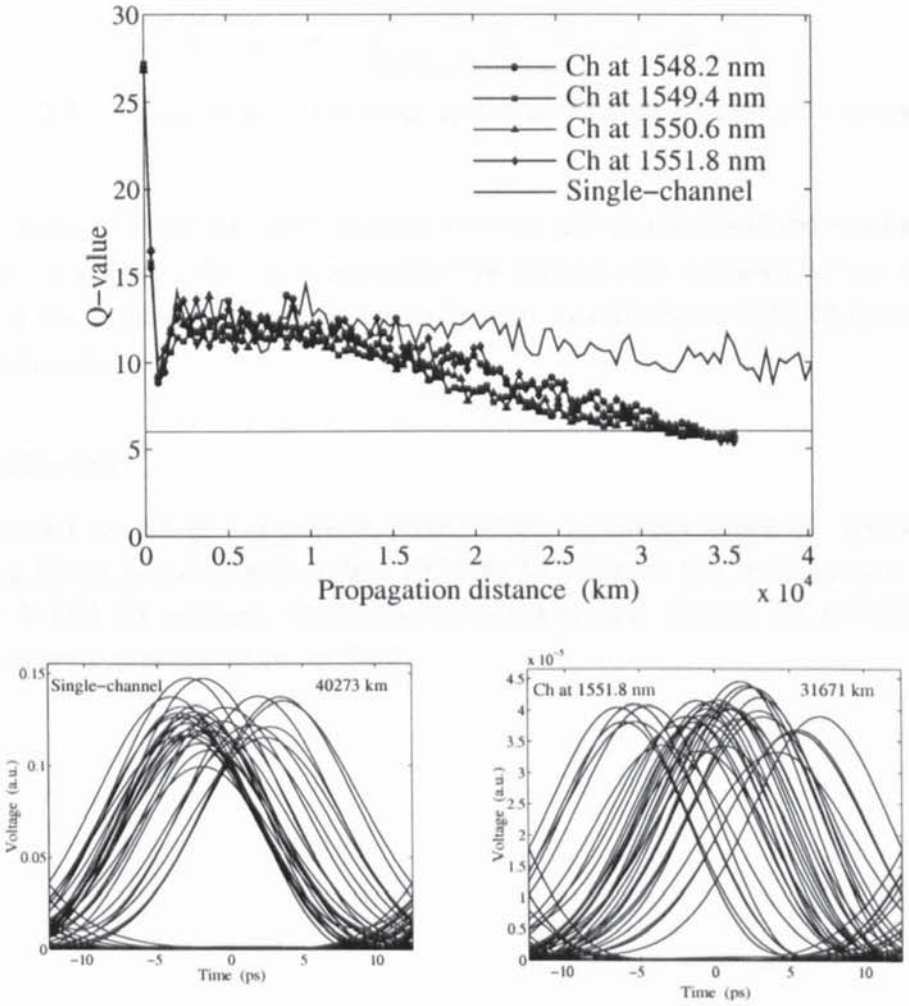

Figure 3.33: Q-values and eye-diagrams for 150 GHz-spaced-40 Gbit s^{-1} × 4 WDM and 40 Gbit s^{-1} single-channel transmission.

eye-diagram after 40000 km transmission. It is seen that the WDM transmission performance is mainly degraded by inter-channel XPM -induced timing jitter. The single-channel eye-diagram is still open at 40000 km, showing that the accumulation of intra-channel timing jitter through the transmission system is not enough at this stage to produce a significant degradation of the Q-factor.

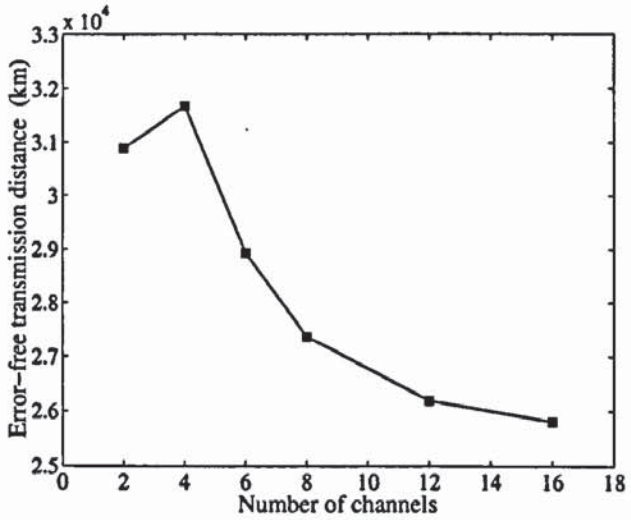

Figure 3.34: Maximum error-free transmission distance versus number of channels.

To demonstrate the flexibility of the proposed technique, we increased the number of channels up to 16. Figure 3.34 shows the maximum error-free transmission distance for the worst channel as a function of the number of channels. It can be seen that 16 channel WDM transmission over 25000 km is achievable.

3.6.4 Conclusion

We have proposed an all-optical passive regeneration technique based on specially designed WDM guiding filters coupled with in-line NOLMs to enhance the transmission performance of 40 Gbit s^{-1} WDM RZ systems. Optimisation of the system allowed for 150 GHz-spaced×16 channel transmission over 25000 km of SMF.

Chapter 4

On the theory of self-similar parabolic optical solitary waves

4.1 Introduction

Self-similarity is a fundamental physical property that has been studied extensively in many areas of physics [84]. In optics, self-similarity techniques have recently been applied to study pulse propagation in normal-dispersion fibre amplifiers. It has been shown that linearly chirped parabolic pulses are approximate self-similar solutions of the NLS equation with gain in the high-intensity limit [90]. These results have been confirmed experimentally [91] and have extended previous theoretical and numerical studies of parabolic pulse propagation in optical fibres [2, 92]. As described in Chapter 1, the generation of high-power self-similar parabolic pulses from fibre amplifiers is of fundamental interest because, aside from its being a further example of self-similar phenomenon in optics, it has wide-ranging practical significance. Indeed, parabolic pulses have potential in ultrafast optics because their linear chirp leads to highly efficient pulse compression [94]. Moreover, they propagate self-similarly in normally dispersive fibre, allowing for highly nonlinear propagation over substantial fibre lenghts without optical wave-breaking [2, 91].

The derivation of parabolically-shaped solutions in [2, 90] is based on the assumption that the linear dispersive term in the equation for the field amplitude is negligible as compared to the nonlinear term, similar to the quasi-classical approximation in quantum mechanics. Though the central core of the solution has already been described in the literature for some physical problems [2, 90], a comprehensive theory has not been presented yet. This chapter is devoted to a detailed mathematical analysis of the solutions of the NLS equation with gain and normal dispersion [134]. The starting point is the analysis of the evolution in the plane time-distance of a parameter defined as the ratio of the linear term to the nonlinear one. This allows us to define three regions on the time axis, that correspond to the core, the tails, and a narrow transition zone in the temporal profile of the asymptotically propagating pulse in the amplifier. The NLS equation is then solved in each of these regions. Specifically, in the inner region the quasi-classical approximation is applied to find a self-similar solution with a parabolic temporal profile. In the outer region we solve the linearized NLS equation. The quasi-classical parabolic solution in the central part is then matched to the linear one through the small intermediate transition region. Following [135], the equation for the field amplitude in the transition region can be reduced to the second Painlevé equation (P_{II}). The asymptotic behaviours of the Painlevé transcendents and the connection problems for the Painlevé equations have been considered in

many works (see e.g. [136]-[142] and references therein). Here, by using the asymptotic results for P_{II} we solve the amplitude matching problem. The construction of the solutions is completed by matching the phase of the field. Our analysis justifies the intuitive assumption made in [2, 90], the parabolic approximation for the pulse shape proving to be valid in the central part of the asymptotic pulse. Moreover, it gives a full description of the shape and the main features of high-power pulses generated in an amplifying medium.

The chapter is organized as follows. First, we present the basic model governing optical pulse propagation in an amplifying medium. In Section 4.3, we review the derivation of self-similar parabolic solutions of the NLS equation in the high-intensity limit, and compare these solutions with the results of numerical simulations. In Section 4.4, we formulate and analytically solve the matching problem. The solutions constructed in this way are shown to reproduce accurately the pulse features observed through numerical simulations. A summary of the results is presented in the concluding section.

4.2 Basic equations

Consider localized optical pulse evolution in an amplifying medium in the absence of gain saturation and for incident pulses with spectral bandwidths less than the amplification bandwidth. Such an analysis is well suited to describe experiments in which high-gain broadband rare-earth fibre amplifiers are used [91, 94]. In this case, pulse propagation can be described by the NLS equation with gain term [143]:

$$i\psi_z - \frac{\beta_2}{2}\psi_{tt} + \sigma|\psi|^2\psi = i\frac{g(z)}{2}\psi, \tag{4.1}$$

where $\psi(z,t)$ is the slowly varying pulse envelope in co-moving system of coordinates, β_2 and σ are the group-velocity dispersion and nonlinearity parameters, respectively, and $g(z)$ is the gain profile along the fibre. We are looking for a solution of Eq. (4.1) of the form

$$\psi(z,t) = a(z)F(\eta,\xi)e^{iC(z)t^2}, \tag{4.2}$$

where new self-similar variables are introduced as

$$\xi = \frac{t}{\tau(z)}, \qquad \frac{\mathrm{d}\eta}{\mathrm{d}z} = \sigma a^2(z). \tag{4.3}$$

Here, $a(z)$ has the same dimensions as $\psi(z,t)$ and describes the evolution of the peak amplitude of the pulse with distance, $\tau(z)$ is a characteristic width, $C(z)$ is a chirp parameter, and $F(\eta,\xi)$ is a normalized, dimensionless function that describes the evolution of the temporal profile through its ξ-dependence; we also allow for an η-dependence to account for contributions to the peak amplitude and the phase. Transformations (4.2) and (4.3) yield coupled equations for a, τ, C, and F:

$$\frac{a_z}{a} = \beta_2 C + \frac{g}{2}, \tag{4.4}$$

$$\frac{\tau_z}{\tau} = -2\beta_2 C, \tag{4.5}$$

$$(C_z - 2\beta_2 C^2)\tau^2 = -\lambda\sigma a^2, \tag{4.6}$$

$$iF_\eta + (|F|^2 + \lambda\xi^2)F - \frac{1}{c(\eta)}F_{\xi\xi} = 0, \qquad c = \frac{2\sigma a^2\tau^2}{\beta_2}, \tag{4.7}$$

where λ is an arbitrary parameter, related to the pulse power. Eqs. (4.4)-(4.6) can be rewritten to yield the relation between a and τ:

$$a^2(z)\tau(z) = a^2(z_0)\tau(z_0)\exp\left[\int_{z_0}^{z} \mathrm{d}z'\, g(z')\right], \tag{4.8}$$

and a second-order equation for τ:

$$\tau_{zz} = \frac{2\beta_2\sigma\lambda a^2}{\tau}, \tag{4.9}$$

subject to the additional boundary condition $(\tau_z)_{z=z_0} = -2\beta_2 C(z_0)\tau(z_0)$. Here z_0 is any initial point.

We separate F into a real amplitude A and a phase Φ, according to

$$F(\eta,\xi) = A(\eta,\xi)e^{i\Phi(\eta,\xi)}, \tag{4.10}$$

to obtain from Eq. (4.7) the "hydrodynamical" system of equations:

$$(A^2)_\eta - \frac{2}{c(\eta)}(A^2\Phi_\xi)_\xi = 0, \tag{4.11a}$$

$$\Phi_\eta + \frac{1}{c(\eta)}\left[\frac{A_{\xi\xi}}{A} - (\Phi_\xi)^2\right] - (A^2 + \lambda\xi^2) = 0. \tag{4.11b}$$

4.3 High-intensity parabolic pulses

First, we consider a possibility of an approximate description of the energy-containing core. Let us define a parameter ϵ as the ratio of the linear dispersive term to the nonlinear term in Eq. (4.11b):

$$\epsilon(\eta,\xi) = \left|\frac{A_{\xi\xi}}{c(\eta)A^3}\right|. \tag{4.12}$$

In this section we concentrate on the propagation properties of high-intensity pulses, or in other words, solutions for which the following condition is satisfied:

$$\epsilon \ll 1. \tag{4.13}$$

This condition corresponds to the so-called quasi-classical limit of Eq. (4.1). Here this means that the effective scale of the change of the field phase with time due to nonlinear effect is much shorter than the characteristic length at which power is significantly changed by dispersion. When such a condition is met, the linear dispersive term in Eq. (4.11b) can be neglected. Note, however, that we keep the terms describing the change of the phase due to linear dispersion. The resulting system of equations on A and Φ reads then

$$\begin{aligned}&(A^2)_\eta - \frac{2}{c(\eta)}(A^2\Phi_\xi)_\xi = 0,\\ &\Phi_\eta - \frac{1}{c(\eta)}(\Phi_\xi)^2 - (A^2 + \lambda\xi^2) = 0.\end{aligned} \tag{4.14}$$

We seek a solution of Eqs. (4.14) having a self-similar form, $A = A(\xi)$. Furthemore, if we assume $\Phi_\xi = 0$, it is easy to find a solution with a parabolic distribution of the intensity:

$$A(\xi) = [\lambda(1-\xi^2)]^{1/2}, \qquad |\xi| \le 1,$$
$$\Phi(\eta) = \lambda\eta. \tag{4.15}$$

This solution yields the following dependence of the pulse energy on the pulse parameters:

$$U = \int_{-\infty}^{+\infty} \mathrm{d}t\, |\psi|^2 = \frac{4}{3}\lambda a^2 \tau. \tag{4.16}$$

We can then summarize equations that model the dynamic evolution of the high-intensity pulse solution of Eq. (4.1). From the amplitude term

$$|\psi(z,t)| = \left[\frac{3U(z)}{4\tau(z)}\right]^{1/2}\left\{1-\left[\frac{t}{\tau(z)}\right]^2\right\}^{1/2} \qquad \text{for } |t| \le \tau(z),$$
$$|\psi(z,t)| = 0 \qquad \text{for } |t| > \tau(z), \tag{4.17}$$

it is clear that the solution corresponds to a pulse with a parabolic intensity profile whose zero-crossing point $\tau(z)$ defines an effective pulse width. In the phase term

$$\arg\psi(z,t) = \lambda\eta(z) + C(z)t^2, \tag{4.18}$$

the solutions for $\eta(z)$ and $C(z)$ are

$$\eta(z) = \eta(z_0) + \left(\frac{3\sigma}{4\lambda}\right)\int_{z_0}^{z} \mathrm{d}z' \frac{U(z')}{\tau(z')}, \tag{4.19}$$
$$C(z) = -(2\beta_2)^{-1}(\mathrm{d}/\mathrm{d}z)\ln\tau(z). \tag{4.20}$$

In Eqs. (4.17)-(4.20), the scaling of the pulse amplitude and width from their initial values can be calculated from

$$U(z) = U(z_0)\exp\left[\int_{z_0}^{z} \mathrm{d}z'\, g(z')\right], \tag{4.21}$$
$$\frac{\mathrm{d}^2\tau}{\mathrm{d}z^2} = \frac{3\beta_2\sigma U(z)}{2\tau^2}. \tag{4.22}$$

Note that Eq. (4.21), which is the expression of the evolution of the pulse energy in the system, is true for all solutions of Eq. (4.1). Therefore, Eq. (4.8) can be also derived directly from (4.21). We point out that the derivation of the solution defined by Eqs. (4.17)-(4.20) is based on the assumption (4.13). This approximation can be justified a posteriori for the parabolic pulse given by Eqs. (4.17)-(4.20) since $\epsilon \approx 2\beta_2/3\sigma\tau U \ll 1$ except close to the pulse edges.

The theoretical predictions from Eqs. (4.17)-(4.22) have been compared with the results of numerical simulations of Eq. (4.1). We have modeled the propagation of Gaussian pulses with a FWHM pulse width of 0.5 ps and an energy of 70 pJ in a fibre amplifier with length of 4 m, an integrated gain of 25 dB, $\sigma = 6 \times 10^{-3}\,\mathrm{W^{-1}\,m^{-1}}$, and $\beta_2 = 35 \times 10^{-3}\,\mathrm{ps^2\,m^{-1}}$. These are realistic parameters in the range expected for high-gain rare-earth-doped fibre amplifiers [90, 94, 144]. We have studied amplification for three commonly encountered gain profiles: (a) $g(z) = g_a \exp(z/z_a)$ with $g_a = 0.668\,\mathrm{m^{-1}}$ and $z_a = 3\,\mathrm{m}$, (b) $g(z) = g_a$ with $g_a = 1.44\,\mathrm{m^{-1}}$, and

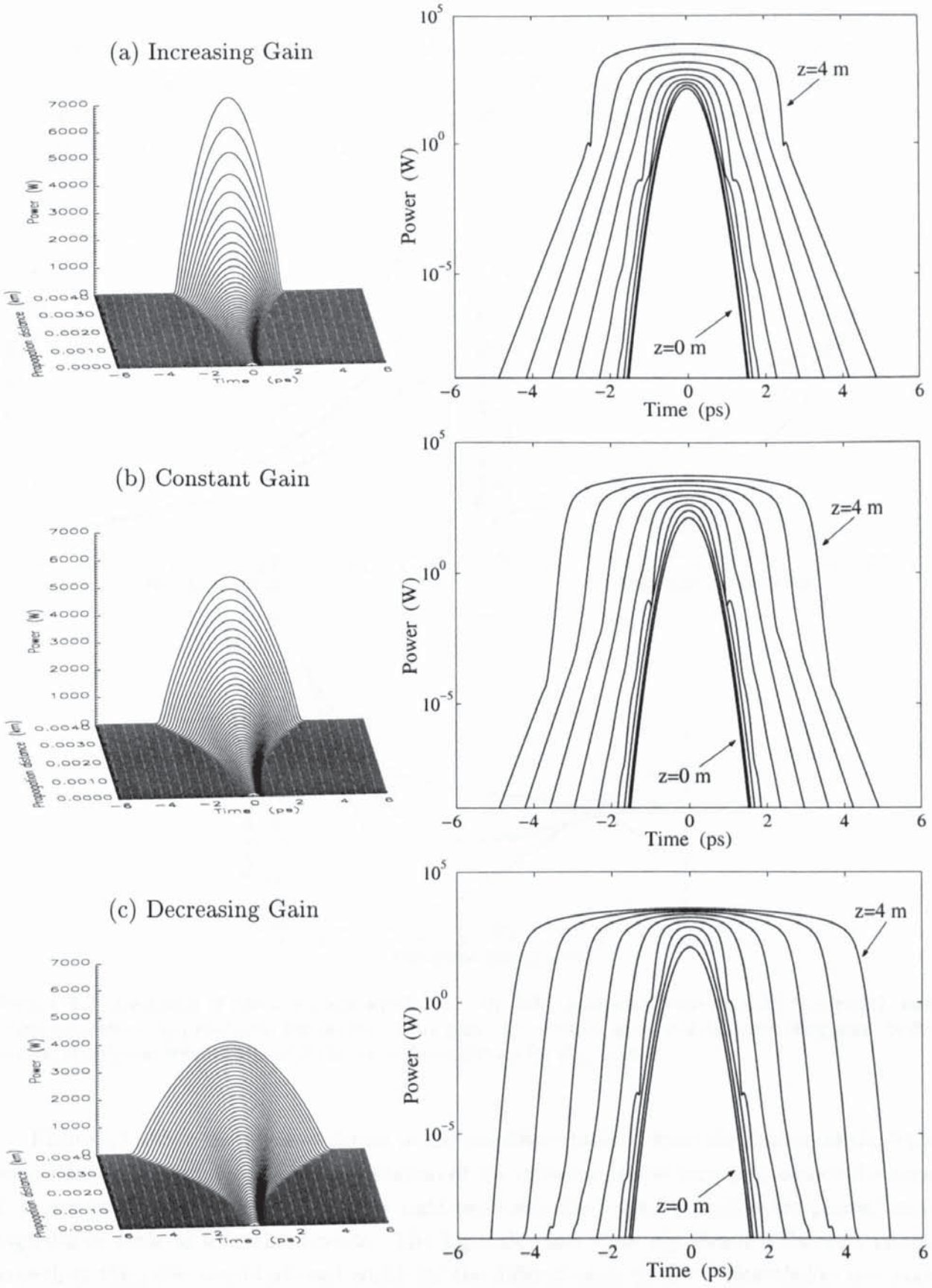

Figure 4.1: Pulse evolution in the amplifier for three different gain distributions. Left, evolution of the intensity profile shown on a linear scale; right, intensity profiles plotted on a logarithmic scale in 0.5 m increments.

(c) $g(z) = g_a \exp(-z/z_a)$ with $g_a = 2.535\,\mathrm{m}^{-1}$ and $z_a = 3\,\mathrm{m}$ [91]. Gain profile (a) simulates the experimental situation of pumping counterdirectionally with the propagating pulse such that the gain increases along the amplifier, profile (b) corresponds to bidirectional pumping with constant gain along the amplifier, and finally profile (c) corresponds to codirectional pumping with decreasing gain along the amplifier.

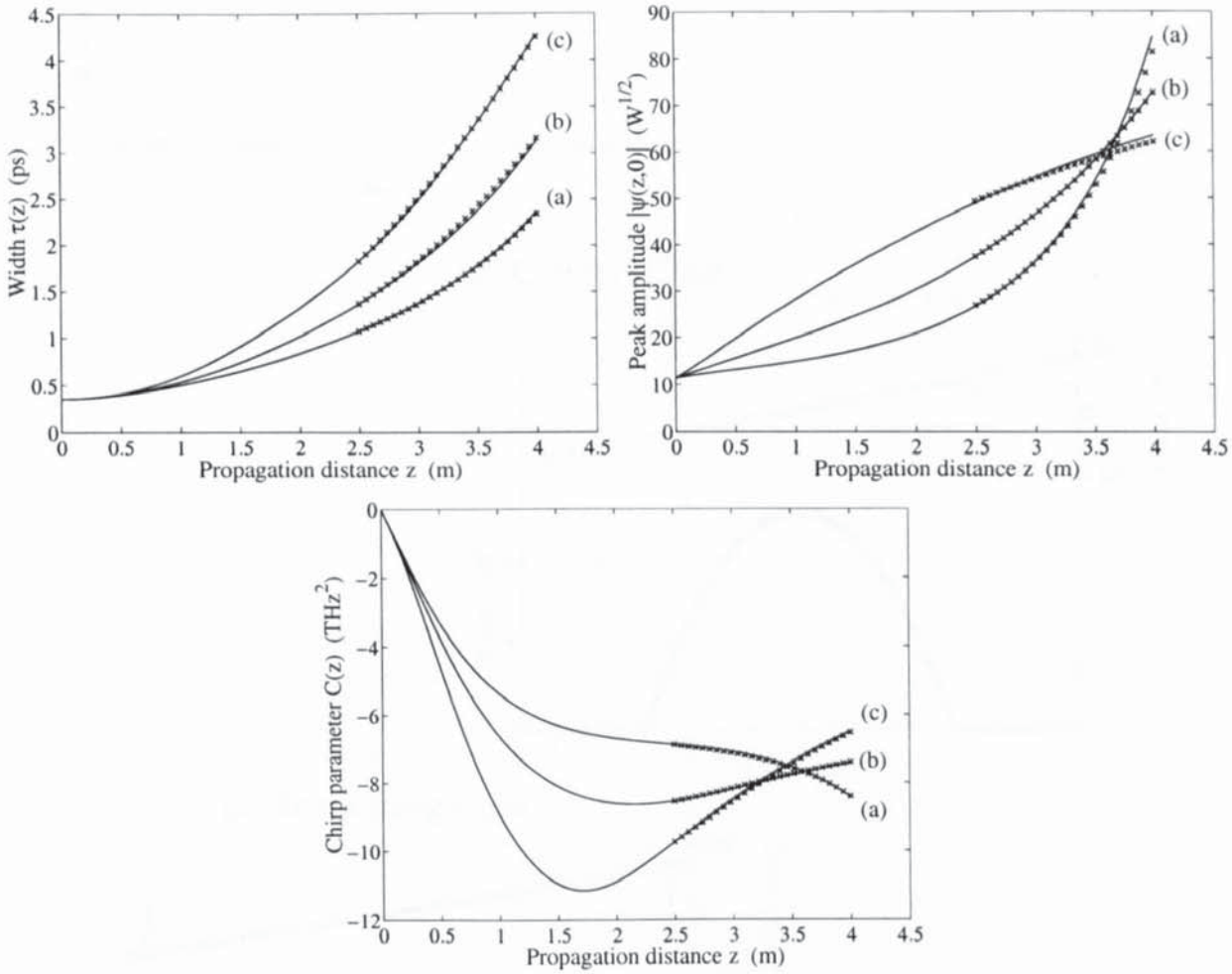

Figure 4.2: Evolution of effective pulse width $\tau(z)$ (top left), peak amplitude $|\psi(z,0)|$ (top right), and chirp parameter $C(z)$ (bottom) for (a) increasing gain, (b) constant gain, and (c) decreasing gain. Solid curves, simulation results; x-marks, theoretical predictions for $z \geq 2.5\,\mathrm{m}$.

Figure 4.1 shows the pulse evolution in the amplifier obtained from simulations of the NLS equation. On the left-hand-side the evolution of the intensity profile with propagation distance is shown on a linear scale, while on the right-hand-side the intensity profiles are plotted on a logarithmic scale in 0.5 m increments. The log-scale plots show significant differences in the growth of the pulse amplitude and width for the different gain profiles. Nonetheless one may see from the linear-scale plots that, for all profiles, as the incident Gaussian pulse is amplified to high intensity, it evolves into a parabolic pulse in the second half of the amplifier. It is also useful to remark here that the initial pulse shape determines only the map toward the parabolic pulse, with the asymptotic pulse characteristics being determined only by the initial pulse energy and the amplifier parameters. The interesting feature emerging from the log-scale plots is that

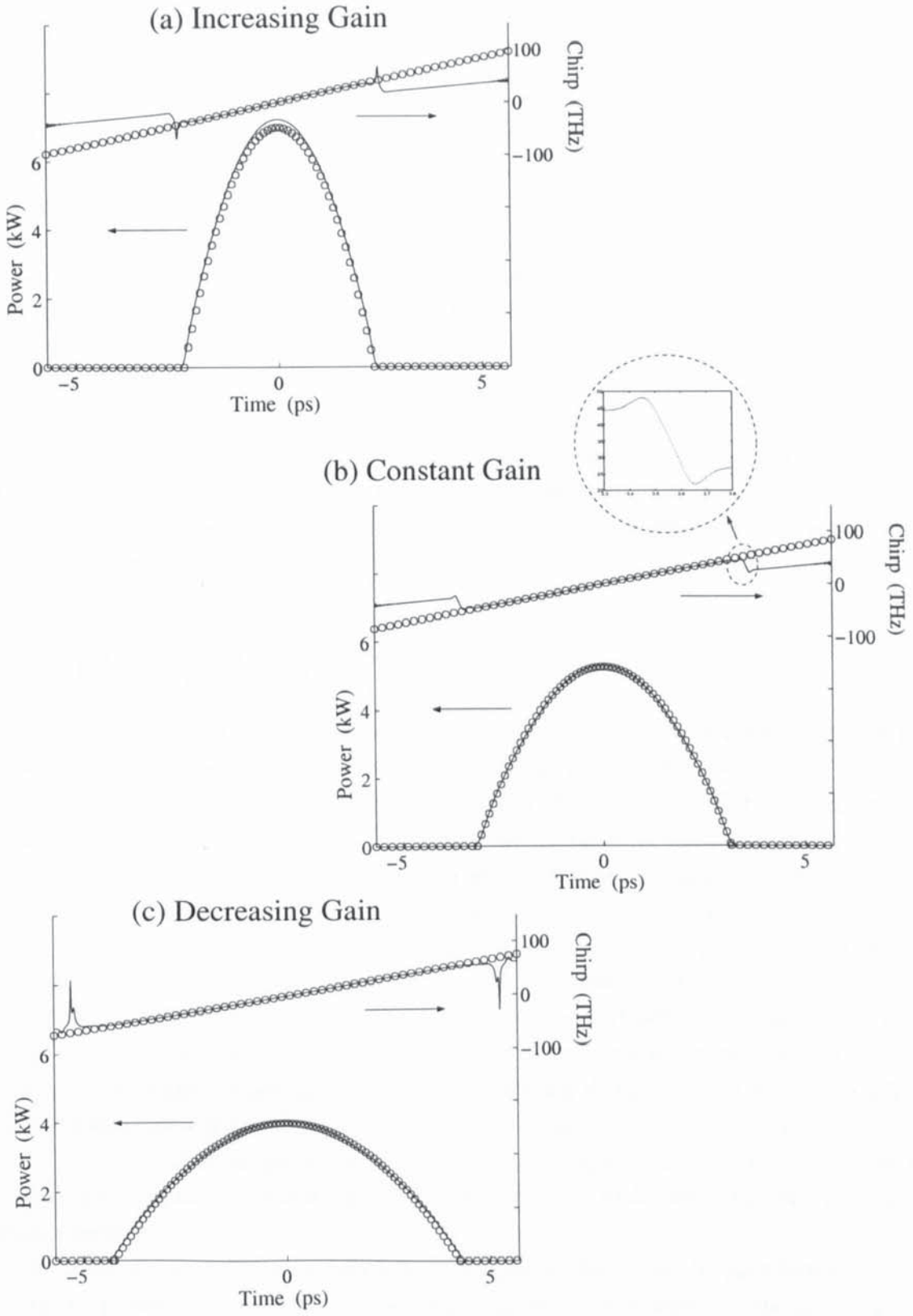

Figure 4.3: Intensity (left axis) and chirp (right axis) of the amplifier output pulse for three different gain profiles. Solid curves, simulation results; circles, theoretical predictions.

the asymptotic pulse presents a self-similar energy-containing parabolic core sourrounded by low-amplitude wings. These tails start developing on the pulse near the points $t = \pm\tau$, i.e. in the region where the linear term neglected in the theory becomes important. Therefore the

description of these tails requires a more detailed analysis of the pulse shape, that we will present in the next section.

Considering the asymptotic parabolic regime that occurs after some initial transition stage, here after a propagation distance of 2.5 m, we can compare the evolution of the pulse parameters from simulations quantitatively with theory. For all gain profiles, Fig. 4.2 shows the evolution of the effective width $\tau(z)$ (solid curves, top left), the peak amplitude $|\psi(z,0)|$ (solid curves, top right), and the chirp parameter $C(z)$ (solid curves, bottom) obtained from fits to the propagating pulse from simulations. These values are in good agreement with the expected results (x-marks) obtained from the solutions of Eqs. (4.22), (4.17), and (4.20), calculated for $z \geq 2.5\,\mathrm{m}$. In addition, the solid curves in Fig. 4.3 show the simulation results for the intensity and chirp (first time derivative of the phase) of the output pulses from the amplifier, compared with the expected results (circles) from Eqs. (4.17)-(4.22). These results confirm the linearly chirped parabolic nature of the output pulses. However, we observe that the pulse chirp remains linear across the whole pulse duration, but it exhibits a change in slope in the pulse tails (see the inset), i.e. where the linear term is not negligible any more. This change will be accounted for in the analysis presented in the next section.

4.4 Matching problem

In the previous section we have demonstrated that the parabolic approximation for the pulse shape can describe the central part of the asymptotically propagating pulse in the amplifying medium. Our aim now is to include in the description the pulse tails. For this purpose, first of all we have studied the evolution in the plane time - distance of the parameter ϵ defined in Eq. (4.12). Figure 4.4 shows the evolution of ϵ as a function of propagation distance z and normalized time ξ calculated from numerical simulation of Eq. (4.1) with constant gain profile. The entire colormap is used for values ranging from 0 to 1, with values greater than 1 rendered with the same color associated to 1. On the top left the variation of ϵ in the full plane (ξ, z) is represented, while the top right picture is a zoom of a narrower region in ξ, that clearly shows the beginnings of the asymptotic regime. The bottom picture shows the variation of ϵ in the asymptotic regime, starting from 2.5 m propagation distance. It is clear from Fig. 4.4 that the transition of ϵ from values < 1 to values > 1 occurs in a narrow region around the points $\xi = \pm 1$, and this is in agreement with our intuitive expectations. One may also see that in the asymptotic regime the transition region does not move with distance (being presented in self-similar variables).

On the basis of these results we define three regions on the ξ-axis, as the schema in Fig. 4.5 shows. As the problem is symmetric in ξ we can limit our considerations to the semiaxis $\xi \geq 0$. Region (I), $0 \leq \xi \leq 1 - \Delta_1$, corresponds to the central part of the asymptotic pulse, where $\epsilon \ll 1$. Region (III), $\xi \geq 1 + \Delta_2$, corresponds to the pulse tails, where $\epsilon \gg 1$. Finally region (II), $1 - \Delta_1 \leq \xi \leq 1 + \Delta_2$, is a transition zone, where $\epsilon \approx 1$. The size of the transition zone is parametrized by $\Delta_1, \Delta_2 \ll 1$. We introduce two different Δ-intervals for the (left and right) regions around the point $\xi = 1$ because of an obvious asymmetry of the solutions relative to this point. In each of the regions we construct an approximate solution of Eq. (4.7), or equivalently of the system (4.11), at fixed η. We then match the solutions at the boundaries.

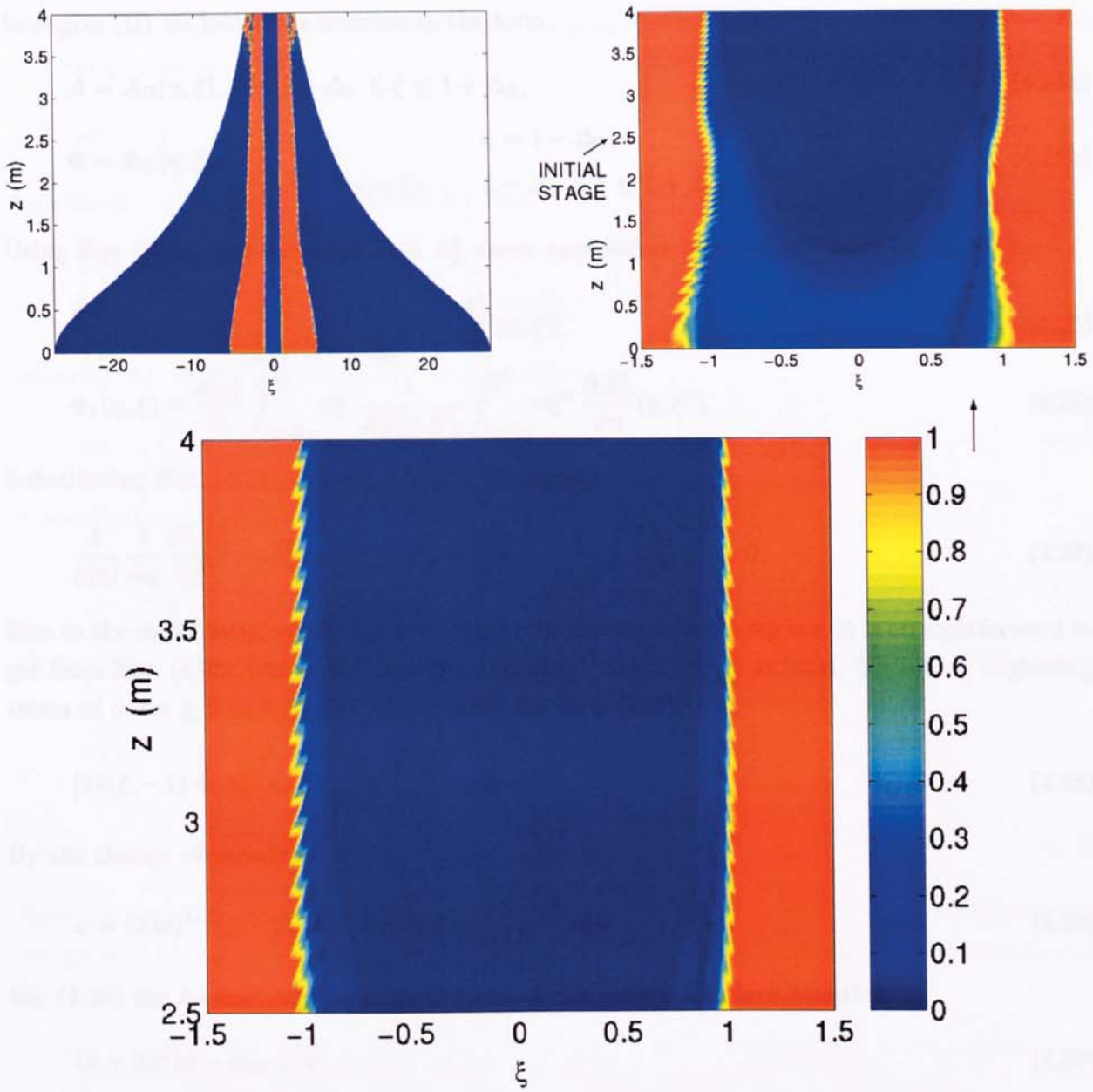

Figure 4.4: Evolution of ϵ as a function of distance z and normalized time ξ. Top left, full plane (ξ, z); top right, $-1.5 \leq \xi \leq 1.5$; bottom, $-1.5 \leq \xi \leq 1.5$ and $z \geq 2.5\,\mathrm{m}$.

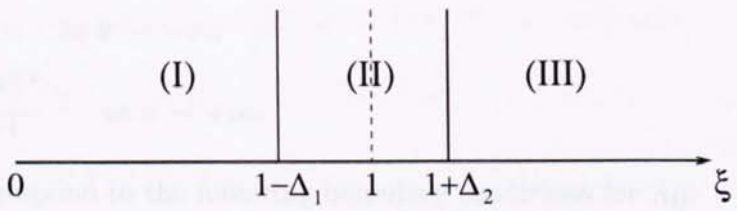

Figure 4.5: Schema of the ξ-regions where Eq. (4.7) is solved.

In region (I) we consider the quasi-classical solution derived in Section 4.3, namely

$$A = A_{\mathrm{I}}(\xi) = [\lambda(1-\xi^2)]^{1/2}, \qquad 0 \leq \xi \leq 1-\Delta_1, \tag{4.23a}$$

$$\Phi = \Phi_{\mathrm{I}}(\eta) = \lambda\eta, \qquad 0 \leq \xi \leq 1-\Delta_1. \tag{4.23b}$$

In region (II) we look for a solution in the form

$$A = A_{\rm II}(\eta,\xi), \qquad 1-\Delta_1 \le \xi \le 1+\Delta_2, \tag{4.24a}$$

$$\Phi = \Phi_{\rm II}(\eta,\xi) = \begin{cases} \lambda\eta, & \xi = 1-\Delta_1, \\ \lambda\eta + \Phi_1(\eta,\xi), & 1-\Delta_1 < \xi \le 1+\Delta_2. \end{cases} \tag{4.24b}$$

Using Eqs. (4.24) and assuming that $A_{\rm II}^2$ never approaches zero, we get from Eq. (4.11a):

$$\frac{\partial\Phi_1}{\partial\xi}(\eta,\xi) = \frac{c(\eta)}{2A_{\rm II}^2(\eta,\xi)} \int_{1-\Delta_1}^{\xi} {\rm d}\xi' \, \frac{\partial A_{\rm II}^2}{\partial\eta}(\eta,\xi'), \tag{4.25}$$

$$\Phi_1(\eta,\xi) = \frac{c(\eta)}{2} \int_{1-\Delta_1}^{\xi} {\rm d}\xi' \, \frac{1}{A_{\rm II}^2(\eta,\xi')} \int_{1-\Delta_1}^{\xi'} {\rm d}\xi'' \, \frac{\partial A_{\rm II}^2}{\partial\eta}(\eta,\xi''). \tag{4.26}$$

Substituting Eqs. (4.24) into Eq. (4.11b), we obtain:

$$\frac{1}{c(\eta)} \frac{1}{A_{\rm II}} \frac{\partial^2 A_{\rm II}}{\partial\xi^2} - A_{\rm II}^2 + \lambda(1-\xi^2) + \frac{\partial\Phi_1}{\partial\eta} - \frac{1}{c(\eta)} \left(\frac{\partial\Phi_1}{\partial\xi}\right)^2 = 0. \tag{4.27}$$

Due to the small variation of $A_{\rm II}^2$ and c with η in the asymptotic regime, it is straightforward to get from Eqs. (4.25) and (4.26) that $\Phi_{1\eta}$ and $(\Phi_{1\xi})^2$ are $O(\Delta_{1,2}^2)$ at least. Therefore, neglecting terms of order ≥ 2 in $\Delta_{1,2}$, Eq. (4.27) takes the form [135]

$$[2\lambda(\xi-1) + A_{\rm II}^2] A_{\rm II} - \frac{1}{c(\eta)} \frac{\partial^2 A_{\rm II}}{\partial\xi^2} = 0. \tag{4.28}$$

By the change of variables

$$x = (2\lambda c)^{1/3}(\xi-1), \qquad \phi = \frac{1}{\sqrt{2}} \left(\frac{c}{4\lambda^2}\right)^{1/6} A_{\rm II}, \tag{4.29}$$

Eq. (4.28) can be rewritten as a special case of the second Painlevé equation

$$(x + 2\phi^2)\phi - \phi_{xx} = 0. \tag{4.30}$$

The boundary conditions to Eq. (4.28) can be formulated in terms of the asymptotic behaviours of the second Painlevé transcendent. For a particular choice of the free parameters, the asymptotics are [139, 137]:

$$\phi \sim \left(-\frac{x}{2}\right)^{1/2} \qquad \text{as } x \to -\infty, \tag{4.31}$$

$$\phi \sim \frac{1}{2\sqrt{\pi}} \frac{e^{-\frac{2}{3}x^{3/2}}}{x^{1/4}} \qquad \text{as } x \to +\infty. \tag{4.32}$$

These formulae correspond to the following boundary conditions for $A_{\rm II}$:

$$A_{\rm II} = [-\lambda(\xi^2-1)]^{1/2} \simeq [-2\lambda(\xi-1)]^{1/2} \qquad \text{at } \xi = 1-\Delta_1, \tag{4.33}$$

$$A_{\rm II} = \frac{1}{\sqrt{\pi}} \left(\frac{\lambda}{2c}\right)^{1/4} \frac{e^{-\frac{2}{3}(2\lambda c)^{1/2}(\xi-1)^{3/2}}}{(\xi-1)^{1/4}} \qquad \text{at } \xi = 1+\Delta_2. \tag{4.34}$$

The solution of the boundary value problem specified by Eqs. (4.28) and (4.33)-(4.34) gives $A_{\rm II}(\eta,\xi)$ (at fixed η). Finally, using $A_{\rm II}(\eta,\xi)$ into Eq. (4.26), we obtain $\Phi_{\rm II}(\eta,\xi)$.

In region (III) we neglect the nonlinear term in Eq. (4.11b) and solve the corresponding linearized equation

$$iF_\eta + \lambda\xi^2 F - \frac{1}{c(\eta)}F_{\xi\xi} = 0. \tag{4.35}$$

Specifically, we look for a solution in the form

$$\begin{aligned} F(\eta,\xi) &= A_{\rm III}(\eta,\xi)e^{i\Phi_{\rm III}(\eta,\xi)} \\ &= \alpha(\eta)G(\eta,\theta)e^{iR(\eta)\xi^2}, \quad \theta = \beta(\eta)\xi, \qquad \xi \geq 1+\Delta_2. \end{aligned} \tag{4.36}$$

Inserting Eq. (4.36) into Eq. (4.35), we find that

$$iG_\eta - \frac{\beta^2(\eta)}{c(\eta)}G_{\theta\theta} = 0 \tag{4.37}$$

is satisfied, provided that

$$\frac{\beta_\eta}{\beta} = \frac{4R}{c}, \qquad \frac{\alpha_\eta}{\alpha} = \frac{2R}{c}, \qquad R_\eta = \frac{4R^2}{c} + \lambda. \tag{4.38}$$

Due to the boundary condition (4.34) coming from zone (II), G has the following asymptotics

$$\begin{aligned} G(\eta,\theta) \sim \alpha^{-1}(\eta)\frac{1}{\sqrt{\pi}}\left(\frac{\lambda}{2c(\eta)}\right)^{1/4} &\frac{e^{-\frac{2}{3}(2\lambda c(\eta))^{1/2}\left(\frac{\theta}{\beta(\eta)}-1\right)^{3/2}}}{\left(\frac{\theta}{\beta(\eta)}-1\right)^{1/4}} \\ &\times e^{i\left[\Phi_{\rm II}\left(\eta,\frac{\theta}{\beta(\eta)}\right)-R(\eta)\frac{\theta^2}{\beta^2(\eta)}\right]} \qquad \text{as } \theta \to \beta(\eta)+0. \end{aligned} \tag{4.39}$$

Here we apply the phase matching condition $\Phi_{\rm III}(\eta,\xi) = \Phi_{\rm II}(\eta,\xi)$ as $\xi \to 1+0$. The parabolic equation (4.37) together with boundary condition (4.39) is solved by the double potential formula [145]

$$G(\eta,\theta) = \frac{1}{2\sqrt{\pi}}\int_0^{b(\eta)} d\eta'\, G(\eta',\beta(\eta)(1+\Delta_2))\frac{\theta}{(b(\eta)-\eta')^{3/2}}e^{-\frac{i\theta^2}{4(b(\eta)-\eta')}}, \tag{4.40}$$

where $\frac{db(\eta)}{d\eta} = \frac{\beta^2(\eta)}{c(\eta)}$.

This completes the construction of the function $F(\eta,\xi)$ for all ξ, at fixed η. The matching conditions here require an appropriate choice of Δ_1 and Δ_2. They should be small enough to ensure the matching between (I) and (II) zones and (II) and (III) zones

$$|x| = (2\lambda c(\eta))^{1/3}|\xi - 1| \gg 1, \qquad |\xi - 1| \ll 1. \tag{4.41}$$

Thus one can choose $\Delta_{1,2}$ from the interval

$$0 < \Delta_{1,2} < (2\lambda c(\eta))^{-\frac{1}{3}+\epsilon}, \qquad 0 < \epsilon < \frac{1}{3}. \tag{4.42}$$

We have compared the solution of the matching problem with the numerical solution of Eq. (4.1). An example is given in Fig. 4.6, that shows the amplitude A of F as a function of ξ, for $0 \leq \xi \leq 1+\Delta_2$, at the final distance in the amplifier. The dashed curve represents the numerical solution, while the solid curve represents the solution of the matching problem specified by Eq. (4.23a) and the solution of Eq. (4.28). The parabolic solution (4.23a) is also plotted for $\Delta_1 = 0$

(dotted curve). We note that parameter Δ_1 should be chosen such that the parabolic solution (4.23a) does not deviate from the numerical one at the point $\xi = 1 - \Delta_1$. The example in Fig. 4.6 corresponds to $\Delta_1 = 0.2$. The value of Δ_2 used in Fig. 4.6 is $\Delta_2 = 0.15$. It can be seen that there is a good agreement between the analytical and the numerical results. As the inset clearly shows, the difference between the analytical and the numerical curves is, in fact, of order of $\Delta_{1,2}^2$, and this is consistent with our expectations, since the lowest order terms neglected in Eq. (4.28) are $O(\Delta_{1,2}^2)$. A fine adjustment of the parameters Δ_1, Δ_2 and λ would improve the accuracy of the theoretical results.

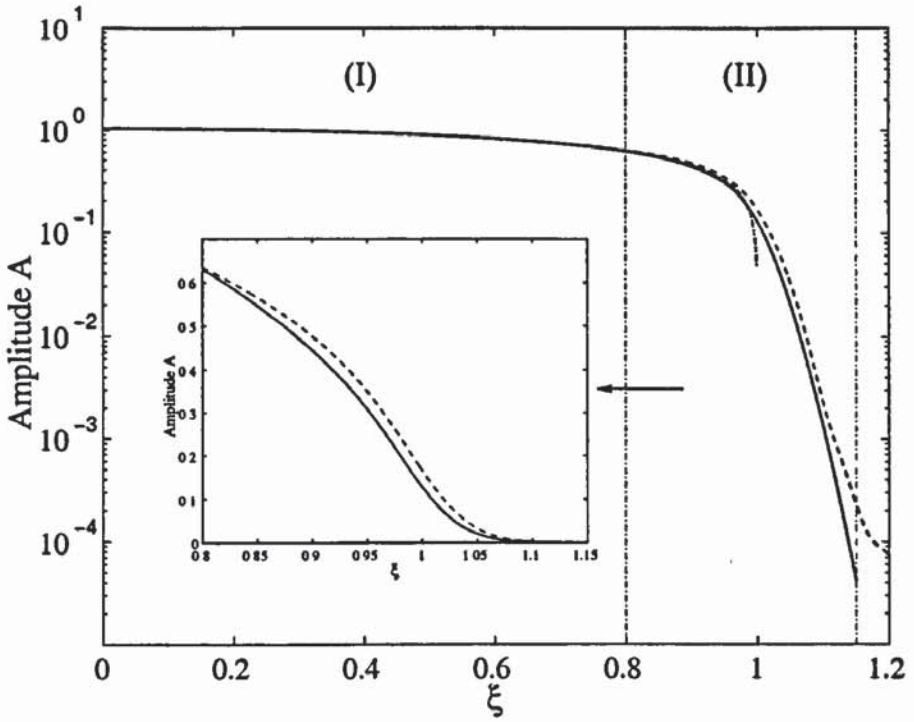

Figure 4.6: Variation of the amplitude A as a function of ξ at the amplifier output. Dashed curve, numerical solution; solid curve, solution of the matching problem for $\Delta_1 = 0.2$ and $\Delta_2 = 0.15$; dotted curve, parabolic solution for $\Delta_1 = 0$. Inset: numerical solution and solution of the matching problem shown on a linear scale.

4.5 Conclusion

We have examined solutions of the NLS equation with gain, that governs optical pulse propagation in a fibre amplifying medium. Quasi-classical solutions with a parabolic temporal profile in the energy-containing core have been accurately analysed theoretically and numerically. We have presented matching of the parabolic solution to the linear low-amplitude tails of the pulse. The theoretical analysis has been shown to reproduce accurately the solution obtained from numerical simulation of the NLS equation.

Chapter 5

Conclusions

This thesis has presented theoretical investigation of some topics concerned with nonlinear optical pulse propagation in optical fibres. Specifically, DM solitons in the regime of weak management, DM autosoliton transmission guided by in-line NOLMs as all-optical regenerators of signals, and self-similar parabolic optical solitary waves in normally dispersive fibres have been studied by means of mathematical analysis and numerical modelling.

Some backgrounds on the development of fibre-optic communication systems and optical solitons and solitary waves have been presented in Chapter 1.

In Chapter 2, the basic model governing the evolution of optical pulses in a fibre link with periodical amplification and dispersion compensation has been introduced, and the derivation of the GT equation describing the slow dynamics of the breathing pulse in the assumption of smallness of the nonlinearity with respect to the local dispersion has been outlined. Then, a perturbation theory of DM solitons for small dispersion map strengths has been developed. In the case of a weak dispersion map, the path-average DM pulse dynamics has been shown to be described by a perturbed form of the NLS equation where the perturbation represents the small effects of the dispersion management. Using a perturbation theory scheme based upon the IST method, an analytical description of the evolution of the path-averaged soliton in the presence of such a perturbation has been given. The analytic expression for the envelope of the DM soliton obtained by the perturbation approach has been shown to correctly predict the energy enhancement arising from the dispersion management. The analytical results have been confirmed by direct numerical simulations.

Currently I am thinking about a possible generalization of the approach presented in Chapter 2, to analyse optical pulse propagation in an optical amplified fibre link with periodical dispersion compensation and in-line control performed by optical bandpass filters and synchronous amplitude modulators. Assuming high local dispersion and accounting for the effect of filters and modulators through their distributed action, it is possible to introduce a path-averaged model that generalizes the GT equation. Then, in the case of a weak dispersion management and distributed model of the control elements, the average pulse dynamics can be analysed using the perturbation theory to the NLS equation. This approach could enable the analytical description of the soliton evolution under the combined action of dispersion management, filtering, and amplitude modulation. It would be interesting to apply the general theory to practical transmission systems. A number of techniques have already been developed in the literature to describe the regime of weak dispersion management (see e.g. [46, 64]). Among them, the multiple-scale

averaging method developed in [64] has proved to be capable of locating the optimal launch points in each period of the dispersion map where the pulses are unchirped [48, 146]. We recall that the use of the chirp-free points as launch points permits to diminish the energy shedding from the input signal into dispersive radiation. Using the asymptotic theory to consider the special case of a two-step dispersion map with an amplifier deployed at a segment junction in each period, it has been demonstrated [48, 146] the existence of "magic" maps, that is a class of dispersion maps that render the location of an optimal (chirp-free) launch point independent of the fibre's dispersion. This is a remarkable finding as it implies that the transmission in different WDM channels can be optimised simultaneously for such maps. Due to the dispersion slope, in fact, different channels have their own frequencies and dispersion characteristics, and therefore in general need to be prechirped differently. By employing magic maps, instead, system performance optimisation can be realized using the same optimal launch point for several channels. Currently I am studying magic dispersion maps with distributed Raman amplification to compensate for the fibre loss. Although the EDFA is the current optical amplifier of choice, recent progress in the development of distributed EDFAs [147] and Raman amplifiers [148] makes them promising candidates to be exploited in future wideband and ultra-high speed systems. The theoretical results that I expect to obtain could be useful for the full optimisation of practical systems employing WDM and distributed Raman amplification. The regime of weak management studied in Chapter 2 and in the above-mentioned works may be considered to not be of much interest, because it loses the well-known advantages offered by strong dispersion management. However, the weak regime still covers many practical situations. Moreover, even though analytical methods developed for weak management are formally valid for map strenghts $S \ll 1$, their predictions can work reasonably well even when the strength of the map is of the order of one; this includes the practically important case when the variations of the local dispersion are much larger than the average (residual) dispersion.

A numerical study of autosoliton transmission in DM fibre systems with periodical in-line optical control performed by NOLMs has been presented in Chapter 3. The basic principles and properties of the NOLM have been described, and the use of in-line NOLMs in conjunction with dispersion management has been addressed as a powerful technique to improve the performance of a transmission system, as it exploits a combination of the effects of dispersion management and the action of NOLMs as saturable absorbers in suppressing the accumulation of noise, dispersive radiation, and pulse distortion, and stabilizing the peak amplitude of pulses. First, the compatibility of NOLMs with dispersion management for achievement of pulse stabilization and long-distance pulse transmission has been demonstrated. Then, the use of in-line NOLMs has been proposed as a general technique for all-optical passive 2R regeneration of RZ data in high bit-rate transmission systems with strong dispersion management. It has been shown that when a system's performance is mainly degraded by amplitude noise and pulse distortion, in-line NOLMs can achieve regeneration and distance-unlimited transmission of the data streams. Specifically, a feasibility of $40\,\mathrm{Gbit\,s^{-1}}$ single-channel stable soliton transmission over unlimited distances in standard fibre has been demonstrated, the tolerance of this result has been investigated, and the proposed method has been extended to $80\,\mathrm{Gbit\,s^{-1}}$ data transmission. It has also been demonstrated that the application of the proposed technique to systems where both amplitude noise and timing jitter are important limiting factors can dramatically improve the

system's performance, allowing for transoceanic transmission distances. Finally, the application of 40 Gbit s^{-1} DM transmission guided by NOLMs to a WDM scheme has been investigated. The use of specially designed WDM guiding filters coupled with NOLMs has been proposed as a regeneration technique to enhance the transmission performance of WDM (40 Gbit s^{-1} × N channel) systems. Optimisation of the system has allowed for 150 GHz-spaced×16 channel transmission over 25000 km of SMF.

The estimate of the NOLM's characteristics imposed by the constraints of different transmission schemes has been based all over Chapter 3 on the approximation of the NOLM's transmissivity by the cw transfer characteristic. Even though this estimate has proved to be good in practice, it would be desirable to develop an analytical model to describe the action of the NOLM on the characteristics of pulses. Transfer functions for the pulse's characteristics are known in the case of other control elements such as filters and modulators, but not yet in the case of NOLMs. The development of a methodological approach to describe the action of NOLMs can be important for properly formulating system design rules as well as for clarifying the fine structure of the autosoliton solutions. Besides the all-optical regeneration function of periodically inserted in-line NOLMs that has been investigated in Chapter 3, another interesting application of NOLMs would be the deployment of one NOLM at the end of a conventional DM line, before the receiver, to study its benefits in terms of improvement of the SNR.

In Chapter 4, a detailed mathematical analysis of the solutions of the NLS equation with gain and normal dispersion, that describes optical pulse propagation in an amplifying medium, has been presented. A quasi-classical self-similar solution with parabolic temporal variation, that corresponds to the energy-containing core of the asymptotically propagating pulse in the amplifying medium, has been constructed. The self-similar core has been matched through Painlevé functions to the solution of the linearized equation, that corresponds to the low-amplitude tails of the pulse. The analytical solution has proved to reproduce accurately the numerically calculated solution of the NLS equation. This analysis justifies the quasi-classical assumption intuitively made in previous works [2, 90], the parabolic approximation for the pulse shape proving to be valid in the central part of the asymptotic pulse. Moreover, it gives a full description of the shape and the main features of high-power pulses generated in an amplifying medium.

In view of their self-similar propagation and the ease with which they can be compressed, parabolic pulses have wide-ranging applications in nonlinear fibre optics. Therefore, it would be interesting to study in detail the properties of the generated parabolic pulses from an amplifier. There are a few important characteristics to be considered: shape control (that must be parabolic), width, power, and chirp. These characteristics depend on the parameters of the input pulse (power, width, and initial chirp) and the characteristics of the fibre (dispersion). The problem would be to study how parameters of the forming asymptotic pulse in the amplifier depend on the input signal parameters and fibre characteristics. This study could be pursued first by numerical analysis, and then by constructing a simple analytical model based on the features observed through numerical simulations. The theoretical results could provide a useful guidance to experiments. Another interesting topic of future investigation could be a detailed analysis of the self-similarity in the generation and stabilization of solitary waves in the NLS equation with gain and anomalous dispersion.

Appendix A

Some features of the Inverse Scattering Transform method

A.1 Unperturbed nonlinear Schrödinger equation

The linear eigenvalue problem associated with the unperturbed form (i.e., $F = 0$) of Eq. (2.11) is [14]-[16]

$$\begin{aligned} &\frac{\partial v_1}{\partial t} + i\zeta v_1 = q v_2, \\ &\frac{\partial v_2}{\partial t} - i\zeta v_2 = -q^* v_1, \end{aligned} \tag{A.1}$$

where $\zeta = \xi + i\eta$ is a complex eigenvalue. Jost function solutions ϕ, $\bar{\phi}$, ψ, and $\bar{\psi}$ are defined by their asymptotic values, for real $\zeta = \xi$,

$$\phi \sim \begin{bmatrix} 1 \\ 0 \end{bmatrix} e^{-i\xi t}, \quad \bar{\phi} \sim \begin{bmatrix} 0 \\ -1 \end{bmatrix} e^{i\xi t}, \quad \text{as } t \to -\infty, \tag{A.2}$$

$$\psi \sim \begin{bmatrix} 0 \\ 1 \end{bmatrix} e^{i\xi t}, \quad \bar{\psi} \sim \begin{bmatrix} 1 \\ 0 \end{bmatrix} e^{-i\xi t}, \quad \text{as } t \to +\infty. \tag{A.3}$$

The relationship between these defines the scattering data a, $\bar{a}$, b, and $\bar{b}$:

$$\begin{aligned} &\phi = a\bar{\psi} + b\psi, \quad \bar{\phi} = -\bar{a}\psi + \bar{b}\bar{\psi}, \\ &\psi = -a\bar{\phi} + \bar{b}\phi, \quad \bar{\psi} = \bar{a}\phi + b\bar{\phi}, \end{aligned} \tag{A.4}$$

where the latter (inverse) expressions are obtained using

$$a\bar{a} + b\bar{b} = 1. \tag{A.5}$$

A squared eigenfunction problem can be associated with Eq. (2.11): introducing the bilinear spinors $\Phi = [\phi_1\psi_1, \phi_2\psi_2]^T$ and $\check{\Phi} = [\phi_1\bar{\psi}_1, \phi_2\bar{\psi}_2]^T$, writing either of these as $[g, h]^T$, and defining $k = (\phi_2\psi_1 + \phi_1\psi_2)/2$ for Φ, and $k = (\phi_2\bar{\psi}_1 + \phi_1\bar{\psi}_2)/2$ for $\check{\Phi}$, leads to the evolution equations

$$\begin{aligned} &\frac{\partial k}{\partial t} = -q^* g + q h, \\ &\frac{\partial g}{\partial t} = -2i\zeta g + 2q k, \\ &\frac{\partial h}{\partial t} = 2i\zeta h - 2q^* k. \end{aligned} \tag{A.6}$$

A formal solution of these leads to the relationship

$$\mathcal{L}\begin{bmatrix} g \\ h \end{bmatrix} - ik_+ \begin{bmatrix} q \\ q^* \end{bmatrix} = \zeta \begin{bmatrix} g \\ h \end{bmatrix}, \tag{A.7}$$

where k_+ denotes $k(t \to +\infty)$, and $\mathcal{L}$ is the integro-differential operator

$$\mathcal{L} = \frac{1}{2i}\begin{bmatrix} -\partial_t - 2qI_+[r\cdot\,] & -2qI_+[q\cdot\,] \\ 2rI_+[r\cdot\,] & \partial_t + 2rI_+[q\cdot\,] \end{bmatrix}. \tag{A.8}$$

Here, $r = -q^*$ as appropriate for Eq. (2.11), and I_+ denotes the integral operator

$$I_+[r\cdot\,]f \equiv I_+[r,f] \equiv \int_t^{+\infty} \mathrm{d}t'\, r(t')f(t'), \tag{A.9}$$

for any function f. Relation (A.7) is satisfied by both Φ and $\check{\Phi}$ with appropriate choice of k_+. For Φ, $k_+ = a/2$; for $\check{\Phi}$, $k_+ = b/2$. In other words,

$$\mathcal{L}\Phi = \zeta\Phi - \frac{a}{2i}\begin{bmatrix} q \\ q^* \end{bmatrix}, \tag{A.10}$$

$$\mathcal{L}\check{\Phi} = \zeta\check{\Phi} - \frac{b}{2i}\begin{bmatrix} q \\ q^* \end{bmatrix}. \tag{A.11}$$

Equations (A.10) and (A.11) can be solved to express both Φ and $\check{\Phi}$ in terms of a formal asymptotic series; from Eq. (A.10), it follows that

$$\Phi = a\sum_{n=0}^{\infty} \frac{1}{(2i\zeta)^{n+1}}(2i\mathcal{L})^n \begin{bmatrix} q \\ q^* \end{bmatrix}. \tag{A.12}$$

We will require also the asymptotic expansion for $\ln a$; this is [16]

$$\ln a = \sum_{n=0}^{\infty} \frac{1}{(2i\zeta)^{n+1}} C_n, \tag{A.13}$$

where the coefficients C_n, the conserved functionals for the unperturbed form of Eq. (2.11), are given by [16]

$$\begin{aligned} C_0 &= \int_{-\infty}^{+\infty} \mathrm{d}t\, |q|^2, \\ C_1 &= \int_{-\infty}^{+\infty} \mathrm{d}t\, q^* \frac{\partial q}{\partial t}, \\ C_2 &= \int_{-\infty}^{+\infty} \mathrm{d}t \left(q^* \frac{\partial^2 q}{\partial t^2} + |q|^4 \right), \end{aligned} \tag{A.14}$$

and so on. We also state the trace formulae, which give the C_n in terms of the spectral data; these are [16]

$$C_n = \sum_{m=1}^{N} \frac{1}{n+1}\left[(2i\zeta_m^*)^{n+1} - (2i\zeta_m)^{n+1}\right] - \frac{1}{\pi}\int_{-\infty}^{+\infty} \mathrm{d}\xi\, (2i\xi)^n \ln\left[1 - |b(\xi, z')|^2\right]. \tag{A.15}$$

The discrete sum gives the contribution to C_n from an arbitrary N-soliton state (here $N = 1$), whereas the integral gives the contribution from the (continuum) radiation modes. Finally, we state the evolution equations for the spectral data; these are [22]

$$\frac{\partial a}{\partial z'} = -\int_{-\infty}^{+\infty} \mathrm{d}t \left[\frac{\partial r}{\partial z'}, -\frac{\partial q}{\partial z'}\right] \Phi, \tag{A.16}$$

$$\frac{\partial b}{\partial z'} = -\int_{-\infty}^{+\infty} \mathrm{d}t \left[\frac{\partial r}{\partial z'}, -\frac{\partial q}{\partial z'}\right] \check{\Phi}. \tag{A.17}$$

Here, $r = -q^*$.

A.2 Evolution equations for the perturbed system

Consider first the derivation of Eq. (2.14). Substituting (A.12) into Eq. (A.16), differentiating Eq. (A.13) with respect to z', then comparing coefficients of $(2i\zeta)^{-(n+1)}$ gives

$$\frac{\mathrm{d}C_n}{\mathrm{d}z'} = \int_{-\infty}^{+\infty} \mathrm{d}t \left[\frac{\partial q^*}{\partial z'}, \frac{\partial q}{\partial z'}\right] (2i\mathcal{L})^n \begin{bmatrix} q \\ q^* \end{bmatrix}. \tag{A.18}$$

We note here that Eq. (2.11), together with its conjugate, can be written in the form [16]

$$\frac{\partial}{\partial z'} \begin{bmatrix} q^* \\ q \end{bmatrix} - \frac{i}{2}(2i\mathcal{L}^A)^2 \begin{bmatrix} -q^* \\ q \end{bmatrix} = \begin{bmatrix} F^* \\ F \end{bmatrix}, \tag{A.19}$$

where $\mathcal{L}^A$ is the formal adjoint of the operator $\mathcal{L}$. We substitute then (A.19) into Eq. (A.18); since

$$(2i\mathcal{L}^A)^m \begin{bmatrix} -q^* \\ q \end{bmatrix} = \begin{bmatrix} -\dfrac{\delta C_m}{\delta q} \\ \dfrac{\delta C_m}{\delta q^*} \end{bmatrix} \tag{A.20}$$

and

$$(2i\mathcal{L})^n \begin{bmatrix} q \\ q^* \end{bmatrix} = \begin{bmatrix} \dfrac{\delta C_n}{\delta q^*} \\ \dfrac{\delta C_n}{\delta q} \end{bmatrix}, \tag{A.21}$$

where $\delta C_m/\delta q$, etc. are functional derivatives of the C_m, and since all C_n functionals commute [16], we get

$$\frac{\mathrm{d}C_n}{\mathrm{d}z'} = \int_{-\infty}^{+\infty} \mathrm{d}t\, [F^*, F](2i\mathcal{L})^n \begin{bmatrix} q \\ q^* \end{bmatrix} \tag{A.22}$$

as required.

Equation (2.15) is found in a similar way. Substituting Eq. (A.19) into Eq. (A.17) gives [23]

$$\frac{\partial b}{\partial z'} = 2i\zeta^2 b + \int_{-\infty}^{+\infty} \mathrm{d}t\, [F^*, F]\check{\Phi}. \tag{A.23}$$

The first term follows using standard manipulations for the unperturbed system, while $\check{\Phi}$ satisfies Eq. (A.11).

References

[1] A. Hasegawa and Y. Kodama, *Solitons in Optical Communications* (Oxford University Press, Oxford, 1995).

[2] D. Anderson, M. Desaix, M. Karlsson, M. Lisak, and M.L. Quiroga-Teixeiro, "Wave-breaking-free pulses in nonlinear-optical fibers", J. Opt. Soc. Am. B **10**, 1185-1190 (1993).

[3] N.S. Kapaney, *Fiber Optics: Principles and Applications* (Academic Press, San Diego, California, 1967).

[4] D. Marcuse, *Theory of Dielectric Optical Waveguides* (2nd ed., Academic Press, San Diego, California, 1991).

[5] A.C. Newell and J.P. Moloney, *Nonlinear Optics* (Addison-Wesley, Redwood City, California, 1992).

[6] G.P. Agrawal, *Nonlinear Fiber Optics* (2nd ed., Academic Press, San Diego, California, 1995).

[7] F. Forghieri, R.W. Tkach, and A.R. Chraplyvy, "Fiber nonlinearities and their impact on transmission systems", in *Optical Fiber Telecommunications*, eds. I.P. Kaminov and T.L. Koch (Academic, San Diego, California, 1997), 196-264.

[8] T. Miya, Y. Terumura, T. Hosaka, and T. Miyasita, "Ultimate low-loss single-mode fibre at 1.55 μm", Electron. Lett. **15**, 106 (1979).

[9] R.J. Mears, L. Reekie, I.M. Janucey, and D.N. Payne, "Low-noise erbium-doped fibre amplifier operating at 1.54 μm", Electron. Lett. **23**, 1026 (1987).

[10] E. Desurvire, J.R. Simpson, and P.C. Becker, "High-gain erbium-doped traveling-wave fiber amplifier", Opt. Lett. **12**, 888 (1997).

[11] C. Lin, H. Kogelnik, and L.G. Cohen, "Optical-pulse equalization of low-dispersion transmission in single-mode fibers in the 1.3 – 1.7 μm spectral region", Opt. Lett. **5**, 476 (1980).

[12] A. Hasegawa and F. Tappert, "Transmission of stationary nonlinear optical pulses in dispersive dielectric fibers. I. Anomalous dispersion", Appl. Phys. Lett. **23**, 142-144 (1973).

[13] L.F. Mollenauer, R.H. Stolen, and J.P. Gordon, "Experimental observation of picosecond pulse narrowing and solitons in optical fiber transmission", Phys. Rev. Lett. **45**. 1095-1098 (1980).

[14] V.E. Zakharov and A.B. Shabat, "Exact theory of two-dimensional self-focusing and one-dimensional self-modulation of waves in nonlinear media", Zh. Eksp. Teor. Fiz. **61**, 118-134 (1971) [Sov. Phys. JETP **34**, 62-69 (1972)].

[15] M.J. Ablowitz, D.J. Kaup, A.C. Newell, and H. Segur, "The inverse scattering transform-Fourier analysis for nonlinear problem", Stud. in Appl. Math. **53**, 249-315 (1974).

[16] M.J. Ablowitz and H. Segur, *Solitons and the Inverse Scattering Transform* (SIAM, Philadelphia, 1981).

[17] A. Hasegawa and Y. Kodama, "Guiding-center soliton in optical fibers", Opt. Lett. **15**, 1443-1445 (1990); "Guiding-center soliton", Phys. Rev. Lett. **66**, 161-164 (1991).

[18] K.J. Blow and N.J. Doran, "Average soliton dynamics and the operation of soliton systems with lumped amplifiers", IEEE Photon. Technol. Lett. **3**, 369-371 (1991).

[19] H. Kubota and M. Nakazawa, "Long-distance optical soliton transmission with lumped amplifiers", IEEE J. Quantum Electron. **26**, 692-700 (1990).

[20] V.I. Karpman and E.M. Maslov, "Perturbation theory for solitons", Zh. Exsp. Teor. Fiz. **73**, 537-559 (1977) [Sov. Phys. JETP **46**, 281-291 (1977)].

[21] V.I. Karpman, "Soliton evolution in the presence of perturbation", Physica Scripta **20**, 462-478 (1979).

[22] D.J. Kaup, "A perturbation expansion for the Zakharov-Shabat inverse scattering transform", SIAM J. Appl. Math. **31**, 121-133 (1976).

[23] D.J. Kaup and A.C. Newell, "Solitons as particles, oscillators, and in slowly changing media: a singular perturbation theory", Proc. R. Soc. Lond. A **361**, 413-446 (1978).

[24] D.J. Kaup, "Perturbation theory for solitons in optical fibers", Phys. Rev. A **42**, 5689-5693 (1990).

[25] J.N. Elgin, "Perturbations of optical solitons", Phys. Rev. A **47**, 4331-4341 (1993); "Soliton propagation in an optical fiber with third-order dispersion", Opt. Lett. **17**, 1409-1410 (1992).

[26] J.P. Gordon, "Dispersive perturbations of solitons of the nonlinear Schrödinger equation", J. Opt. Soc. Am. B **9**, 91-97 (1992).

[27] E.A. Kuznetsov, A.V. Mikhailov, and I.A. Shimokhin, "Nonlinear interaction of solitons and radiation", Physica D **87**, 201 (1995).

[28] J.P. Gordon and H.A. Haus, "Random walk of coherently amplified solitons in optical fiber transmission", Opt. Lett. **11**, 665 (1986).

[29] J.P. Gordon, "Interaction forces among solitons in optical fibers", Opt. Lett. **8**, 596 (1983).

[30] L.F. Mollenauer, S.G. Evangelides, and J.P. Gordon, "Wavelength division multiplexing with solitons in ultra-long distance transmission using lumped amplifiers", J. Lightwave Technol. **9**, 362 (1991).

[31] P.V. Mamyshev and L.F. Mollenauer, "Pseudo-phase-matched four-wave mixing in soliton wavelength-division multiplexing transmission", Opt. Lett. **21**, 396 (1996).

[32] S. Wabnitz, Y. Kodama, and A.B. Aceves, "Control of optical soliton interactions", Opt. Fiber Technol. **1**, 187 (1995).

[33] A. Mecozzi, J.D. Moores, H.A. Haus, and Y. Lai, "Soliton transmission control", Opt. Lett. **16**, 1841-1843 (1991).

[34] M. Matsumoto and A. Hasegawa, "Numerical study of the reduction of instability in bandwidth-limited amplified soliton transmission", Opt. Lett. **18**, 897 (1993).

[35] L.F. Mollenauer, J.P. Gordon, and S.G. Evangelides, "The sliding-frequency filter: an improved form of soliton jitter control", Opt. Lett. **17**, 1575 (1992).

[36] H. Kubota and M. Nakazawa, "Soliton transmission control in time and frequency domains", IEEE J. Quantum Electron. **29**, 2189-2197 (1993).

[37] S. Wabnitz, "Suppression of soliton interaction by phase modulation", Electron. Lett. **29**, 1711 (1993).

[38] Y. Kodama, M. Romagnoli, and S. Wabnitz, "Soliton stability and interactions in fiber lasers", Electron. Lett. **28**, 1981-1983 (1992).

[39] F.M. Knox, W. Forysiak, and N.J. Doran, "10 Gbit/s soliton communication systems over standard fiber at 1.55 μm and the use of dispersion compensation", J. Lightwave Technol. **13**, 1955 (1995).

[40] N.J. Smith, F.M. Knox, N.J. Doran, K.J. Blow, and I. Bennion, "Enhanced power solitons in optical fibres with periodic dispersion management", Electron. Lett. **32**, 54-55 (1996).

[41] M. Nakazawa and H. Kubota, "Construction of a dispersion-allocated soliton transmission line using conventional dispersion-shifted nonsoliton fibers", Japan J. Appl. Phys. **34**, L681-L683 (1995).

[42] I. Gabitov and S.K. Turitsyn, "Averaged pulse dynamics in a cascaded transmission system with passive dispersion compensation", Opt. Lett. **21**, 327-329 (1996); "Breathing solitons in optical fiber links", Pis'ma Zh. Eksp. Teor. Fiz. **63**, 814-819 (1996) [JETP Lett. **63**, 861-866 (1996)].

[43] N.J. Smith, N.J. Doran, F.M. Knox, and W. Forysiak, "Energy scaling characteristics of solitons in strongly dispersion-managed fibers", Opt. Lett. **21**, 1981-1983 (1996).

[44] J.H.B. Nijhof, N.J. Doran, W. Forysiak, and A. Berntson, "Energy enhancement of dispersion managed solitons and WDM", Electron. Lett. **34**, 481-482 (1998).

[45] M. Nakazawa, H. Kubota, A. Sahara, and K. Tamura, "Marked increase in the power margin through the use of a dispersion-allocated soliton", IEEE Photon. Technol. Lett. **8**, 1088-1090 (1996).

[46] A. Hasegawa, Y. Kodama, and A. Maruta, "Recent progress in dispersion-managed soliton transmission technologies", Opt. Fiber Technol. **3**, 197-213 (1997).

[47] T. Georges and B. Charbonnier, "Reduction of the dispersive wave in periodically amplified links with initially chirped solitons", IEEE Photon. Technol. Lett. **9**, 127-131 (1997).

[48] T.S. Yang, W.L. Kath, and S.K. Turitsyn, "Optimal dispersion maps for wavelength-division-multiplexed soliton transmission", Opt. Lett. **23**, 597 (1998).

[49] J.H.B. Nijhof, N.J. Doran, W. Forysiak, and F.M. Knox, "Stable soliton-like propagation in dispersion managed systems with net anomalous, zero and normal dispersion", Electron. Lett. **33**, 1726-1727 (1997).

[50] N.J. Smith, W. Forysiak, and N.J. Doran, "Reduced Gordon-Haus jitter due to enhanced power solitons in strongly dispersion managed systems", Electron. Lett. **32**, 2085-2086 (1996).

[51] G.M. Carter, J.M. Jacob, C.R. Menyuk, E.A. Golovchenko, and A.N. Pilipetskii, "Timing-jitter reduction for a dispersion-managed soliton system: experimental evidence", Opt. Lett. **22**, 513-515 (1997).

[52] C. Kurtzke, "Suppression of fiber nonlinearities by appropriate dispersion management", IEEE Photon. Technol. Lett. **5**, 1250-1253 (1993).

[53] T. Yu, E.A. Golovchenko, A.N. Pilipetskii, and C.R. Menyuk, "Dispersion-managed soliton interactions in optical fibers", Opt. Lett. **22**, 793-795 (1997).

[54] A. Hasegawa, S. Kumar, and Y. Kodama, "Reduction of collision-induced timing jitters in dispersion managed soliton transmission system", Opt. Lett. **21**, 39 (1996).

[55] A.M. Niculae, W. Forysiak, A.J. Gloag, J.H.B. Nijhof, and N.J. Doran, "Soliton collisions with wavelength-division multiplexed systems with strong dispersion management", Opt. Lett. **23**, 1354-1356 (1998).

[56] M. Wald, I.M. Uzunov, F. Lederer, and S. Wabnitz, "Optimization of periodically dispersion compensated breathing soliton transmissions", IEEE Photon. Technol. Lett. **9**, 1670 (1997).

[57] I. Gabitov, E.G. Shapiro, and S.K. Turitsyn, "Optical pulse dynamics in fiber links with dispersion compensation", Opt. Commun. **134**, 317-329 (1996); "Asymptotic breathing pulse in optical transmission systems with dispersion compensation", Phys. Rev. E **55**, 3624 (1997).

[58] J.N. Kutz, P. Holmes, S.G. Evangelides Jr., and J.P. Gordon, "Hamiltonian dynamics of dispersion managed breathers", J. Opt. Soc. Am. B **15**, 87-96 (1998).

[59] V.S. Grigoryan and C.R. Menyuk, "Dispersion-managed soliton at normal average dispersion", Opt. Lett. **23**, 609-611 (1998).

[60] T. Georges, "Soliton interaction in dispersion-managed links", J. Opt. Soc. Am. B **15**, 1553 (1998).

[61] T.I. Lakoba, J. Yang, D.J. Kaup, and B.A. Malomed, "Conditions for stationary pulse propagation in the strong dispersion management regime", Opt. Commun. **149**, 366-375 (1998).

[62] S.K. Turitsyn and E.G. Shapiro, "Variational approach to the design of optical communication systems with dispersion management", Opt. Fiber Technol. **4**, 151-188 (1998); E.G. Shapiro and S.K. Turitsyn, "Theory of guiding-center breathing soliton propagation in optical communication systems with strong dispersion management", Opt. Lett. **22**, 1544-1546 (1998).

[63] S.K. Turitsyn, T. Schäfer, and V.K. Mezentsev, "Generalized root-mean-square momentum method to describe chirped return-to-zero signal propagation in dispersion-managed fiber links", IEEE Photon. Tecnol. Lett. **11**, 203-205 (1999).

[64] T.S. Yang and W.L. Kath, "Analysis of enhanced-power solitons in dispersion-managed optical fibers", Opt. Lett. **22**, 985-987 (1997).

[65] M.J. Ablowitz and G. Biondini, "Multiscale pulse dynamics in communication systems with strong dispersion management", Opt. Lett. **23**, 1668-1670 (1998).

[66] S.K. Turitsyn and V.K. Mezentsev, "Dynamics of self-similar dispersion-managed soliton presented in the basis of chirped Gauss-Hermite functions", JETP Lett. **67**, 640-646 (1998); S.K. Turitsyn, T. Schäfer, and V.K. Mezentsev, "Self-similar core and oscillatory tails of a path-averaged chirped dispersion-managed optical pulse", Opt. Lett. **23**, 1351 (1998).

[67] S.K. Turitsyn, A.B. Aceves, C.K.R.T. Jones, V. Zharnitsky, and V.K. Mezentsev, "Hamiltonian averaging in soliton-bearing systems with a periodically varying dispersion", Phys. Rev. E **59**, 1-4 (1999).

[68] T.I. Lakoba and D.J. Kaup, "Shape of stationary pulse in strong dispersion management regime", Electron. Lett. **34**, 1124-1125 (1998).

[69] L.F. Mollenauer and P.V. Mamyshev, "Massive wavelength-division multiplexing with solitons", IEEE J. Quantum Electron. **34**, 2089 (1998).

[70] G.M. Carter and J.M. Jacob, "Dynamics of solitons in filtered dispersion-managed systems", IEEE Photon. Technol. Lett. **10**, 546-548 (1998).

[71] M. Matsumoto, "Analysis of filter control of dispersion-managed soliton transmission", J. Opt. Soc. Am. B **15**, 2831-2837 (1998).

[72] M. Matsumoto, "Time-domain transmission control of dispersion-managed solitons", Electron. Lett. **34**, 2155-2157 (1998).

[73] A. Sahara, T. Inui, T. Komukai, H. Kubota, and M. Nakazawa, "40-Gb/s RZ transmission over a transoceanic distance in a dispersion managed standard fiber using a modified inline synchronous modulation method", J. Lightwave Technol. **18**, 1364-1373 (2000).

[74] A. Tonello, A.D. Capobianco, S. Wabnitz, O. Leclerc, B. Dany, and E. Pincemin, "Stability and optimization of dispersion managed soliton control", Opt. Lett. **25**, 1496 (2000).

[75] M. Matsumoto, "Instability of dispersion-managed solitons in a system with filtering", Opt. Lett. **23**, 1901-1903 (1998).

[76] P.V. Mamyshev, "All-optical data regeneration based on self-phase modulation effect", Tech. Dig. of ECOC'98, Munick, Germany (1998).

[77] N.J. Doran and D. Wood, "Nonlinear optical loop mirror", Opt. Lett. **13**, 56-58 (1988).

[78] M.E. Fermann, F. Haberl, M. Hofer, and H. Hochreiter, "Nonlinear amplifying loop mirror", Opt. Lett. **15**, 752-754 (1990).

[79] N.J. Smith and N.J. Doran, "Picosecond soliton transmission using concatenated nonlinear optical loop-mirror intensity filters", J. Opt. Soc. Am. B **12**, 1117-1125 (1995).

[80] M. Matsumoto, H. Ikeda, and A. Hasegawa, "Suppression of noise accumulation in bandwidth-limited soliton transmission by means of nonlinear loop mirrors", Opt. Lett. **19**, 183-185 (1994).

[81] I. Gabitov, D.D. Holm, B.P. Luce, and A. Mattheus, "Recovery of solitons with nonlinear amplifying loop mirrors", Opt. Lett. **20**, 2490-2492 (1995).

[82] I. Gabitov, D.D. Holm, and B.P. Luce, "Low-noise picosecond soliton transmission by use of concatenated nonlinear amplifying loop mirrors", J. Opt. Soc. Am. B **14**, 1850-1855 (1997).

[83] P. Harper, I.S. Penketh, S.B. Alleston, I. Bennion, and N.J. Doran, "10 Gbit/s dispersion managed soliton propagation over 200 Mm without active control", Electron. Lett. **34**, 1997-1998 (1998).

[84] G.I. Baremblatt, *Scaling, Self-Similarity, and Intermediate Asymptotics* (Cambridge University Press, Cambridge, 1996).

[85] P.J. Olver, *Applications of Lie Groups to Differential Equations* (Springer, Berlin, 1986).

[86] A.A. Afanas'ev, V.I. Kruglov, B.A. Samson, R. Jakyte, and V.M. Volkov, "Self-action of counterpropagating axially symmetrical light-beams in a transparent cubic-nonlinearity medium", J. Mod. Opt. **38**, 1189-1202 (1991).

[87] C.R. Menyuk, D. Levi, and P. Winternitz, "Self-similarity in transient stimulated Raman-scattering", Phys. Rev. Lett. **69**, 3048-3051 (1992).

[88] T.M. Monro, P.D. Millar, L. Paladin, and C.M. de Sterke, "Self-similar evolution of self-written waveguides", Opt. Lett. **23**, 268-270 (1998).

[89] M. Soljacic, M. Segev, and C.R. Menyuk, "Self-similarity and fractals in soliton supporting systems", Phys. Rev. E **61**, R1048-R1051 (2000).

[90] V.I. Kruglov, A.C. Peacock, J.M. Dudley, and J.D. Harvey, "Self-similar propagation of high-power parabolic pulses in optical fiber amplifiers", Opt. Lett. **25**, 1753-1755 (2000).

[91] M.E. Fermann, V.I. Kruglov, B.C. Thomsen, J.M. Dudley, and J.D. Harvey, "Self-similar propagation and amplification of parabolic pulses in optical fibers", Phys. Rev. Lett. **84**, 6010-6013 (2000).

[92] K. Tamura and M. Nakazawa, "Pulse compression by nonlinear pulse evolution with reduced optical wave breaking in erbium-doped fiber amplifiers", Opt. Lett. **21**, 68-70 (1996).

[93] P.A. Bélanger, L. Gagnon, and C. Paré, "Solitary pulses in an amplified nonlinear dispersive medium", Opt. Lett. **14**, 943-945 (1989).

[94] A. Galvanauskas and M.E. Fermann, Postdeadline Papers of CLEO'2000, CPD 3-1 (2000).

[95] L. Gagnon and P.A. Bélanger, "Adiabatic amplification of optical solitons", Phys. Rev. A **43**, 6187-6193 (1991).

[96] K.J. Blow, N.J. Doran, and D. Wood, "Trapping of energy into solitary waves in amplified nonlinear dispersive systems", Opt. Lett. **12**, 1011-1013 (1987); "Generation and stabilization of short soliton pulses in the amplified nonlinear Schrödinger equation", J. Opt. Soc. Am. B **5**, 381-391 (1988).

[97] R. Trebino, K.W. DeLong, D.N. Fittinghoff, J.N. Sweetser, M.A. Krumbugel, B.A. Richman, and D.J. Kane, "Measuring ultrashort laser pulses in the time-frequency domain using frequency-resolved optical gating", Rev. Sci. Instrum. **68**, 3277-3295 (1997).

[98] D.J. Jones, H.A. Haus, L.E. Nelson, and E.P. Ippen, "Stretched-pulse generation and propagation", IEICE Trans. Electron. **E81-C**, 180-188 (1998).

[99] V.E. Zakharov, "Propagation of optical pulses in nonlinear systems with varying dispersion", in *Optical soliton: Theoretical challenges and industrial perspectives*, eds. V.E. Zakharov and S. Wabnitz (Springer-Verlag, Berlin, 1999), 73-89.

[100] V.E. Zakharov and S.V. Manakov, "On propagation of short pulses in strong dispersion managed optical lines", Pis'ma Zh. Exsp. Teor. Fiz. **70**, 573-576 (1999) [JETP Lett. **70**, 578-582 (1999)].

[101] S. Boscolo, J.H.B. Nijhof, and S.K. Turitsyn, "A perturbative analysis of dispersion-managed solitons", Physica Scripta **62**, 479-485 (2000).

[102] S.K. Turitsyn, T. Schäfer, K.H. Spatschek, and V.K. Mezentsev, "Path-averaged chirped optical soliton in dispersion-managed fiber communication lines", Opt. Commun. **163**, 122-158 (1999).

[103] N.J. Smith, N.J. Doran, W. Forysiak, and F.M. Knox, "Soliton transmission using periodic dispersion compensation", IEEE J. Lightwave Technol. **15**, 1808-1822 (1997).

[104] J.H.B. Nijhof, W. Forysiak, and N.J. Doran, "The averaging method for finding exactly periodic dispersion-managed solitons", IEEE J. of Selected Topics in Quantum Electron. **6**, 330-336 (2000).

[105] I. Shake, H. Takara, K. Mori, S. Kawanishi, and Y. Yamabayshi, "Influence of inter-bit four-wave mixing in optical TDM transmission", Electron. Lett. **34**, 1600-1601 (1998).

[106] R.-J. Essiambre, B. Mikkelsen, and G. Raybon, "Intra-channel cross-phase modulation and four-wave mixing in high-speed TDM systems", Electron. Lett. **35**, 1576-1578 (1999).

[107] P.V. Mamyshev and N.A. Mamysheva, "Pulse-overlapped dispersion-managed data transmission and intrachannel four-wave mixing", Opt. Lett. **24**, 1456-1458 (1999).

[108] A. Mecozzi, C.B. Clausen, and M. Shtaif, "Analysis of intrachannel nonlinear effects in highly dispersed optical pulse transmission", IEEE Photon. Technol. Lett. **12**, 392-394 (2000); "System impact of intra-channel nonlinear effects in highly dispersed optical pulse transmission", IEEE Photon. Technol. Lett. **12**, 1633-1635 (2000).

[109] R.I. Killey, H.J. Thiele, V. Mikhailov, and P. Bayvel, "Reduction of intrachannel nonlinear distortion in 40-Gb/s-based WDM transmission over standard fiber", IEEE Photon. Technol. Lett. **12**, 1624-1626 (2000).

[110] D.S. Govan, N.J. Smith, F.M. Knox, and N.J. Doran, "Stable propagation of solitons with increased energy through the combined action of dispersion management and periodic saturable absorption", J. Opt. Soc. Am. B **14**, 2960-2966 (1997).

[111] T. Hirooka and S. Wabnitz, "Stabilisation of dispersion-managed soliton transmissions by nonlinear gain", Electron. Lett. **35**, 655-657 (1999); "Nonlinear gain control of dispersion-managed soliton amplitude and collisions", Opt. Fiber Technol. **6**, 109 (2000)..

[112] S. Boscolo, J.H.B. Nijhof, and S.K. Turitsyn, "Autosoliton transmission in dispersion-managed systems guided by in-line nonlinear optical loop mirrors", Opt. Lett. **25**, 1240-1242 (2000).

[113] S. Boscolo, S.K. Turitsyn, and K.J. Blow, "All-optical passive regeneration of 40 Gbit/s soliton data stream using dispersion management and in-line NOLMs", Electron. Lett. **37**, 112-113 (2001).

[114] S. Boscolo, S.K. Turitsyn, and K.J. Blow, "Study of the operating regime for all-optical passive 2R regeneration of dispersion-managed RZ data at 40 Gbit/s using in-line NOLMs", IEEE Photon. Technol. Lett. **14**, 30-32 (2002).

[115] S. Boscolo, S.K. Turitsyn, and K.J. Blow, "All-optical passive quasi-regeneration in transoceanic 40 Gbit/s return-to-zero transmission systems with strong dispersion management", Opt. Commun., In Press.

[116] S. Boscolo, S.K. Turitsyn, K.J. Blow, and J.H.B. Nijhof, "Passive regeneration in 40 Gbit/s-based WDM dispersion-managed RZ transmission systems by in-line NOLMs", Submitted to Opt. Fiber Technol.

[117] S. Boscolo, S.K. Turitsyn, and K.J. Blow, "All-optical passive 2R regeneration for N×40 Gbit/s WDM transmission using NOLM and novel filtering technique", Submitted to Electron. Lett.

[118] K.J. Blow, B.K. Nayar, and N.J. Doran, "Experimental demonstration of optical soliton switching in a all-fiber nonlinear Sagnac interferometer", Opt. Lett. **14**, 754-756 (1989).

[119] M.N. Islam, E.R. Sunderman, R.H. Stolen, W. Pleibel, and J.R. Simpson, "Soliton switching in a fiber nonlinear loop mirror", Opt. Lett. **14**, 811-813 (1989).

[120] A.L. Steele, "Pulse-compression by an optical-fiber loop mirror constructed from 2 different fibers", Electron. Lett. **29**, 1971-1972 (1993).

[121] M. Matsumoto, A. Hasegawa, and Y. Kodama, "Adiabatic amplification of solitons by means of nonlinear amplifying loop mirrors", Opt. Lett. **19**, 1019-1021 (1994).

[122] S.B. Alleston, P. Harper, I.S. Penketh, I. Bennion, N.J. Doran, and A.D. Ellis, "1000 km transmission of 40 Gbit/s single channel RZ data over dispersion managed standard (non-dispersion shifted) fibre", Electron. Lett. **35**, 823-824 (1999).

[123] A.H. Gnauck, S.-G. Park, J.M. Wiesenfeld, and L.D. Garrett, "Highly dispersed pulses for 2×40 Gbit/s transmission over 800 km of conventional singlemode fibre", Electron. Lett. **35**, 2218-2219 (1999).

[124] A.R. Pratt, H. Murai, H.T. Yamada, and Y. Ozeki, "40 Gbit/s single channel transmission over 3120 km of dispersion managed standard fibre", Tech. Dig. of ECOC'2000, Munick, Germany, vol. 4, pp. 43-44 (2000).

[125] M. Nakazawa, K. Suzuki, E. Yamada, H. Kubota, Y. Kimura, and M. Takaya, "Experimental demonstration of soliton data transmission over unlimited distances with soliton control in time and frequency domains", Electron. Lett. **29**, 729-730 (1993).

[126] O. Leclerc, P. Brindel, D. Rouvillain, B. Dany, E. Pincemin, E. Desurvire, C. Duchet, A. Shen, F. Blache, E. Grard, A. Coquelin, M. Goix, S. Bouchoule, and P. Nouchi, "2×40 Gbit/s WDM optically regenerated dispersion-managed transmission over 10000 km with narrow channel spacing", Electron. Lett. **36**, 58-59 (2000).

[127] D. Breuer, F. Küppers, A. Mattheus, E.G. Shapiro, I. Gabitov, and S.K. Turitsyn, "Symmetrical dispersion compensation for standard monomode-fiber-based communication systems with large amplifier spacing", Opt. Lett. **22**, 982-984 (1997).

[128] C.M. Weinert, R. Ludwig, W. Pieper, D. Breuer, K. Peterman, and F. Küppers, "40 Gb/s and 4×40 Gb/s TDM/WDM standard fiber transmission", IEEE J. Lightwave Technol. **17**, 2276-2284 (1999).

[129] K. Tanaka, I. Morita, M. Suzuki, and N. Edagawa, "40 Gbit/s-based DWDM systems with SMF-based dispersion flattened transmission line", Tech. Dig. of ROSC International Workshop 2000, Japan (2000).

[130] D. LeGuen, S. Del Burgo, M.L. Moulinard, D. Grot, M. Henry, F. Favre, and T. Georges, "Narrow band 1.02 Tbit/s (51×20 Gbit/s) soliton DWDM transmission over 1000 km of standard fiber with 100 km amplifier spans", Postdeadline Papers of OFC/IOOC'99, San Diego, California, PD4 (1999).

[131] T. Tsuritani, A. Agata, K. Imai, K. Tanaka, T. Miyakawa, N. Edagawa, and M. Suzuki, "35 GHz-spaced-20 GBPS$\times$100 WDM RZ transmission over 2700 km using SMF-based dispersion flattened fiber span", Postdeadline Papers of ECOC'2000, Munick, Germany, PD1.5 (2000).

[132] K. Suzuki, H. Kubota, A. Sahara, and M. Nakazawa, "640 Gbit/s (40 Gbit/s$\times$16 channel) dispersion-managed DWDM soliton transmission over 1000 km with spectral efficiency of 0.4 bit/Hz", Electron. Lett. **36**, 443-445 (2000).

[133] S. Bigo, "Improving spectral efficiency by ultra-narrow optical filtering to achieve multiterabit/s capacities", Tech. Dig. of OFC'2002, Anaheim, California, WX3, pp. 362-364 (2002).

[134] S. Boscolo, S.K. Turitsyn, V.Yu. Novokshenov, and J.H.B. Nijhof, "Self-similar parabolic optical solitary waves", Invited to Special Issue of Theoretical and Mathematical Physics.

[135] V.E. Zakharov and E.A. Kuznetsov, "Quasiclassical theory of three-dimensional wave collapse", Zh. Eksp. Teor. Fiz. **91**, 1310-1324 (1986) [Sov. Phys. JETP **64**, 773-780 (1986)].

[136] H. Segur and M.J. Ablowitz, "Connection results for the second Painlevé equation", Physica D **3**, 165-184 (1981).

[137] S.P. Hastings and J.B. McLeod, "A boundary value problem associated with the second Painlevé transcendent and the Korteweg-de Vries equation", Arch. Rational Mech. Anal. **73**, 31-51 (1980).

[138] P.A. Clarkson and J.B. McLeod, "A connection formula for the second Painlevé transcendent", Arch. Rational Mech. Anal. **103**, 97-138 (1988).

[139] A.R. Its and V.Yu. Novokshenov, *The Isomonodromic Deformation Method in the Theory of Painlevé Equations*, Lecture Notes in Math. **1191** (Springer-Verlag, Berlin, 1986).

[140] A.R. Its and A.A. Kapaev, "The method of isomonodromy deformations and connection formulas for the second Painlevé transcendent", Math. USSR Izvestiya **31**, 193-207 (1988).

[141] N. Joshi and M.D. Kruskal, "The connection problem for Painlevé transcendents", Physica D **18**, 215-216 (1986); "An asymptotic approach to the connection problem for the first and the second Painlevé equations", Phys. Lett. A **130**, 129-137 (1988); "The Painlevé connection problem: an asymptotic approach I", Stud. Appl. Math. **86**, 315-376 (1992).

[142] N. Joshi, "Asymptotic Studies of the Painlevé Equations", in *The Painlevé Property, One Century Later*, ed. R. Conte, CRM Series in Mathematical Physics (Springer-Verlag, New York, 1999), 181-227.

[143] E. Desurvire, *Erbium-Doped Fiber Amplifiers: Principles and Applications* (Wiley, New York, 1994).

[144] B. Deutsch and T. Pfeiffer, "Chromatic dispersion of erbium-doped silica fibers", Electron. Lett. **28**, 303-305 (1992).

[145] O.A. Ladyženskaja, V.A. Solonnikov and N.N. Ural'ceva, *Linear and Quasi-Linear Equations of Parabolic Type*, American Mathematical Society, Translations of Mathematical Monographs **23**.

[146] S.K. Turitsyn, M. Fedoruk, T.S. Yang, and W.L. Kath, " "Magic" dispersion maps for multichannel soliton transmission", IEEE J. Quantum Electron. **36**, 290-299 (2000).

[147] A. Altuncu, L. Noel, W.A. Pender, A.S. Siddiqui, T. Widdowson, A.D. Ellis, M.A. Newhouse, A.J. Antos, G. Kar, and P.W. Chu, "40 Gbit/s error free transmission over a 68 km distributed erbium doped fibre amplifier", Electron. Lett. **32**, 233-234 (1996).

[148] T. Naito, T. Tanaka, K. Torii, N. Shimojoh, and H. Nakamoto, "A broadband distributed Raman amplifier for bandwidths beyond 100 nm", Tech. Dig. of OFC'2002, Anaheim, California, TuR1, pp. 116-117 (2002).

Publications

1. Journal articles

1. S. Boscolo, J.H.B. Nijhof, and S.K. Turitsyn, "A perturbative analysis of dispersion-managed solitons", Physica Scripta **62**, 479-485 (2000).

2. S. Boscolo, J.H.B. Nijhof, and S.K. Turitsyn, "Autosoliton transmission in dispersion-managed systems guided by in-line nonlinear optical loop mirrors", Opt. Lett. **25**, 1240-1242 (2000).

3. S. Boscolo, S.K. Turitsyn, and K.J. Blow, "All-optical passive regeneration of 40 Gbit/s soliton data stream using dispersion management and in-line NOLMs", Electron. Lett. **37**, 112-113 (2001).

4. S. Boscolo, S.K. Turitsyn, and K.J. Blow, "Study of the operating regime for all-optical passive 2R regeneration of dispersion-managed RZ data at 40 Gbit/s using in-line NOLMs", IEEE Photon. Technol. Lett. **14**, 30-32 (2002).

5. S. Boscolo, S.K. Turitsyn, and K.J. Blow, "All-optical passive quasi-regeneration in transoceanic 40 Gbit/s return-to-zero transmission systems with strong dispersion management", Opt. Commun., In Press.

6. S. Boscolo, S.K. Turitsyn, K.J. Blow, and J.H.B. Nijhof, "Passive regeneration in 40 Gbit/s-based WDM dispersion-managed RZ transmission systems by in-line NOLMs", Submitted to Opt. Fiber Technol.

7. S. Boscolo, S.K. Turitsyn, V.Yu. Novokshenov, and J.H.B. Nijhof, "Self-similar parabolic optical solitary waves", Invited to Special Issue of Theoretical and Mathematical Physics.

8. S. Boscolo, S.K. Turitsyn, and K.J. Blow, "All-optical passive 2R regeneration for N×40 Gbit/s WDM transmission using NOLM and novel filtering technique", Submitted to Electron. Lett.

2. Conferences

1. S. Boscolo, "Path-averaged optical solitons in dispersion-managed fibre communication lines: a perturbative description", Tech. Dig. of Second Conference on Postgraduate Research in Electronics, Photonics and Related Fields (PREP 2000), Nottingham, UK, 399-404 (Apr. 2000).

2. S. Boscolo, J.H.B. Nijhof, and S.K. Turitsyn, "A perturbative analysis of dispersion-managed solitons", RCP264: Inverse Problems and Nonlinearity, Theory and Applications, Montpellier, France (Jun. 2000).

3. S. Boscolo, J.H.B. Nijhof, and S.K. Turitsyn, "Auto-solitons guided by in-line nonlinear optical loop mirrors in dispersion-managed communication systems", Tech. Dig. of Conference on Lasers and Electro-Optics Europe 2000 (CLEO/Europe-IQEC 2000), Nice, France, CThE28, p. 306 (Sept. 2000).

4. S. Boscolo, S.K. Turitsyn, and K.J. Blow, "All-optical passive regeneration of 40 Gbit/s soliton data stream using dispersion-management and in-line nonlinear optical loop mirrors", Tech. Dig. of Conference on Optical Fiber Communications (OFC 2001), Anaheim, California, USA, MF6 (Mar. 2001).

5. S. Boscolo, S.K. Turitsyn, and K.J. Blow, "Stabilization of dispersion-managed soliton transmission in systems with very large map strength by in-line nonlinear optical loop mirrors", Tech. Dig. of Nonlinear Guided Waves and Their Applications (NLGW 2001), Clearwater, Florida, USA, MC71, pp. 248-250 (Mar. 2001).

6. S. Boscolo, S.K. Turitsyn, and K.J. Blow, "Working parameter region for soliton all-optical passive regeneration using dispersion management and nonlinear optical loop mirrors", Tech. Dig. of 15th International Conference on Lasers and Electrooptics in Europe (CLEO/Europe-EQEC Focus Meetings 2001), Munich, Germany, p. 267 (Jun. 2001).

7. S. Boscolo and S.K. Turitsyn, "Stable self-similar parabolic optical solitary waves", Nonlinear Evolution Equations and Dynamical Systems XVth Meeting (NEEDS 2001), Cambridge, UK (Jul. 2001).

8. S. Boscolo, S.K. Turitsyn, and K.J. Blow, "All-optical passive 2R regeneration of dispersion-managed RZ data at 40 and 80 Gbit/s using in-line NOLMs", Tech. Dig. of 14th Annual Meeting of the IEEE Lasers and Electro-Optics Society (LEOS 2001), San Diego, California, USA, MK2, pp. 83-84 (Nov. 2001).

9. S. Boscolo and S.K. Turitsyn, " "Magic" dispersion maps with distributed Raman amplification", Accepted to 16th Workshop on Nonlinear Evolution Equations and Dynamical Systems (NEEDS 2002), Cadiz, Spain (Jun. 2002).

10. S. Boscolo, S. Waiyapot, and S.K. Turitsyn, "A perturbation approach for dispersion-managed solitons controlled by filters and amplitude modulators", Accepted to Nonlinear Physics: Theory and Experiment. II, Gallipoli, Italy (Jun. 2002).

11. S. Boscolo, S.K. Turitsyn, and K.J. Blow, "All-optical passive 2R regeneration for N×40 Gbit/s WDM transmission using NOLM and novel filtering technique", Submitted to 23th European Conference on Optical Communication (ECOC 2002), Copenaghen, Denmark (Sept. 2002).

12. S. Boscolo, S.K. Turitsyn, V.Yu. Novokshenov, and J.H.B. Nijhof, "On the theory of self-similar parabolic optical solitary waves", Submitted to Nonlinear Guided Waves and Their Applications (NLGW 2002), Stresa, Italy (Sept. 2002).

3. Patent

1. S. Boscolo, S.K. Turitsyn, and K.J. Blow, "Optical Pulse Regenerating Transmission Lines", British Patent No. 0100603.0 .